AN IMPROVED STRUCTURAL MECHANICS MODEL FOR THE FRAPCON NUCLEAR FUEL PERFORMANCE CODE

By

Alexander James Mieloszyk

B.S., Nuclear Engineering (2010)

Oregon State University

SUBMITTED TO THE DEPARTMENT OF NUCLEAR SCIENCE AND ENGINEERING
IN PARTIAL FULFILLMENT OF THE REQUIREMENTS FOR THE DEGREE OF

MASTER OF SCIENCE IN NUCLEAR SCIENCE AND ENGINEERING
AT THE
MASSACHUSETTS INSTITUTE OF TECHNOLOGY

JUNE 2012

Signature of Author: _____
Alexander James Mieloszyk
Department of Nuclear Science and Engineering
May 18, 2012

Certified By: _____
Mujid S. Kazimi, Ph. D.
TEPCO Professor of Nuclear Engineering
Thesis Supervisor

Certified By: _____
Ronald G. Ballinger, Ph. D.
Professor of Nuclear Science and Engineering
Thesis Reader

Accepted By: _____
Mujid S. Kazimi, Ph. D.
TEPCO Professor of Nuclear Engineering
Chairman, Committee on Graduate Students

An Improved Structural Mechanics Model for the FRAPCON Nuclear Fuel Performance Code

by

Alexander James Mielosyzk

Submitted to the Department of Nuclear Engineering on May XX, 2012 in partial fullfillment for the degree of Masters of Science in Nuclear Science and Engineering

ABSTRACT

In order to provide improved predictions of Pellet Cladding Mechanical Interaction (PCMI) for the FRAPCON nuclear fuel performance code, a new model, the FRAPCON Radial-Axial Soft Pellet (FRASP) model, was developed. This new model uses 1.5D structural mechanics to represent both the fuel pellet and cladding along with their interaction via interfacial forces. The fuel pellet and cladding are modeled as concentric annular cylinders using similar governing equations with slight differences to allow for cracking of the semi-brittle fuel matrix and plastic behavior in a ductile cladding. By accounting for the structural mechanics of the fuel pellet, FRASP allows for stress-induced deformations which were previously unattainable with the rigid pellet model used by FRAPCON.

Because of the significant differences between FRAPCON's previous mechanical model, FRACAS-I, and FRASP, simply replacing the treatment of PCMI within the code was not a viable option. This led to a complete replacement of FRACAS-I and all associated fuel rod structural calculations. Feedback effects are likely to result from such a major change due to the complexity of nuclear fuel simulation. The potential for these feedback effects dictated a preliminary validation of FRASP against FRACAS-I for typical case. This evaluation was not limited to the investigation of mechanical parameters, but covered a wide variety of predicted parameters by the new and unaltered versions of FRAPCON. The differences which were found in this validation were limited in nature and easily attributable to the differing assumptions of FRASP and FRACAS-I.

The newly developed mechanical model was used with the improved fuel behavior models of FRAPCON-EP (Enhanced Performance) to assess the mechanical behavior of fuel rods with a composite silicon carbide (SiC) cladding under Pressurized Water Reactor (PWR) conditions. The fuel rod designs were selected to match previously chosen values for both solid and annular fuel pellets under current and uprated power conditions. Unlike FRACAS-I, which is hindered by the rigid pellet model, FRASP was able to successfully analyze PCMI behavior with the more rigid SiC, even though "hard contact" of the fuel and cladding was encountered.

Simulations using the improved models showed that the SiC clad fuel rods may not provide adequate safety margins at the desired burnup, or simply fail to achieve their desired final burnup. Previous analyses which relied on FRAPCON-3.3 may have been overly optimistic in this regard. The new, more conservative predictions are largely due to FRASP's treatment of the inner radius of the annular fuel pellets, which was assumed not to change in previous versions of FRAPCON. These new findings suggest that SiC fuel rod general design and operation require further optimization.

Thesis Supervisor: Mujid S. Kazimi
Title: TEPCO Professor of Nuclear Science and Engineering

Thesis Reader: Ronald G. Ballinger
Title: Professor of Nuclear Science and Engineering

ACKNOWLEDGEMENTS

First, I would like to thank my advisor, Professor Kazimi, for directing me towards this project and continuing to support it. The guidance that he provided me since my arrival at MIT has been crucial to both my personal development and the completion of this thesis.

Both the Fuel Development and Fuel Cycle research groups here at MIT have taught me vast amounts about the field of nuclear fuel design, of which I was completely ignorant upon my arrival. I owe a tremendous thanks to Dr. David Carpenter as he helped me navigate the labyrinth that is FRAPCON's structure. The power histories used for the evaluation of the SiC clad fuel rods used in this study are wholly a result of the diligence of Dr. Edward Pilat, for which I am very grateful.

My fellow students within the Nuclear Science and Engineering Department and at MIT in general have provided me with a better community than I had thought possible. Knowing them has made me a better person in every sense. I have had the privilege of knowing and sharing an office with Tyrell Arment for the last two years and owe him a mountain of thanks for his friendship.

I am also deeply thankful for the patience and support given to me by my girlfriend, Becky Asher. I consider it my great fortune to have found her here.

Lastly, I would like to thank my father and mother, Jim and Karyn Mieloszyk. For the last 24 years they have given me the tools to reach this point in my life and have provided unconditional love and support at every turn. My life will always be driven by the lessons they taught me about how success is truly defined.

Contents

List of Figures 6

List of Tables 10

Nomenclature 11

1 Introduction 15
- 1.1 Background . . . 15
  - 1.1.1 LWR Fuel Rod Design . . . 15
  - 1.1.2 Pellet-Cladding Interaction (PCI) . . . 16
- 1.2 Nuclear Fuel Rod Simulation . . . 18
  - 1.2.1 FRAPCON-3 Fuel Performance Code . . . 20
  - 1.2.2 FRACAS-I Mechanical Model . . . 22
  - 1.2.3 FRAPCON-EP Fuel Performance Code . . . 24
- 1.3 Need for an Improved Mechanical Model within FRAPCON . . . 25
- 1.4 Objectives and Scope . . . 27

2 Model Development 28
- 2.1 Model Assumptions of FRASP . . . 28
- 2.2 Steady State Behavior . . . 33
- 2.3 Fuel Pellet Cracking . . . 38
- 2.4 Inelastic Behavior . . . 43
  - 2.4.1 Instantaneous Plastic Straining . . . 43
  - 2.4.2 Cladding Creep . . . 46
  - 2.4.3 Calculation of Permanent Strain Components . . . 48
- 2.5 Contact Regimes . . . 49
- 2.6 PCMI Model . . . 51
- 2.7 Incorporation of FRASP into FRAPCON . . . 59
- 2.8 SiC Cladding Model Changes . . . 64

3 Preliminary Validation 70
- 3.1 Validation Case . . . 71
- 3.2 Validation Results . . . 74

4 Analyses of SiC Clad Fuel Rods Using FRAPCON-EP **92**
4.1 Power History Evaluation 94
4.2 Base Zircaloy-Clad Case 101
4.3 SiC-Clad Solid Pellet Case 112
4.4 SiC-Clad Annular Pellet Case 124
4.5 10% Uprated SiC-Clad Annular Pellet Case 134
4.6 Discussion of SiC Clad PWR Fuel Designs 141

5 Summary and Recommendations for Future Work **143**
5.1 Summary of FRASP Development and Preliminary Validation 143
5.2 Summary of FRAPCON-EP Analysis of SiC Clad Fuel Rods 144
5.3 Recommendations for Future Uses of and Improvements to FRASP 146
5.4 Recommendations for Future Analyses of SiC Clad Fuel Rods 147

Bibliography **149**

Appendix A: FRAPCON Inputs **153**

List of Figures

1-1 **Picture of cladding failure due to a MPS (Williamson et al., 2012)** 18
1-2 **Typical fuel pin parameters that influence fuel-cladding heat transfer coefficient (Beyer et al., 1975)** 19
1-3 **Simplified FRAPCON-3 flowchart (Berna et al., 1997)** 22

2-1 **Illustration of fuel rod nodalization applied by FRAPCON-3** 30
2-2 **Comparison of the arithmetic and integral averaged fuel pellet temperatures** 32
2-3 **Comparison of the arithmetic and integral averaged cladding temperatures** 32
2-4 **Visualization of secant method iteration** 36
2-5 **Illustration of plenum and coolant pressure application** . . . 37
2-6 **Illustration of axial forces acting on the fuel pellet** 38
2-7 **Hoop stress within the fuel pellet resulting from thermal expansion** 39
2-8 **Photograph of a cracked fuel pellet** (Marchal et al., 2009) 40
2-9 **Photograph of a fuel pellet which has experienced crack healing (Sercombe et al., 2012)** 43
2-10 **Uniaxial stress-strain curve of unirradiated Zircaloy at 300K** 44
2-11 **Illustration of FRASP's instantaneous plastic strain methodology** 46
2-12 **Illustration of the fuel and cladding behavior in the various contact regimes** 50
2-13 **Flow chart of FRASP's treatment of pellet-cladding contact** 52
2-14 **Illustration of the application of interfacial coupling forces** . 53
2-15 **Illustration of the axial force's directions of application** . . . 54
2-16 **Illustration of the primary and secondary effects of applying interfacial forces** 56
2-17 **Simplified flow chart of FRASP's partially separated PCMI solution process** 58
2-18 **Changes to the code structure of FRAPCON to incorporate FRASP** 60
2-19 **Visualization of the modified solution direction for the implementation of FRASP** 62

2-20 Example of the differences in cladding local and average hoop stress . . . 64
2-21 Triplex SiC cladding design (Carpenter et al., 2010) . . . 65

3-1 Axial peaking profile used in the preliminary validation . . . 73
3-2 Fuel pellet outer and cladding inner radii predicted by FRASP for the peak LHGR axial node . . . 74
3-3 Fuel pellet outer and cladding inner radii predicted by FRACAS-I for the peak LHGR axial node . . . 75
3-4 Labeled description of fuel-cladding gap behavior over the fuel rod's lifetime . . . 76
3-5 Maximum fuel pellet temperature of the peak LHGR axial node . . . 78
3-6 Illustration of stress-induced fuel pellet deformation predicted by FRASP . . . 79
3-7 Difference in the calculated total cladding strain components by FRASP and FRACAS-I . . . 80
3-8 Difference in the calculated permanent cladding strain components by FRASP and FRACAS-I . . . 81
3-9 Difference in calculated cladding axial strains between FRASP and FRACAS-I . . . 82
3-10 Permanent cladding axial strain calculated for the peak LHGR axial node . . . 83
3-11 Permanent cladding radial strain calculated for the peak LHGR axial node . . . 83
3-12 Difference in calculated cladding axial strains between FRASP and FRACAS-I . . . 84
3-13 Average cladding axial stress observed for the peak LHGR axial node . . . 85
3-14 Average cladding hoop stress observed for the peak LHGR axial node . . . 86
3-15 Interfacial pressure observed for the peak LHGR axial node 86
3-16 Average cladding radial stress observed for the peak LHGR axial node . . . 87
3-17 Total observed cladding axial elongation throughout the fuel rod lifetime . . . 88
3-18 Plenum pressure observed throughout the fuel rod lifetime . 89
3-19 Void volume observed throughout the fuel rod lifetime 89
3-20 Difference in the size of the fuel-cladding gap size observed between FRASP and FRACAS-I . . . 90
3-21 Difference in the maximum fuel pellet temperature observed between FRASP and FRACAS-I . . . 91

4-1 Power history characteristic of those used in previous studies 95

4-2 Peaking factor history of the peak burnup assembly from SIMULATE results 96
4-3 Power history of the peak burnup assembly 97
4-4 Adapted power histories of the peak burnup fuel rod 98
4-5 BOL axial power shape associated with each irradiation cycle 99
4-6 MOL axial power shape associated with each irradiation cycle 99
4-7 EOL axial power shape associated with each irradiation cycle 100
4-8 Axial LHGR distribution throughout the fuel rod lifetime . 100
4-9 Power histories of the BOL and EOL peak LHGR nodes . . 101
4-10 Fuel pellet radius of the axial node with the BOL peak LHGR 103
4-11 Cladding inner radius of the axial node with the BOL peak LHGR 104
4-12 Gap thickness of the axial node with the BOL peak LHGR . 105
4-13 Cladding hoop strain at EOL for the Zircaloy clad fuel rod . 106
4-14 Total axial cladding elongation of the Zircaloy clad fuel rod 107
4-15 Difference in maximum fuel temperature between FRAPCON-EP and FRAPCON-3.3 throughout the lifetime of the Zircaloy clad fuel rod 108
4-16 Difference in maximum fuel temperature between FRAPCON-EP and FRAPCON-3.4 throughout the lifetime of the Zircaloy clad fuel rod 108
4-17 Average temperature of the the fuel stack throughout the lifetime of the Zircaloy clad fuel rod 110
4-18 Observed FGR throughout the lifetime of the Zircaloy clad fuel rod 111
4-19 Observed plenum pressure throughout the lifetime of the Zircaloy clad fuel rod 112
4-20 Inner cladding radius of the axial node with the BOL peak LHGR for the SiC clad solid pellet case 113
4-21 Fuel-cladding thickness of the axial node with the BOL peak LHGR for the SiC clad solid pellet case 114
4-22 Average temperature of the the fuel stack throughout the lifetime of the SiC clad solid pellet case 115
4-23 Observed FGR throughout the lifetime of the SiC clad solid pellet case 116
4-24 Observed plenum pressure throughout the lifetime of the SiC clad solid pellet case 117
4-25 Total axial cladding elongation of the SiC clad solid pellet case 118
4-26 Maximum interfacial pressure throughout the lifetime of the SiC clad solid pellet case 119
4-27 Observed EOL fuel outer radii of the SiC clad solid pellet case 120
4-28 Interfacial pressure observed at EOL of the SiC clad solid pellet case 121
4-29 Cladding hoop strain at EOL of the SiC clad solid pellet case 122
4-30 Cladding hoop strain at MOL of the SiC clad solid pellet case 123

4-31 Difference in predicted cladding axial strain observed by FRAPCON-EP and FRAPCON-3.3 for the SiC clad solid pellet case . . . 124
4-32 Comparison of the burnup between the solid and annular pellet cases . . . 125
4-33 Average temperature of the the fuel stack throughout the lifetime of the SiC clad annular pellet case . . . 126
4-34 Observed FGR throughout the lifetime of the SiC clad annular pellet case . . . 127
4-35 Observed plenum pressure throughout the lifetime of the SiC clad annular pellet case . . . 127
4-36 Inner cladding radius of the axial node with the BOL peak LHGR for the SiC clad annular pellet case . . . 128
4-37 Cladding hoop strain at EOL of the SiC clad annular pellet case . . . 129
4-38 Maximum interfacial pressure throughout the lifetime of the SiC clad annular pellet case . . . 130
4-39 Observed EOL fuel outer radii of the SiC clad annular pellet case . . . 131
4-40 Inner fuel pellet radius of the axial node with the BOL peak LHGR for the SiC clad annular pellet case . . . 132
4-41 Observed EOL fuel inner radii of the SiC clad annular pellet case . . . 133
4-42 Comparison of FRAPCON-EP and FRAPCON-3.3 EOL fuel outer radii with and without the addition of FRASP's predicted inner surface displacement for the SiC clad annular pellet case . . . 134
4-43 Comparison of initial and uprated average fuel rod power histories . . . 136
4-44 Comparison of the burnup between the solid and uprated annular pellet cases with the FRAPCON-EP's last point of expected cladding survival marked . . . 137
4-45 Cladding hoop strain at EOL of the uprated case . . . 138
4-46 Comparison of FRAPCON-EP and FRAPCON-3.3 EOL fuel outer radii with and without the addition of FRASP's predicted inner surface displacement for the uprated case . . . 139
4-47 Maximum interfacial pressure throughout the lifetime of the uprated case . . . 140
4-48 Interfacial pressure observed at EOL of the uprated case . . . 140

List of Tables

3.1 **Fuel rod parameters for the preliminary validation of FRASP** 71
3.2 **Reactor conditions for the preliminary validation of FRASP** 72

4.1 **Current Seabrook core conditions** 93
4.2 **Description of cases to be analyzed** 93
4.3 **Solid pellet fuel rod parameters** 102
4.4 **10% Uprated Seabrook core conditions** 135

Nomenclature

$\dot{\epsilon^c}$	Creep strain rate
$\dot{Q}_{core}$	Total core power
ϵ^*	Equivalent strain
ϵ^{Perm}	Permanent strain
ϵ^{Reloc}	Relocation strain
ϵ^S	Swelling strain
ϵ^{ThEx}	Thermal expansion strain
ϵ_θ	Hoop strain
ϵ_{Ave}	Area averaged strain
ϵ_r	Radial strain
$\epsilon_{z,cont}$	Axial strain at onset of PCMI
ϵ_z	Axial strain
ν	Poisson's Ratio
Φ	Fast neutron fluence
σ^*	Equivalent stress
σ_θ	Hoop stress
σ_{Ave}	Area averaged stress
σ_r	Radial stress
$\sigma_{ultimate}$	Ultimate stress
σ_{yield}	Yield stress
σ_z	Axial stress

BU_{Core} Core average burnup

F_{Ext} External force

F_{Fric} Friction force

F_{weight} Weight force

MW_t Mega-Watt thermal

N_{crack} Number of cracks

P_{cool} Coolant pressure

P_{plenum} Plenum pressure

r^{As-fab} As-fabricated radius

r_{ci} Cladding inner radius

r_{co} Cladding outer radius

r_{fo} Fuel outer radius

r_{void} Fuel inner void radius

UO_2 Uranium Oxide

V_{gap} Fuel-cladding gap gas volume

V_{inter} Inter-pellet gas volume

V_{plenum} Plenum gas volume

V_{total} Total gas volume

A Area

BOL Beginning-of-Life

BWR Boiling Water Reactor

E Young's Modulus

EFPD Effective Full Power Days

EOL End-of-Life

FEA Finite Element Analysis

FGR Fission Gas Release

FRACAS-I FRAPCON-3 mechanical model

FRACAS-I FRAPCON-3 mechanical model

FRAPCON Steady-state single rod fuel performance code

FRAPCON Steady-state single rod fuel performance code

FRAPCON-EP FRAPCON for Enhanced Performance

FRAPTRAN Fuel Rod Analysis Program Transient

FRASP FRAPCON Radial-Axial Soft Pellet

ft foot

K Kelvin

k Thermal conductivity

kgU Kilograms of uranium

kW Kilo-Watt

LHGR Linear Heat Generation Rate

LOCA Loss of Coolant Accident

LWR Light Water Reactor

m Meter

min Minute

MOL Middle-of-Life

MOX Mixed oxide fuel

MPa Mega-Pascals

MPS Missing Pellet Surface

MWd Mega-Watt days

N Number of radial nodes

n Moles of gas

NRC Nuclear Regulatory Commission

PCI Pellet Cladding Interaction

PCI Pellet Cladding Interaction

PCMI Pellet Cladding Mechanical Interaction

PWR Pressurized Water Reactor

q' Linear heat generation rate

q"' Volumetric heat generation rate

R Universal gas constant

RBWR Reduced moderation Boiling Water Reactor

SCC Stress Corrosion Cracking

SiC Silicon Carbide

T Temperature

t Time

u Radial displacement

Chapter 1

Introduction

1.1 Background

During the course of any reactor operation, the primary safety goal is to prevent the release of radioactive material to the environment. From the perspective of non-accident reactor management, this goal is accomplished by maintaining the integrity of both the fuel pellet matrix and fuel rod cladding, therein permanently capturing the radioactive products of nuclear fission within the fuel rod itself. In order to insure fuel pins stay within acceptable margins of safety during operations, fuel performance codes have been developed to analyze the behavior of individual fuel rods throughout their lifetime producing power within the reactor.

1.1.1 LWR Fuel Rod Design

All 104 commercial reactors in the United States are Light Water Reactors (LWRs) of either of two designs, the Pressurized Water Reactor (PWR) and the Boiling Water Reactor (BWR). Both reactor designs utilize light water as both the neutron moderator and the coolant for cylindrical fuel rods with similar fuel and cladding materials. The base component of both reactor designs is the nuclear fuel rod, which is grouped into square assemblies that are positioned to create a roughly cylindrical reactor core. While the specific fuel rod design parameters, e.g. pellet dimensions, cladding thick-

ness, gap size, cladding material, etc., have varied greatly since the first commercial reactors were built in the 1950's, all have made use of cylindrical pellets containing enriched uranium sheathed within a metallic tube which is then charged with inert gas and sealed (Lustman, 1981).

The current US nuclear fleet makes use of ceramic uranium oxide (UO_2) clad in Zircaloy, a zirconium based metallic alloy, with a long and successful operating history (Lustman, 1981). Current fuel pellet designs have evolved from simple cylinders to include dished ends, to mitigate uneven thermal expansion, as well as chamfered edges, to alleviate Pellet-Cladding Mechanical Interaction (PCMI). Likewise, the specific alloying components and material processing of Zircaloy have changed since its initial implementation to improve general performance.

Thanks in large part to improved fuel design, manufacturing techniques, and operational management, fuel rod failures in modern LWRs fall well below 10 failures per 100,000 rods and are experiencing generally decreasing trends, both domestically and overseas, and for both PWRs and BWRs (Rusch, 2008; Dangouleme et al., 2010). While this is a success rate greater than 99.99%, the fact that each core is comprised of ~50,000 fuel rods (Seabrook, 2007) causes this low failure rate to translate to a number of fuel rod failures per operational core. Because reactors are operated on relatively long cycles, typically 18 months between reloads, every individual failed fuel rod, which may dictate modified operation or potentially core shutdown, is viewed by reactors operators to be very expensive. This economic incentive to prevent fuel failures largely drives the continued improvements in both fuel rod design and simulation.

1.1.2 Pellet-Cladding Interaction (PCI)

During the course of irradiation in the reactor, the initial fuel-cladding gap eventually closes, bringing the two components of the fuel rod into contact with one another. This closure is driven by two mechanisms: (1) the creep down of the cladding material, caused by the pressure gradient between the reactor coolant and the fuel rod internal gas pressures, and (2) the swelling of the fuel pellet, caused by the accu-

mulation of fission products and radiation damage. While PCI is traditionally used as an umbrella term for any interaction between the fuel pellet's outer surface and cladding's inner surface, PCMI specifically describes only the structural behavior of the fuel pellet and cladding once they come in direct contact.

In current reactor operation, PCI accounts for approximately 1% and 19% of total fuel rod failures in PWRs and BWRs, respectively (Rusch, 2008). The failure of fuel rods via PCI tends to be more prevalent in BWRs due to the more dramatic power shifting associated with their operation, though the addition of an inner cladding liner of pure zirconium has been adopted to help mitigate this issue (Knief, 1992). While it is not the dominant failure mode for either reactor type, the prevention of PCI related failures is still relevant to the nuclear industry.

Fuel rod failures associated with PCI are generally segregated into two categories, classical PCI and non-classical PCI. Classical PCI failure is classified as a combined combined chemical and mechanical process, e.g. iodine assisted Stress Corrosion Cracking (SCC), and non-classical PCI is classified as being purely mechanical, e.g. Missing Pellet Surfaces (MPSs).

The onset of PCI generally leads to tensile stresses being applied to the cladding as it is deformed to accommodate the growth of the fuel pellet associated with irradiation swelling. These tensile stresses in association with the presence of corrosive iodine, a fission product released from the fuel pellet, leads to SCC of the cladding, and ultimately classical PCI fuel failure. Because fuel pellet cracking accelerates the the release of iodine from the fuel matrix and acts as a stress concentrator on the inner surface of the cladding, SCC tends to occur on the cladding surface directly adjacent to fuel cracks.

Non-classical PCI fuel failures typically result from the mechanical failure of the cladding due to the concentration of interfacial stresses associated with the deviation of the fuel pellet from a purely cylindrical shape. These deviations include the hour-glassing and cracking of the fuel pellet during normal reactor operations and the potential for MPSs, shown in Figure 1-1. Because non-classical PCI fuel failures are the result of highly localized stresses, limited to the size of a single fuel pellet,

and stochastic behavior, like cracking, their characterization has historically been challenging. Currently, models are being developed to better predict this behavior with advanced Finite Element Analysis (FEA) on increasingly fine scales (Williamson et al., 2012; Thourvenin et al., 2007; Sercombe et al., 2012).

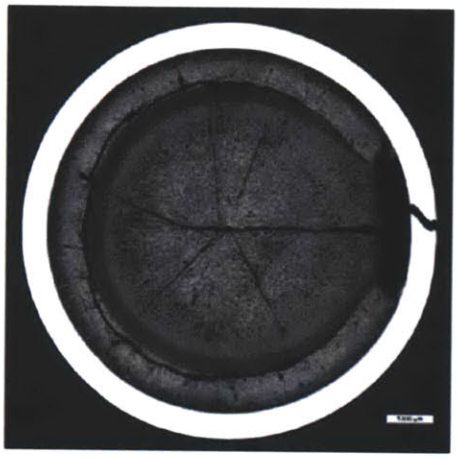

Figure 1-1: **Picture of cladding failure due to a MPS (Williamson et al., 2012)**

Because of these known failure mechanisms, the cladding strain of individual fuel rods, typically resulting from PCMI, is applied as a limiting criterion for reactor operation. Cladding hoop strain greater than 1% is not permitted in US commercial reactors due to concerns associated with PCI failure and to assure appropriate safety margin in accident scenarios (NRC, 2007).

1.2 Nuclear Fuel Rod Simulation

Ultimately, all nuclear reactor simulations are performed to ensure that the operations of the reactor do not threaten the integrity of the fuel rod and other radiation barriers. Fuel rod simulation is the application of known operational parameters acting on the fuel rod, like the Linear Heat Generation Rate (LHGR), neutron flux, cladding surface temperature, etc., to the individual components of the fuel rod and determining the resulting behavior. Due to the complexity of modeling their behavior

and lack of direct interaction with one another, nuclear fuel rods are simulated on an individual basis.

In simulating nuclear fuel rod behavior, three general aspects have to be considered: thermal, mechanical, and chemical. Thermally, the temperature profiles of the cladding and fuel pellets are dependent on both mechanical and chemical effects, such as the size of the fuel-cladding gap and buildup of cladding oxidation. The structural state of the fuel rod is also dependent on thermal and chemical effects, such as thermal expansion and material property changes. Many chemical effects, like Fission Gas Release (FGR) and SCC, are also driven by the thermal and mechanical state of the fuel rod, like temperature gradients and cladding stress. The complexity of nuclear fuel rod simulation is exemplified in Figure 1-2.

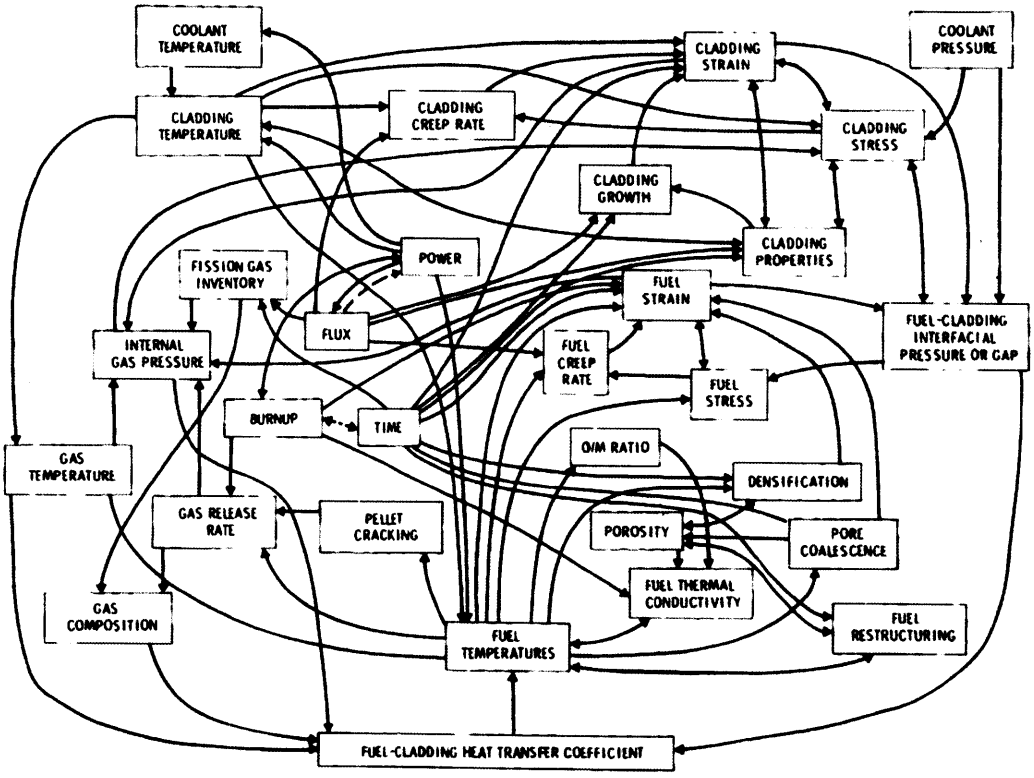

Figure 1-2: **Typical fuel pin parameters that influence fuel-cladding heat transfer coefficient (Beyer et al., 1975)**

Because of the complexity of modeling the coupled behavior of nuclear fuel rods, solutions are typically found by decoupling the individual models. The solutions from these decoupled models then act as parameters for finding the solutions to other decoupled models. This level of separation then dictates some form of iteration to guarantee that all of the individual models provide one another with correct parameters. This complexity introduces the possibility of compounding feedback effects which often result in widely varying predictions from various fuel performance codes for identical cases (Herranz et al., 2011).

1.2.1 FRAPCON-3 Fuel Performance Code

Because individual fuel rod parameters are used as criteria for the regulation of commercial reactors, the US Nuclear Regulatory Commission (NRC) developed and benchmarked the FRAPCON-3 steady-state single rod fuel performance code, written in FORTRAN, to provide the agency with its own nuclear fuel rod simulation capabilities. The most recent version of the code, FRAPCON-3.4, was released in April, 2010 and is the latest in the evolution of NRC-sponsored fuel performance codes (Geelhood et al., 2010). For the analysis of rapid transients, the NRC sponsored the development of a separate fuel performance code, FRAPTRAN, which uses FRAPCON-3 to provide initial conditions for analysis.

As it has been developed specifically for the simulation and regulation of current commercial LWRs, FRAPCON-3 has been constructed to simulate only UO_2 fuel clad in Zircaloy, of varying types, under well-characterized neutron energy spectrums characteristic of thermal reactors. This well defined design space does have the advantage of the long operating history associated with these specific conditions, as well as having a considerable amount of experimental data to support it. As a result, FRAPCON-3 relies heavily on engineering-scale correlations to describe the behavior of individual models, such as fuel swelling or cladding oxidation. FRAPCON-3 has also been heavily validated and benchmarked for these conditions (Lanning et al., 1997). Because of its role in the regulation of US commercial reactors, FRAPCON-3 has been purposefully constructed to provide conservative fuel performance solutions.

As is common with fuel performance codes, FRAPCON-3 separates the solution of individual fuel rod behaviors into independent models which are then arranged into an iterative scheme to provide information to one another and allow for feedback effects. For each time step, FRAPCON-3 iterates to converge on solutions for two parameters: the fuel-cladding gap temperature difference and the gas pressure within the rod. Thermal and mechanical calculations are performed in order to iterate on the temperature drop across the fuel-cladding gap for each axial node along the height of fuel rod, which then provides the information needed for iterating on the gas pressure in the fuel rod. All of these iterative processes are then repeated for each time step through the duration of the fuel rod's irradiation. All of these iterations are performed using a quasi-steady-state assumption, i.e. using constant conditions for each time step. A simplified flowchart of FRAPCON-3's iterative process is illustrated in Figure 1-3.

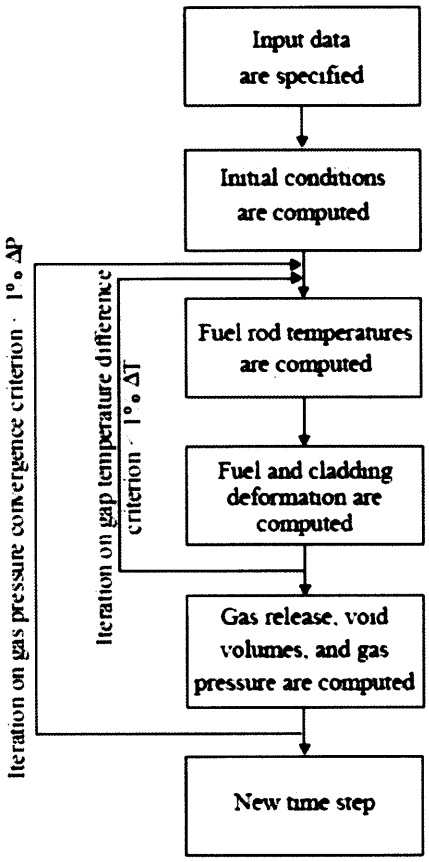

Figure 1-3: **Simplified FRAPCON-3 flowchart (Berna et al., 1997)**

1.2.2 FRACAS-I Mechanical Model

At the heart of FRAPCON-3 is the FRACAS-I mechanical model, which is used to find the structural state of the cladding throughout the lifetime of the fuel rod. For finding the size of the fuel-cladding gap, necessary to find the associated temperature difference, FRACAS-I is used to calculate the steady-state cladding deformation. Between the steady-state fuel performance calculations, FRACAS-I is also used to calculate the transient cladding creep.

Due to a diameter to thickness ratio of approximately 20 or greater for the cladding of nuclear fuel rods, FRACAS-I is able to apply the thin shell approximation to solve for the structural mechanics of the cladding. The use of the thin shell model provides

FRACAS-I with a rather straight forward set of governing equations which can be solved quickly and accurately using simple linear algebra. This speed is critical to FRAPCON-3's performance, as cladding deformation plays a fundamental role in determining the fuel-cladding temperature drop needed for the iteration processes.

Less appropriate than FRACAS-I's use of the thin shell approximation, however, is the assumption driving its treatment of PCMI, the rigid pellet model. Should FRAPCON-3 determine that the fuel pellet and cladding are in contact with one another, the rigid pellet model implies that the fuel pellet is not deformable via feedback from the cladding and the interfacial radius is determined entirely by the outer fuel pellet radius. Under these conditions, FRACAS-I uses the thin shell model to infer the structural state of the cladding based on the deformation dictated by the growth of the fuel pellet.

While FRACPON-3 utilizes FRACAS-I to calculate all cladding deformations via the thin shell model, the fuel pellet dimensions are found using a much simpler methodology. Rather than applying any form of structural mechanics, fuel strains are simply added to the original nodal lengths and thicknesses, as shown in Equation 1.1, which are then used to find the total deformations, without any consideration of stresses within the fuel pellet. Due to the empirical nature of the models dictating fuel growth strains within FRAPCON-3, this method is generally appropriate. However, under PCMI conditions the possibility of stress-induced fuel pellet deformation is wholly neglected.

$$L = L_0 \times \left(1 + \sum \epsilon_i\right) \tag{1.1}$$

Along with updated models, FRAPCON-3.4 also included an option to use a newly incorporated FEA model(Geelhood et al., 2010). However, limited information is available on the workings of this new model and FRACAS-I is still considered the primary mechanical model within FRAPCON-3.4.

1.2.3 FRAPCON-EP Fuel Performance Code

In the analyses of fuel rod designs for advanced reactor concepts, like the Reduced moderation Boiling Water Reactor (RBWR), many of the conditions assumed by FRAPCON-3, including maximum burnup, fuel temperature, and neutron spectrum, were found to lie beyond the range of the empirical models developed for traditional LWR operation (Lerch, 2010; Karahan et al., 2011). The need for fuel performance analysis of these innovative designs resulted in the development of a new version of the code, named FRAPCON Enhanced Performance (EP). The primary goal of FRAPCON-EP is to apply more mechanistic models to the previously empirical relations used by FRAPCON-3. By adopting these new models, FRAPCON-EP is intended to provide reactor designers with a more versatile fuel performance code that allows for the simulation of innovative reactor designs extending beyond the scope of current LWRs, allowing for temperatures and burnups up to 2500K and 100 MWd/kgU.

As the initial development of FRAPCON-EP predates the release of FRAPCON-3.4, it is based on modifications to the structure of FRAPCON-3.3, including its use of FRACAS-I. To date, these modifications have been limited to the fuel pellet behavior, but the models associated with the cladding are identical to those of FRAPCON-3.3. These EP modifications include (Lerch, 2010):

- New thermal conductivity for $UO_2$and mixed oxide (MOX)
- New swelling model
- Modified fission gas release model
- Accounting for oxygen to metal ratio effects with burnup
- Axial cesium migration

While all of the modified models affect the fuel rod simulation, the new swelling model has the most effect on the behavior of the fuel rod. As opposed to the old swelling model of FRAPCON-3, which is linear and only dependent on the burnup (Luscher

and Geelhood, 2011), the new swelling model in FRAPCON-EP is separated into three components, solid fission product swelling, fission gas swelling, and RIM porosity swelling. These new models account for fuel temperature effects and interfacial pressure in addition to the burnup. By accounting for these additional parameters the new model better accounts for fuel pellet swelling, especially at high temperatures (>1500K) (Karahan et al., 2010).

1.3 Need for an Improved Mechanical Model within FRAPCON

For the simulation of normal LWR operation, the assumptions of FRACAS-I are not unreasonable and their use does not hinder the general accuracy of FRAPCON-3's predictions. However, situations and designs exist which challenge the validity of these assumptions. In an effort to allow FRAPCON-EP to better model fuel rod structural behavior under these challenging conditions, the FRAPCON Radial-Axial Soft Pellet (FRASP) model has been developed.

The rigid pellet model used by FRACAS-I in FRAPCON-3 has been shown to provide overly conservative solutions for the cladding strain under PCI conditions (Geelhood et al., 2010). This is largely due to the lack of structural feedback between the fuel pellet and cladding when the two are in contact. Because fuel rods may spend the majority of their operational lifetime experiencing PCI (fuel-cladding gap closure can occur within the first 70 days of a total residency time of approximately 1500 days in a PWR), as well as its importance in predicting fuel rod failure, the conservatism of the rigid pellet model can limit the design space for the development of new fuel rods.

Congruent with the philosophy dictating FRAPCON-3's development, the rigid pellet model utilized in FRACAS-I's evaluation of cladding deformation consistently provides conservative estimates of fuel rod structural behavior. The development of FRASP is intended to alleviate some of this conservatism by adopting new models

which remove some of the underlying assumptions of FRACAS-I. By making use of 1.5D structural mechanics for both the fuel pellet and cladding and coupling the mechanical interaction of both components, FRASP is dismissing the previously used rigid pellet and thin shell models. The development of FRASP is aimed specifically to address previous concerns associated with FRACAS-I's treatment of PCMI for three specific situations: power ramping, the use of silicon carbide (SiC) cladding, and high (>1%) cladding strain in high burnup reactor designs.

Power ramping, defined by relatively large increases in local power over relatively short time periods, results in very large cladding stresses and deformations which create a desire for an improved mechanical model. While not fast enough to warrant a transient analysis, ramps are typically on the order of 6-10 kW/m/min (Massih et al., 2005). The fuel pellet thermal expansion associated with power ramps leads to large cladding stresses and, in some cases, cladding failure. Because BWRs are controlled using the movement of control blades, power ramping, in a very localized sense, may be experienced during reactor start up and operation. This localized power ramping partially accounts for the high PCI related fuel rod failures observed in BWRs. As failures caused by power ramping are driven by PCMI behavior, better characterization of the feedback between the fuel pellet and cladding would be very valuable for BWR operations.

Because of interest in replacing Zircaloy with ceramic SiC cladding in current LWRs, previous studies have focused on characterizing SiC clad fuel rod behavior with FRAPCON-3.3 (Carpenter, 2006). Because of the brittle nature of SiC, cladding deformations dictated by the rigid pellet model have resulted in the prediction of cladding failure immediately upon the onset of PCMI. However, this use of the rigid pellet model fails to account for any stress-induced pellet deformation which may allow for a period of PCMI prior to brittle fracture of the cladding.

Lastly, the analysis of some innovative new reactor designs have resulted in the prediction of cladding strains significantly higher than the NRC regulatory limit of 1%, due to the high burnup levels they may experience (Karahan et al., 2011). While these reactor designs intend to use innovative fuel materials, they currently make use of

existing Zircaloy cladding, which validates the use of LWR cladding limits. While high strain rates are still likely to be predicted, the incorporation of FRASP is expected to provide fuel designers with more reliable results than FRACAS-I, especially at very high burnups.

1.4 Objectives and Scope

The objective of this work is to incorporate a new mechanical model, FRASP, into FRAPCON-EP to allow for improved analysis of PCMI than is currently achievable with the FRACAS-I model. The development of FRASP aims to apply an annular 1.5D structural mechanics model to both the fuel pellet and cladding. This new model has been written in FORTRAN and developed to be incorporated directly into the structure of FRAPCON-3, utilizing parameters from, and providing information to, existing models.

Preliminary validation of FRASP has been performed by comparing the performance of the modified and unaltered versions of FRAPCON-3.3. While this is not a rigorous validation against experimental findings, it does allow for the quantification of potential effects associated with upgrading the code's mechanical model. Because of the highly coupled nature of fuel rod simulation, this form of validation also allows for the observation of feedback effects on the non-mechanical parameters which may result.

Finally, FRAPCON-EP, complete with FRASP and SiC cladding material properties, has been used to evaluate innovative new fuel rod designs for a PWR. These evaluations are compared to a version of FRAPCON-3.3 which has previously been modified to simulate SiC clad fuel rods. These evaluations demonstrate that while existing versions of FRAPCON-3 can easily be modified to evaluate new fuel rod designs, their emphasis on modeling existing LWR fuel rods hinders their ability to accurately predict the behavior of new designs.

Chapter 2

Model Development

The objective of developing FRASP is to model the behavior of the fuel rod using quasi-steady-state, 1.5D cylindrical structural mechanics. Interfacial pressure and axial friction will be used to couple the behavior of the fuel pellet and cladding under PCMI conditions. This requires models for elastic as well as plastic behavior, fuel cracking, creep behavior, and the application of interfacial coupling forces. The use of these new models marks a dramatic departure from the previous treatment of the structural state of the fuel rod in FRAPCON and requires the complete replacement of the FRACAS-I model.

While FRASP has been developed with the primary intention of incorporation in FRAPCON-EP, it has been constructed to be capable of operating within any version of FRAPCON-3. This is the result of the fact that all versions of FRAPCON-3 make use of the same general code structure, with the differentiation between versions being generally limited to modifications to the individual models.

2.1 Model Assumptions of FRASP

Both the pellet and cladding are assumed to be axisymmetric not only by FRASP, but FRAPCON in general. Local power levels are based on a 1D axial peaking profile provided by the user and 1D radial power profiles calculated within FRAPCON. Cladding surface temperatures are also calculated, or input by the user, assuming no

azimuthal variation in temperature. For these reasons, temperatures throughout the fuel pin are assumed to be azimuthally uniform. Since FRASP does not explicitly model discrete cracks and no temperature gradient exists azimuthally, no pertinent structural information could be gained by dismissing the axisymmetric assumption. FRASP is not considered to be fully 2D, however, due to its treatment of axial strain. At each axial position of a given cylinder, fuel or cladding, the axial strain is calculated via an axial force balance and applied uniformly across the entire material area. This methodology has been previously applied with good results in other fuel performance codes, such as LIFE and FEAST (Karahan, 2009; Olander, 1976).

For time dependent calculations, e.g. creep, FRASP applies a quasi-static-state assumption. This approach first finds the time independent structural state of the fuel pellet and cladding. This structural state is then used to evaluate the appropriate transient strain rates, which are assumed to be constant throughout the interval between time steps. Using this assumption, the differential strains are found and applied to finding the steady-state behavior of the next time step. By adopting a quasi-steady-state model, FRASP is able to capture time dependent effects using steady-state structural mechanics.

The fuel pellet and cladding are modeled separately by FRASP as two concentric annular cylinders. These cylinders are each segmented axially and radially into rings, which are treated numerically as individual nodes, as illustrated in Figure 2-1. In performing its structural state calculations, FRASP treats each axial node as an individual cylindrical section; and coupling the behavior of multiple axial nodes is accomplished via axial force communication. For its nodalization of the fuel rod, FRASP utilizes the axial and radial segmentation for fuel stack and the axial segmentation for the cladding which previously exist from the initialization of FRAPCON's main structure.

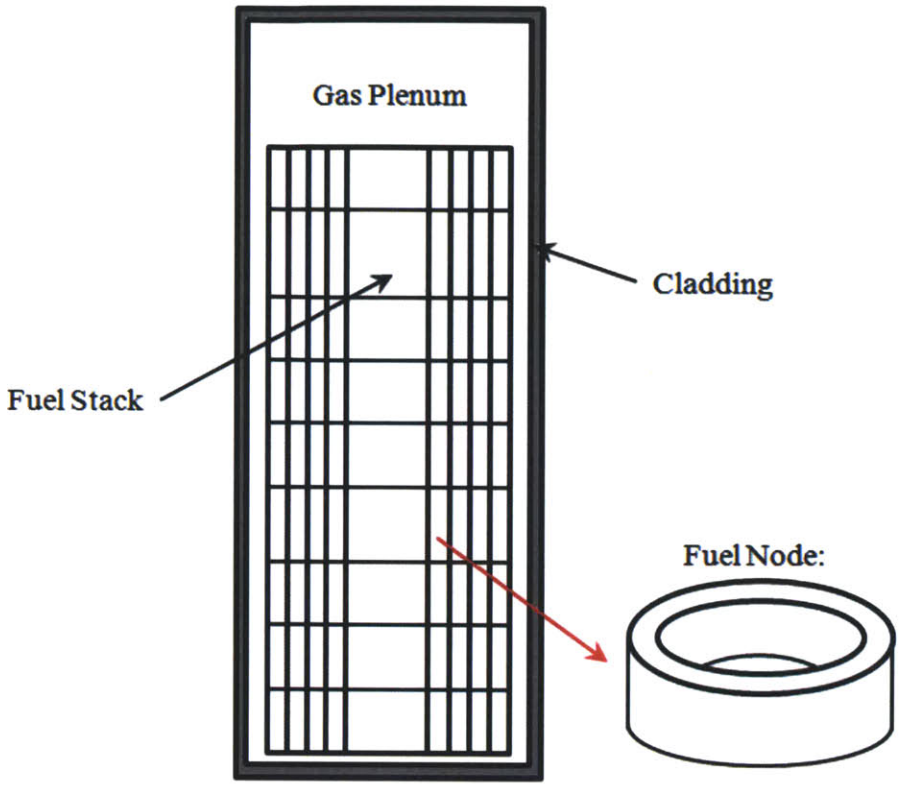

Figure 2-1: **Illustration of fuel rod nodalization applied by FRAPCON-3**

It is worth noting that the mechanical model of the fuel pellet uses FRAPCON's thermal nodalization rather than that utilized for fission gas release. This is due to the fact that FRAPCON calculates fuel temperature, swelling, thermal expansion, and densification based on the thermal nodalization, eliminating the need for FRASP to replicate the calculations. For cladding structural mechanics calculations within FRAPCON, FRACAS-I treats the cladding as radially uniform. While FRASP is capable of being run with any number of radial nodes in the cladding, these studies utilize four radial nodes. Sensitivity studies revealed FRASP to be insensitive to the use of any more than four radial nodes.

Within FRASP, each node is assumed to be homogeneous with regard to its material properties and structural state. The material properties are based nodal average temperature and conditions. This is in conflict with FRAPCON's thermal model, which calculates only temperatures at the fuel node boundaries and cladding surfaces.

Within the fuel, FRASP uses the arithmetic mean of the node boundary temperatures, as in Equation 2.2, rather than calculating the true area averaged temperature of the node using Equations 2.1 and 2.3(Todreas and Kazimi, 1990). Likewise, the cladding node temperatures are also calculated using Equation 2.2 rather than the more formal solution using Equations 2.4 and 2.1(Todreas and Kazimi, 1990).

$$T_{i,Ave} = \frac{\int_{A_i} T(r)dA}{\int_{A_i} dA} = \frac{\int_{r_i}^{r_{i+1}} T(r)rdr}{\int_{r_i}^{r_{i+1}} rdr} \tag{2.1}$$

$$T_{i,Ave} \approx \frac{T_i + T_{i+1}}{2} \tag{2.2}$$

$$\left(\frac{1}{r}\right)\frac{d}{dr}\left[k_{fuel}(r)\frac{dT_{fuel}}{dr}\right] + q'''(r) = 0 \tag{2.3}$$

$$T_{clad}(r) = \frac{q'}{2\pi k_{clad}} ln\left(\frac{r_o}{r}\right) + T_o \tag{2.4}$$

By using these assumptions with temperatures provided by FRAPCON, there is no need for FRASP to directly perform any thermal calculations. For the purposes of FRASP's implementation into FRAPCON, this simplified the amount of information that needs to be incorporated and increased the speed with which it is processed. The relatively small error associated with these assumptions is illustrated in Figures 2-2, and 2-3 for typical radial temperature profiles for the fuel pellet and cladding.

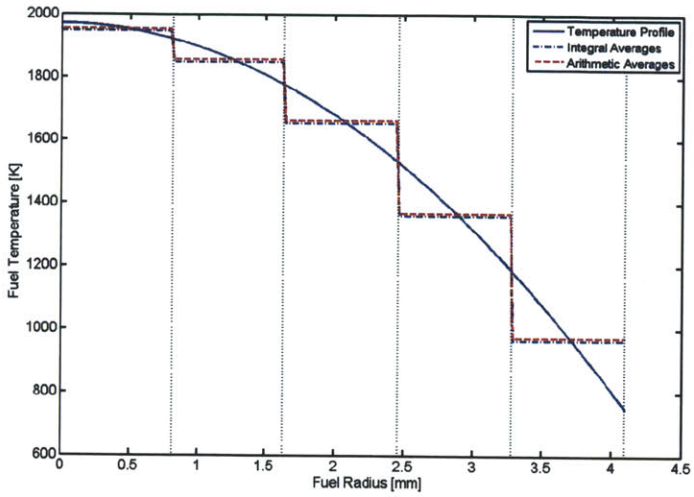

Figure 2-2: Comparison of the arithmetic and integral averaged fuel pellet temperatures

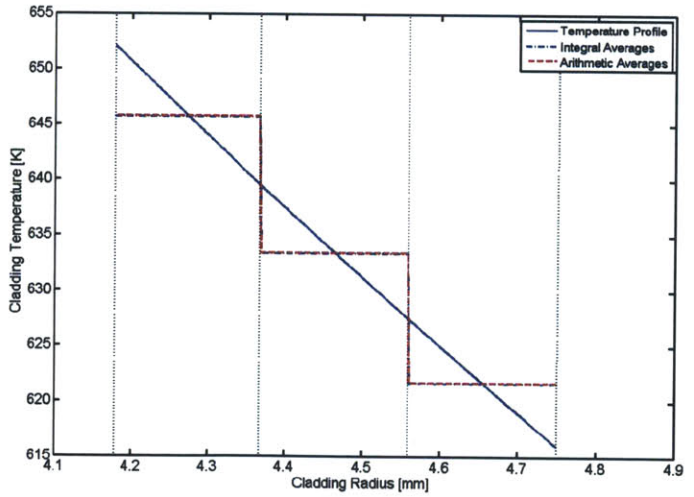

Figure 2-3: Comparison of the arithmetic and integral averaged cladding temperatures

2.2 Steady State Behavior

Under steady-state conditions, FRASP applies thermal expansion, swelling and permanent strains to find the radial, hoop, and azimuthal stresses within each node by using Equations 2.5, 2.6, and 2.7. The radial strain is assumed to be equal to the radially differentiated radial displacement and the hoop strain is equal to the radial displacement divided by the radius, as shown in Equations 2.8 and 2.9. Using these definitions allows for the stresses to be related directly to the radial displacement. Unlike the radial and hoop strains, the axial strain is based on an axial force balance and requires an iterative process, as discussed later. By convention, negative stresses are compressive, while positive values indicate tension.

$$\sigma_r = \frac{E}{1+\nu}\left[\epsilon_r + \frac{\nu}{1+2\nu}\left(\epsilon_r + \epsilon_\theta + \epsilon_z - \sum_{m=r,\theta,z}\left[\epsilon_m^{ThEx} + \epsilon_m^{S}\right]\right) - \left(\epsilon_r^{ThEx} + \epsilon_r^{S} + \epsilon_r^{Perm}\right)\right] \tag{2.5}$$

$$\sigma_\theta = \frac{E}{1+\nu}\left[\epsilon_\theta + \frac{\nu}{1+2\nu}\left(\epsilon_r + \epsilon_\theta + \epsilon_z - \sum_{m=r,\theta,z}\left[\epsilon_m^{ThEx} + \epsilon_m^{S}\right]\right) - \left(\epsilon_\theta^{ThEx} + \epsilon_\theta^{S} + \epsilon_\theta^{Perm}\right)\right] \tag{2.6}$$

$$\sigma_z = \frac{E}{1+\nu}\left[\epsilon_z + \frac{\nu}{1+2\nu}\left(\epsilon_r + \epsilon_\theta + \epsilon_z - \sum_{m=r,\theta,z}\left[\epsilon_m^{ThEx} + \epsilon_m^{S}\right]\right) - \left(\epsilon_z^{ThEx} + \epsilon_z^{S} + \epsilon_z^{Perm}\right)\right] \tag{2.7}$$

$$\epsilon_r = \frac{du}{dr} \tag{2.8}$$

$$\epsilon_\theta = \frac{u}{r} \tag{2.9}$$

The axisymmetric radial deformation, Equation 2.10, of each node is solved for in FRASP via finite difference, as shown in Equation 2.11. The integration constants of

each node, C_{1i} and C_{2i}, are solved such that equal radial displacements and stresses are imposed at each internal node boundary. Compressive radial stresses, to match either gas, interfacial, or coolant pressure, are applied to the internal and external faces of each annular cylinder as boundary conditions. The integration constants can be found by combining the boundary conditions, Equation 2.12, with the displacement and radial stress equations, Equations 2.11 and 2.5, thereby allowing for the calculation of the cylinder's structural state. It should be noted that the inner and outer radii of the cylinder are denoted as $r_{1,inner}$ and $r_{N,outer}$, where N is the total number of radial nodes. For numerical reasons, $r_{1,inner}$ cannot equal zero and is given a minimum value of 1μm.

$$\frac{d}{dr}\left[\frac{1}{r}\frac{d(ru)}{dr}\right] = \left(\frac{1-2\nu}{1-\nu}\right)\left(\frac{d\epsilon_r^{Perm}}{dr} + \frac{\epsilon_r^{Perm} - \epsilon_\theta^{Perm}}{r}\right) + \left(\frac{1+\nu}{1-\nu}\right)\frac{d}{dr}\left(\epsilon_r^{ThEx} + \epsilon_r^{S}\right) \tag{2.10}$$

$$u(r) = \frac{C_{1i}}{r} + C_{2i}r + \left(\frac{1+\nu}{1-\nu}\right)\left(\epsilon_r^{ThEx} + \epsilon_r^{S}\right)_i \frac{r^2 - r_{i-1}^2}{2r} + \frac{1}{2}\left(\frac{1-2\nu}{1-\nu}\right)\left[\left(\epsilon_r^{Perm} + \epsilon_\theta^{Perm}\right)_i \frac{r^2 - r_{i-1}^2}{2r} + \left(\epsilon_r^{Perm} + \epsilon_\theta^{Perm}\right)_i r ln\left(\frac{r}{r_{i-1}}\right)\right] \tag{2.11}$$

$$\begin{aligned} u\left(r_{i,outer}\right) &= u\left(r_{i+1,inner}\right),\ 1 < i < N-1 \\ \sigma_r\left(r_{i,outer}\right) &= \sigma_r\left(r_{i+1,inner}\right),\ 1 < i < N-1 \\ \sigma_r\left(r_{1,inner}\right) &= P_{Inner} \\ \sigma_r\left(r_{N,outer}\right) &= P_{Outer} \end{aligned} \tag{2.12}$$

The integration constants used in calculating the displacements of each radial node are solved using the secant method. This is accomplished, as shown in Equation 2.13, by treating the radial stress of the outer surface, for which a known value exists, a function of the internal surface pressure and one of the integration constants of the inner most node, in this case C_1. Initial and perturbed guesses for C_1 are then made

and used to find associated values for the external radial stress. These values are then used to linearly extrapolate a solution for the C_1 value which would satisfy the given boundary condition, shown in equations 2.14 and 2.15. The previous guess is then stored and the process is repeated until the external radial stress is found to have converged within an acceptable margin of the boundary condition, as demonstrated by Figure 2-4 (Atkinson and Han, 2004). The secant method is very robust for this application and is significantly faster than other suggested solution methods, like binomial search or power iteration.

$$\sigma_r\left(r_{N,outer}\right) = f\left(C_1,\, P_{inner}\right) = P_{Outer} \tag{2.13}$$

$$m = \frac{\sigma_r\left(C_1'\right) - \sigma_r\left(C_1\right)}{C_1' - C_1} \tag{2.14}$$

$$C_1' = \frac{P_{Outer} - \sigma_r\left(C_1\right)}{m} + C_1 \tag{2.15}$$

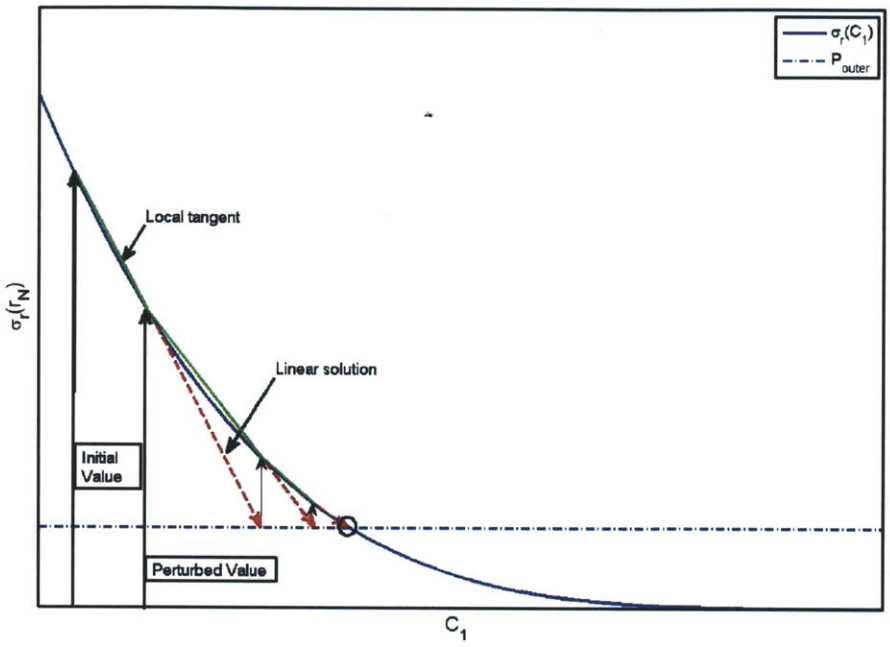

Figure 2-4: **Visualization of secant method iteration**

The axial strain used to calculate stresses is found for each cylindrical component based on an axial force balance. As the quasi-steady-state assumption used in FRASP requires the components to be at rest, all forces in the axial direction are required to have a net sum of zero. Within each annulus, the internal axial stresses act as a normal force against external forces. These external forces include the weight of the annular column, plenum pressure, coolant pressure, and interfacial friction, as shown in Equations 2.16 and 2.17. Figure 2-5 illustrates how plenum and coolant pressures are applied to the top of the fuel and cladding. Forces are only communicated downward through the annular columns, as the base is assumed to be the fixed support and the top of the rod is assumed to be unconstrained. The axial segmentation of the fuel pellets prevent tensile forces from being communicated downward through the fuel stack. However, because the cladding is comprised of one continuous tube, cladding tensile forces can be communicated downward. The interfacial axial friction component is used to couple the axial straining of the fuel and cladding during PCMI

and is applied equally to the fuel and cladding, as will be discussed in Section 2.6. By convention, positive external forces are compressive.

$$F_{Ext}^{fuel} = \pi \left(r_{fo}^2 - r_{void}^2 \right) P_{plenum} + \sum F_{fric} + \sum F_{weight}^{fuel} \tag{2.16}$$

$$F_{Ext}^{clad} = \pi r_{co}^2 P_{cool} - \pi r_{ci}^2 P_{plenum} - \sum F_{fric} + \sum F_{weight}^{clad} \tag{2.17}$$

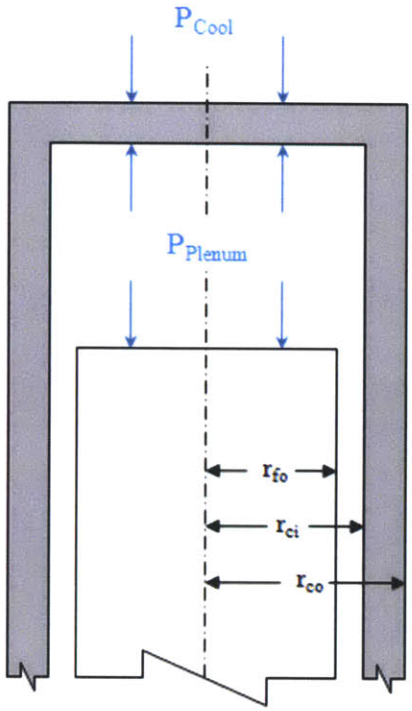

Figure 2-5: **Illustration of plenum and coolant pressure application**

All external forces are assumed to be applied uniformly across the annulus, while the axial stresses have been calculated at different radial locations, shown in Figure 2-6 for the fuel pellet. As such, the axial stresses are integrated over the cross sectional area of the annulus to achieve the force balance as shown in Equation 2.18. By assuming the axial strain to be radially constant and integrating via finite difference, the axial strain can be found.

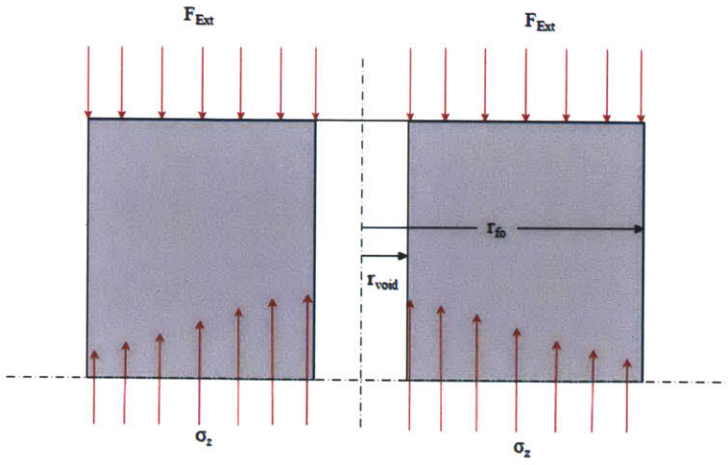

Figure 2-6: **Illustration of axial forces acting on the fuel pellet**

$$F_{Ext} = -2\pi \int_{r_{inner}}^{r_{outer}} \sigma_z(r)\, r dr \tag{2.18}$$

Because calculating the axial strain requires components, such as the radial and hoop strains which are intrinsically dependent on the axial strain, FRASP is required to iterate to find it. This is accomplished by applying a simple power iteration scheme which uses an initial strain guess and iterates using previously found values until a satisfactory degree of convergence is achieved (Sjoden, 2009). For an initial guess, FRASP uses an area weighted average of the axial thermal expansion and growth strains, shown in Equation 2.19.

$$\epsilon_{z,o} = \frac{\int_A \left[\epsilon^{ThEx}(r) + \epsilon^S(r)\right] dA}{\int_A dA} \approx \frac{\sum \left(\epsilon_i^{ThEx} + \epsilon_i^S\right) \times \left(r_i^2 - r_{i-1}^2\right)}{\left(r_{N,outer}^2 - r_{1,inner}^2\right)} \tag{2.19}$$

2.3 Fuel Pellet Cracking

During reactor operation, the temperature gradient within the fuel pellet (see Figure 2-2) leads to radially non-uniform thermal expansion of the fuel pellet. The hotter internal regions of the fuel pellet experience more thermal expansion strain, placing tensile stresses on the external region the fuel and compressive stresses on the

internal region, as illustrated in Figure 2-7. Should these tensile stresses exceed the fracture stress of the fuel material, the fuel pellet will crack. Because the cladding is assumed to only experience fracture under conditions not applicable to the modeling limits of FRAPCON, FRASP does not account for cracking in the cladding.

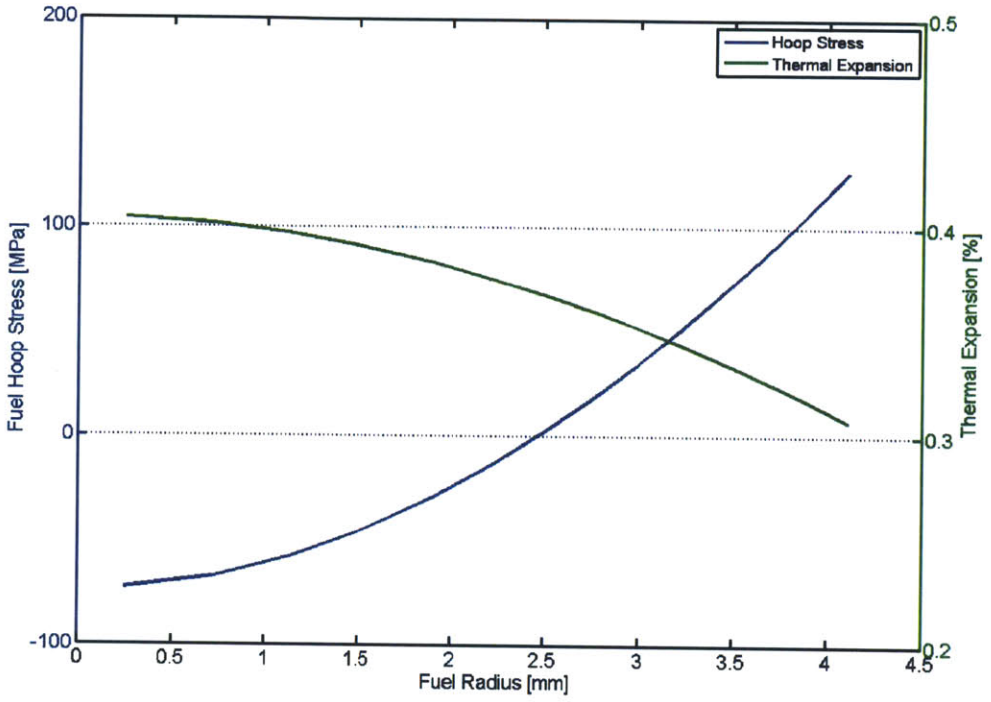

Figure 2-7: **Hoop stress within the fuel pellet resulting from thermal expansion**

Fuel cracking directly affects many aspects of fuel performance, including thermal conductivity, fission gas release, free gas volume, structural mechanics, etc (Bernaudat, 1995). Figure 2-8 shows a cracked fuel pellet cross section with radial and circumferential cracks. Axial cracks occur but have less impact on fuel mechanics because of the fuel stack is already axially segmented into individual pellets.

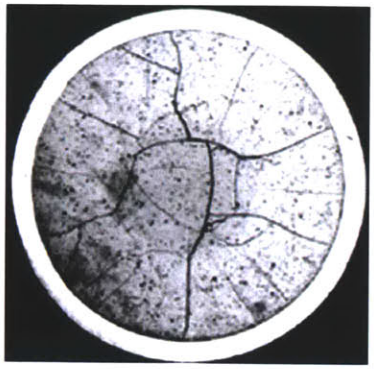

Figure 2-8: **Photograph of a cracked fuel pellet** (Marchal et al., 2009)

As the fuel pellet cracks, the fragments shift and relocate, introducing space into the pellet's interior. This shifting acts to effectively decrease the fuel–cladding gap. Because of this gap reduction, the relocation of the cracked pellet has important implications for fuel performance. For FRASP to capture this effect, an effective cracking relocation strain is utilized. Because this strain represents the physical space introduced into the pellet by cracking, rather than the size of solid elements, the relocation strain is not included in the stress and solid displacement calculations of FRASP. Rather, FRASP simply adds the relocation strain component onto the size of the fuel pellet after the calculated radial displacements have been applied. This is accomplished by adjusting the radial location of each individual node's outer boundary, as shown in Equation 2.20. As the application of the relocation strain is intended to only affect location of the outer boundary, it is applied uniformly to all radial boundaries.

$$r_{i,outer} = r_{i,outer}^{As-fab} + u\left(r_{i,outer}\right) + \epsilon^{Reloc}\left(r_{i,outer}^{As-fab} - r_{i,inner}^{As-fab}\right) \tag{2.20}$$

As can be observed from Figure 2-8, radial cracks within the pellet introduce non-uniformity along the azimuthal axis. This heterogeneity is in conflict with the axisymmetric assumption utilized by FRASP. Modeling each individual crack would be beyond the scope of a fast model's capabilities, as well as numerically unfeasible for the entire fuel stack. Therefore, in order to accommodate cracking behavior within the

structural behavior of the fuel pellet, FRASP utilizes the smeared cracking approach, which modifies the mechanical parameters based on cracking within each radial node. The effects of cracking on the Young's Modulus and Poisson Ratio can be calculated by Equations 2.21 and 2.22. (Jankus and R.W., 1972) The smeared cracking approach effectively causes the fuel to be modeled as being less stiff with each additional crack, thereby decreasing the stress within the cracked region.

$$E' = \left(\frac{2}{3}\right)^{N_{crack}} E \tag{2.21}$$

$$\nu' = \left(\frac{1}{2}\right)^{N_{crack}} \nu \tag{2.22}$$

The fuel material is assumed to be brittle below a threshold temperature, which is calculated by FRAPCON. At temperatures above this threshold, FRASP assumes that the fuel exhibits ductile behavior and does not crack. Below this transition temperature, the pellet is assumed to fracture and not experience plastic straining (Callister, 2007). Because only radial cracks affect the assumptions incorporated into FRASP, they are the only crack type assumed to occur in the smeared cracking model. It is assumed that the radial cracks are the result of the hoop stresses exceeding the fuel's fracture stress, perpendicular to the radial plane. As the compressive fracture stress is approximately an order of magnitude larger than the tensile fracture stress only tensile hoop stress is assumed to cause cracking (Olander, 1976).

To find the number of cracks in each nodal ring, FRASP begins by calculating the structural state of each node within the fuel pellet. The code then compares the hoop and fracture stresses of each node beginning at the first node exterior to the ductile-brittle transition radius. If the hoop stress is found to be greater than the fracture stress of the fuel, a crack is initiated and is extended radially from the initiating point through each node out to the external surface of the fuel pellet, as demonstrated in Equation 2.23. FRASP then recalculates the steady-state structural state of the pellet with updated mechanical properties and the process is repeated until no additional cracking occurs or the maximum number of cracks is reached.

$$\sigma_{\theta,i} > \sigma_{frac} \Rightarrow N'_{crack}(r \rightarrow r_{fo}) = N_{crack}(r \rightarrow r_{fo}) + 1 \tag{2.23}$$

A sensitivity study of large LHGRs showed that allowing high numbers of cracks led to non-physical crack effects manifesting in the form of fuel contraction. To prevent this non-physical behavior from occurring, a 10 crack limit was established. Because FRASP assumes that every crack, regardless of initiating point, results in a crack on the outermost node, no cracking is allowed anywhere in the fuel pellet after the outermost node reaches the crack limit. In lower power situations, limiting the number of allowed cracks has shown to have negligible effects on fuel performance results. Previous studies have shown that fuel pellets typically contain approximately eight radial cracks during typical reactor operations (Sercombe et al., 2012), lending an element of physicality to the limit of 10 cracks within FRASP. While fuel pellets have been shown to experience increased cracking during power ramps (Sercombe et al., 2012), these effects tend to result in non-physical behavior within FRASP and are thus ignored.

If the stresses between pellet fragments are compressive and the temperature is sufficiently high, cracks in the fuel pellet have been observed to be partially removed from the fuel pellet via crack healing (Olander, 1976). This process of healing is largely the result of the thermal diffusion of material between the fragments. However, because crack healing is highly dependent on the temperature of the fuel material, it tends to be limited to within a certain radius. As the radial cracks then all extend to the same radius, this leads to circumferential pellet cracking by "bridging" the interior points of the radial cracks (Bernaudat, 1995), as shown in Figure 2-9. Due to the level of uncertainty associated with the implementation of crack healing, the occurrence of this phenomena is currently neglected by FRASP.

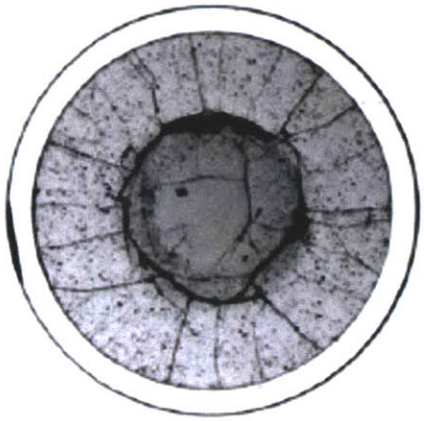

Figure 2-9: **Photograph of a fuel pellet which has experienced crack healing (Sercombe et al., 2012)**

2.4 Inelastic Behavior

Unlike the brittle fuel pellet, the cladding, which is assumed to be a ductile metal, is not expected to experience fracture during normal operations, though it will experience inelastic behavior. While the fuel can behave similarly at elevated temperatures, the effects of fuel inelastic behavior are expected to be minimal and are thus neglected by FRASP. Permanent, i.e. inelastic and unrecoverable, straining of the cladding can be the consequence of either instantaneous plastic strain due to elastically exceeding the yield stress or creep strain acting to relieve stress of periods of time. These permanent strains are calculated by FRASP and applied to the mechanical calculations, which to this point have only been elastic in nature.

2.4.1 Instantaneous Plastic Straining

In order to assess the need for the application instantaneous plastic strain, FRASP must first determine the uniaxial yield stress of the cladding material. The yield stress is identified as the transition point between linear elastic behavior and plastic behavior on the uniaxial stress strain curve. In determining the value of the yield stress, FRASP takes a similar approach to FRACAS-I by finding the intersection of

the elastic and plastic strain curves (Berna et al., 1997). Then transition between elastic and plastic behavior is identified in Figure 2-10 which illustrates the elastic and plastic uniaxial stress-strain curves for unirradiated Zircaloy at 300K. While materials are traditionally treated as experiencing plastic behavior after straining 0.2% beyond the transition point (Callister, 2007), FRASP assumes yielding to occur at the exact intersection of the elastic and plastic strain curves. Assuming that the behavior transitions from elastic to plastic at the exact intersection prevents numerical complications associated with assuming elastic behavior continues for 0.2% strain beyond the intersection. Given the uncertainty associated with the correlations being used, this is not an inappropriate assumption (Geelhood et al., 2008). It should be noted that the yield point will move as permanent strains added, shifting the linear elastic curve to the right.

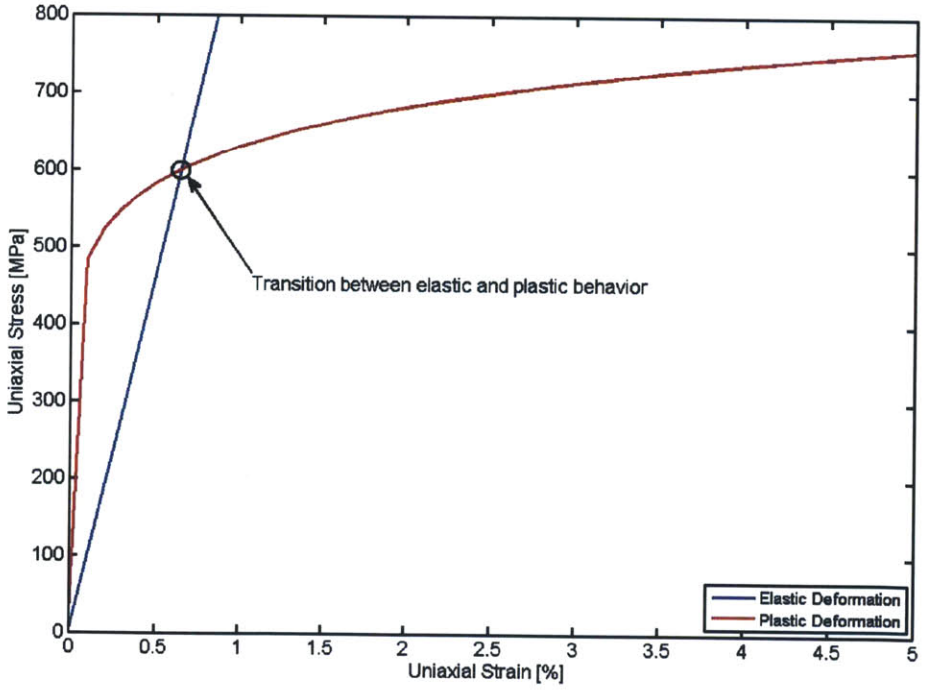

Figure 2-10: **Uniaxial stress-strain curve of unirradiated Zircaloy at 300K**

In assessing instantaneous plastic straining, FRASP uses the von Mises assumption that the cladding stress and strain components can be compared to the uniaxial stress-strain behavior using Equations 2.24 and 2.25 to find the equivalent stress and strain.

$$\sigma^* = \frac{1}{\sqrt{2}} \left[(\sigma_r - \sigma_\theta)^2 + (\sigma_r - \sigma_z)^2 + (\sigma_\theta - \sigma_z)^2 \right]^{1/2} \tag{2.24}$$

$$\epsilon^* = \frac{\sqrt{2}}{3} \left[(\epsilon_r - \epsilon_\theta)^2 + (\epsilon_r - \epsilon_z)^2 + (\epsilon_\theta - \epsilon_z)^2 \right]^{1/2} \tag{2.25}$$

After finding the yield stresses associated with each radial node's applicable conditions, temperature, fluence, plastic strain, etc., FRASP compares them against the elastically calculated equivalent stresses. If a node is found to have an equivalent stress exceeding the yield stress, an equivalent plastic strain of 0.0001% is added to the total permanent strain of that node. If instantaneous plastic straining is found to occur within the cladding, FRASP then recalculates the structural state and yield stresses of the cladding utilizing the modified permanent strain components and checks to determine if further plastic deformations are warranted. Iteration continues in this fashion until the addition of plastic strain to the inelastically behaving node(s) is found to have an equivalent stress equal to the yield stress, indicating the node's deformation lies along the uniaxial stress-strain curve. This process is illustrated for a single node in Figure 2-11. Note that Figure 2-11 is purely illustrative and not to scale.

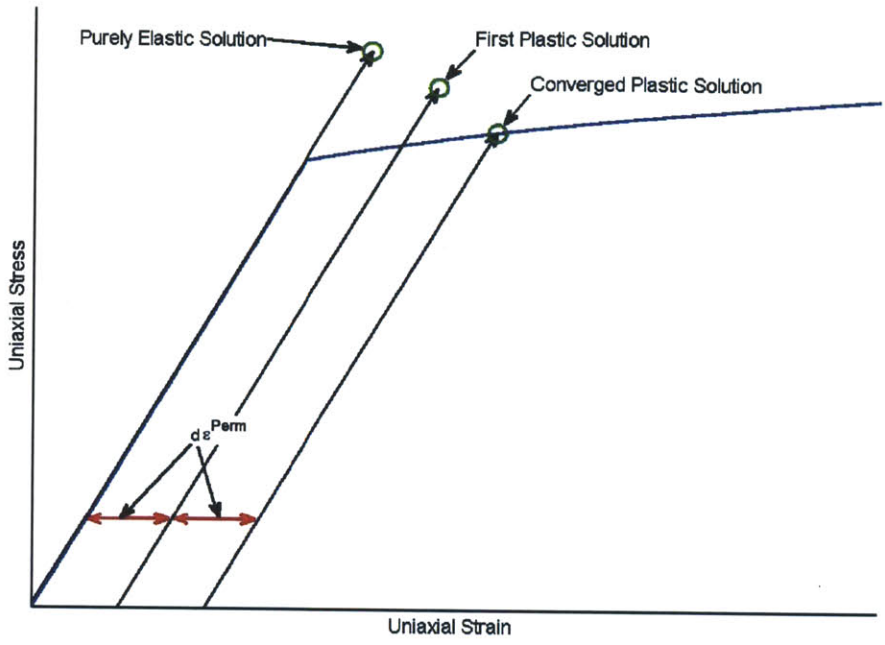

Figure 2-11: **Illustration of FRASP's instantaneous plastic strain methodology**

Though the use of such a small differential equivalent strain for instantaneous plastic strain calculations does cause FRASP to slow down, it is necessary to insure that the equivalent stress always converges to the yield stress value. Experience with FRASP has shown that such instantaneous plastic behavior is characteristic primarily of large power ramps and is rarely experienced in other applications of FRASP. As these ramps tend to be confined to individual time steps, the increased calculation times are not a hindrance of the user.

2.4.2 Cladding Creep

In addition to instantaneous plastic strain, FRASP also accounts for time dependent creep straining. This creep behavior acts to relieve stress in the cladding and is responsible for a significant portion of fuel-cladding gap closure. The creep strain rate is calculated at individual time steps based on the cladding steady-state stress

levels. As it is dependent on the structural state of the cladding, creep is a strong function of the cladding internal and external pressures.

Similar to FRACAS-I, FRASP takes a quasi-steady-state approach to the application of creep strains. At each individual time step, FRASP finds the steady-state structural state of the cladding based on current conditions. The stresses associated with this structural state are then applied in finding the equivalent creep strain rate associated with that time step. Using a finite difference approach, shown in Equation 2.26, the calculated equivalent creep strain rate is then multiplied by the size of the time step to find the differential equivalent creep which will occur over the course of that particular time step.

$$\triangle \epsilon^c (t_i) \approx \dot{\epsilon^c} \times (t_i - t_{i-1}) \tag{2.26}$$

Due to the length of time steps used by FRAPCON, typically several days in duration, FRASP utilizes an intermediate time loop for creep calculations. For each user input time step, FRASP provides steady-state structural information to FRAPCON for use in the fuel-cladding gap size and plenum pressure iteration processes. After FRAPCON determines the steady-state condition of the fuel, cladding, and plenum gas under current conditions, FRASP further segments the large input time step into smaller creep time steps, typically less than ten hours. These smaller time steps are then used to find and apply cladding creep strains.

Experience with FRASP has shown that the high cladding stresses associated with instantaneous yielding lead to extremely large creep rates. When these large rates are applied over time steps on the order of several hours, they result in unrealistically large differential creep strains which can lead to numerical instability within FRASP. In order to counter this effect, the size of the time steps used in calculating creep effects were further reduced to one minute if instantaneous plastic straining was found to have occurred during steady-state calculations. While this does slow down the operation of FRAPCON, its effect is very limited for two reasons. The first is that there are no gap size or plenum pressure iterations occurring as FRASP performs this intermediate

creep loop, which means the structural calculations need only be performed once. The second reason is that, again, instantaneous plastic straining occurrence tends to be associated with power ramps, which by their nature occur over small time steps.

2.4.3 Calculation of Permanent Strain Components

In order for the differential strains calculated for the instantaneous plastic and creep behaviors to be utilized by FRASP, they must be converted from equivalent strains into individual permanent strain components. In applying these strains, FRASP assumes incompressibility with respect to permanent strains, as shown in Equation 2.27. (Olander, 1976) This assumption of incompressibility conserves material volume as permanent strains are applied.

$$\epsilon_r^{perm} + \epsilon_\theta^{perm} + \epsilon_z^{perm} = 0 \tag{2.27}$$

To satisfy conservation of volume, FRASP applies the Prandlt-Reuss Flow Rule, in the form of Equations 2.28, 2.29, and 2.30 (Olander, 1976). These equations apply the stress components within the each node to the incremental equivalent strain to find the differential strain components. It is these individual differential components which are added to the total permanent strains and incorporated into FRASP's structural state calculations.

$$\triangle\epsilon_r = \left(\frac{\triangle\epsilon^*}{\sigma^*}\right)\left[\sigma_r - \frac{1}{2}(\sigma_\theta + \sigma_z)\right] \tag{2.28}$$

$$\triangle\epsilon_\theta = \left(\frac{\triangle\epsilon^*}{\sigma^*}\right)\left[\sigma_\theta - \frac{1}{2}(\sigma_r + \sigma_z)\right] \tag{2.29}$$

$$\triangle\epsilon_z = \left(\frac{\triangle\epsilon^*}{\sigma^*}\right)\left[\sigma_z - \frac{1}{2}(\sigma_\theta + \sigma_r)\right] \tag{2.30}$$

2.5 Contact Regimes

Prior to pellet-cladding contact, FRASP's primary role within FRAPCON is to provide information on the displacements of the fuel and cladding. While cladding stresses are reported by FRASP under open gap conditions, these values are of limited importance relative to fuel performance and differ only slightly from FRACAS-I's thin shell approximation. Conversely, the fuel temperature, which has feedback effects on the majority of relevant fuel performance parameters, is extremely sensitive to the size of the fuel-cladding gap, which is based on the fuel outer and cladding inner radii found by FRASP.

As the fuel pellet swells and the cladding creeps down, due to the higher coolant pressure, the two components eventually come into contact. Fuel-cladding contact is defined by FRAPCON as occurring when the fuel outer and cladding inner radii come within a predetermined distance of one another. This minimum gap thickness is based on fuel pellet and cladding surface roughness and is used to maintain a convective heat transfer component between the surfaces. Maintaining this minimum gap thickness is a necessary condition for FRASP's PCMI model.

Mechanically, the cracking relocation of the fuel pellet introduces the possibility of soft contact between the fuel and cladding. Because relocation strain simply represents the introduction of empty space to the interior of the fuel pellet, it can be assumed that further shifting of the pellet can consume some of that space. Upon initial contact with the cladding, the fuel radius is dictated by the inner radius of the cladding as the relocation strain is recovered. This period of relocation recovery due to contact with the cladding is referred to as soft contact. Similar to FRACAS-I, FRASP allows for recovery of up to one half of the fuel relocation strain without the onset of hard contact and, with it PCMI. The recovery of relocation strain is simply applied by reducing the effective relocation strain, with a minimum of one half of its original value, to force the fuel outer radius to equal the cladding inner radius, less the minimum gap thickness. This minimum of one half the original relocation value was selected to match the previous treatment of soft contact by FRACAS-I.

After the recovery of relocation strain via soft contact reaches its minimum limit, FRASP considers the fuel pellet and cladding to be in hard contact. The onset of hard contact marks the start of PCMI, and the two terms are synonymous. During hard contact, the fuel pellet continues to grow due to swelling, causing the cladding to expand to accommodate the growth. Unlike the open gap regime, FRASP's primary role under hard contact conditions is not to predict the gap size, as it is a predetermined minimum value, but to assess the conditions necessary to couple the fuel and cladding. Figure 2-12 illustrates the different fuel-cladding contact regimes.

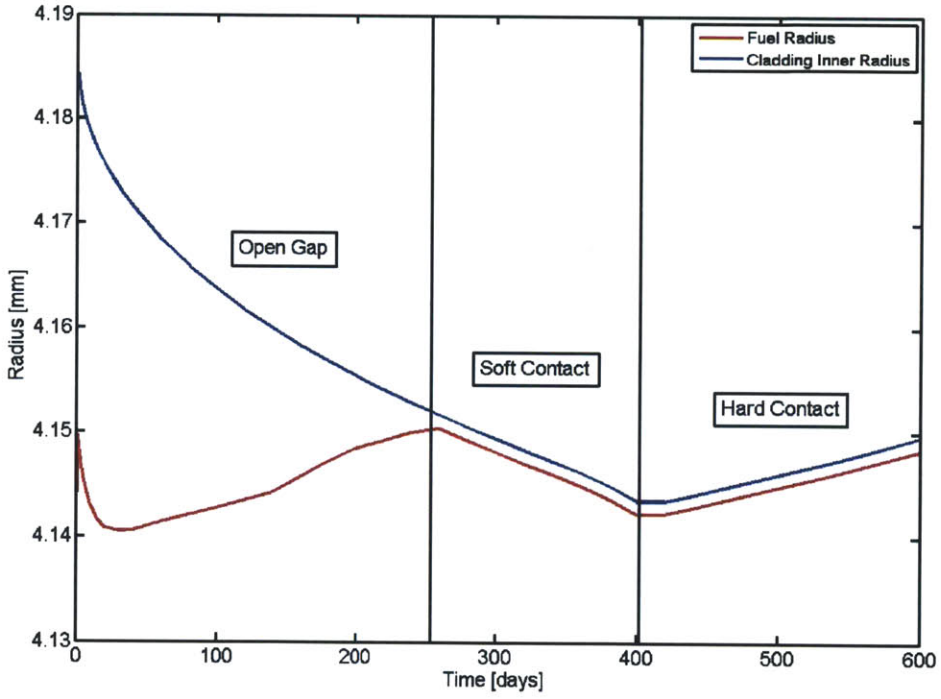

Figure 2-12: **Illustration of the fuel and cladding behavior in the various contact regimes**

2.6 PCMI Model

Within FRASP, PCMI is not considered to occur until the fuel pellet and cladding deformations are coupled via interfacial pressure and axial friction. While the cladding acts to reduce the radius of the fuel pellet during soft contact, no interfacial pressure or axial friction is applied. For these reasons, FRASP only utilizes its PCMI model after soft contact consumes half of the fuel pellet's relocation strain and hard contact begins.

Until the onset of PCMI between the fuel pellet and cladding, FRASP treats both models completely independently, with the exception of relocation strain recovery dying soft contact. After the start of hard contact, FRASP continues to perform the internal calculations associated with the fuel pellet and cladding models in separated fashion. However, under these conditions the two models are no longer fully independent; instead they become coupled together by using interfacial pressure and axial friction as boundary conditions. By separating the structural state calculations of the fuel pellet and cladding and then evaluating PCMI criteria within a higher level code structure, FRASP is able to avoid many potential numerical errors which could result from non-physical behavior that may occur in the course of coupling the two components, particularly the overlapping of fuel pellet and cladding radii. Figure 2-13 illustrates the general method used for evaluating the interfacial conditions of PCMI.

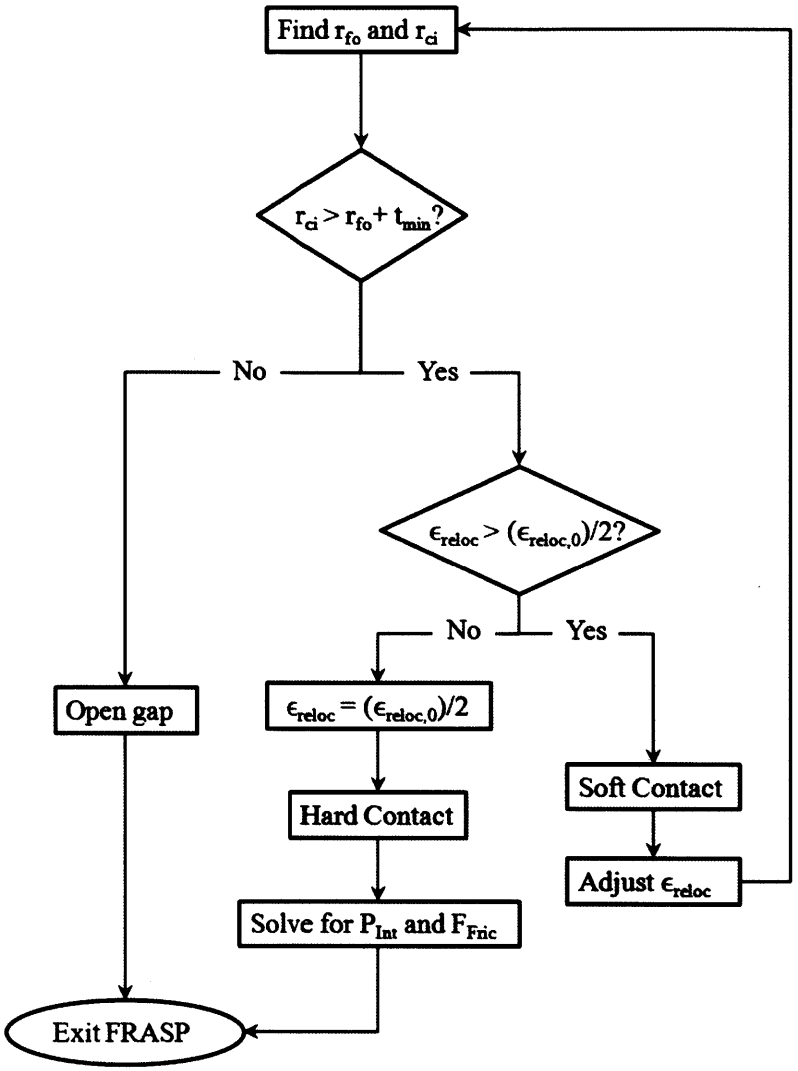

Figure 2-13: **Flow chart of FRASP's treatment of pellet-cladding contact**

Physically, the interfacial pressure and axial friction are simply forces applied to each node in hard contact. Both forces are applied in equal and opposite quantities to the fuel pellet and cladding. Figure 2-14 shows how the coupling components are applied to the interface between a fuel pellet and the cladding. As with all of FRASP's calculations, the PCMI coupling forces are found for each axial node independently, with the only axial communication coming via the axial force balance.

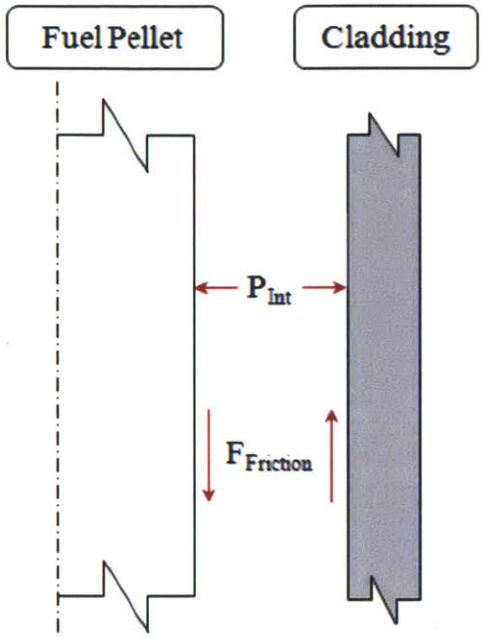

Figure 2-14: **Illustration of the application of interfacial coupling forces**

Interfacial pressure is a radial stress which acts on the exterior surface of the fuel pellet and interior surface of the cladding. Though it physically represents the radial interfacial coupling force, it is convenient to treat it as a compressive stress, as this is already a boundary condition for the radial displacement of the fuel pellet and cladding models. In accordance with FRASP's general assumptions, this compressive stress is applied in an azimuthally and axially uniform manner over the surfaces of the axial node of interest.

The primary purpose of applying interfacial pressure is to force the radial displacements of the fuel pellet external and cladding internal surfaces to support a minimum gap size. Increased interfacial pressure tends to cause the fuel pellet to radially contract while causing the cladding to radially expand.

Axial friction is applied in FRASP as an external force within the axial force balance. While the axial friction force physically acts on the interfacial surfaces of the fuel pellet and cladding, it is applied as a uniform force due to FRASP's assumption of evenly distributed external axial forces. Unlike interfacial pressure, friction can act in either a compressive or tensile manner. Because of this, the sign convention for

axial friction is defined as being compressive on the fuel and tensile on the cladding for positive values and vice versa for negative values, as shown in Figure 2-15. Like other axial forces, friction forces can be communicated axially, according to the calculation of the axial strain components discussed in Section 2.2.

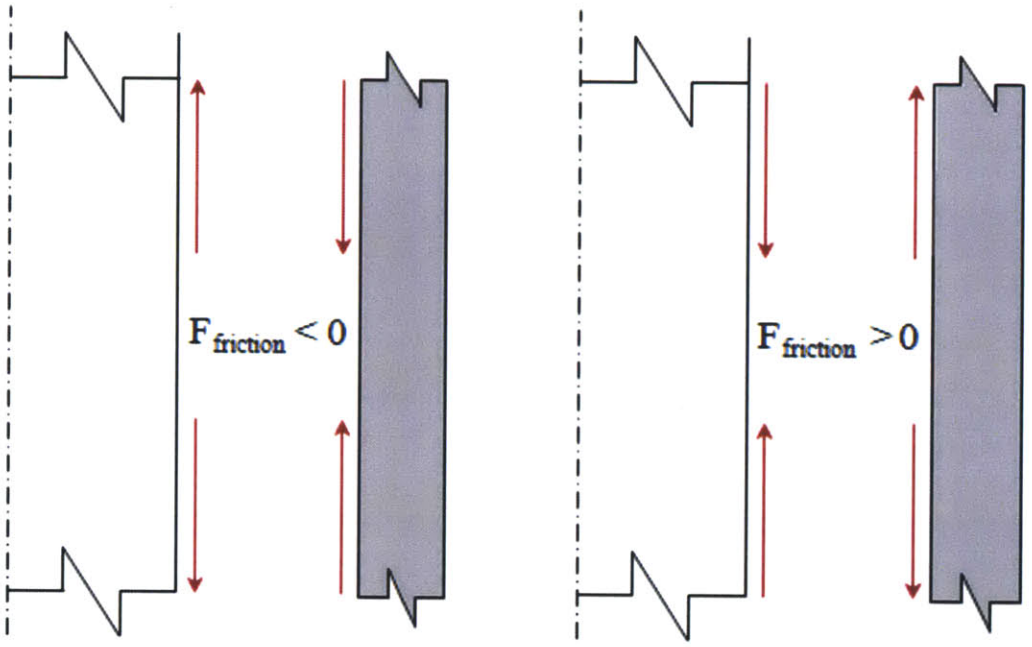

Figure 2-15: **Illustration of the axial force's directions of application**

Axial friction is applied primarily to couple the axial expansion of the fuel pellet and cladding after the onset of hard contact. In reality the maximum friction force that could be applied would be a function of the interfacial pressure and a static friction coefficient. Because of the difficulty of determining and appropriate friction coefficient (Sercombe et al., 2012) FRASP duplicates the assumption of axial locking between the two components used by FRACAS-I during hard contact (Berna et al., 1997).

Axial locking is defined by forcing the total axial elongation that occurs under PCMI conditions to be equal for both the fuel pellet and cladding. The axial elongation is then defined by the initial node length and the change in axial strain after the onset of hard contact, as shown in Equation 2.31. Because the initial node length of both the fuel pellet and cladding are equal, as defined by the initial nodalization

of the fuel rod, the axial expansion of the two components can be directly compared using their axial strains. The condition of axial locking is then defined by Equation 2.32, which dictates that the fuel and cladding length changes must be equal after hard contact. Note that $\epsilon_{z,cont}$ represents the axial strain value immediately prior to the start of PCMI.

$$\triangle L_z = L \times (\epsilon_z - \epsilon_{z,cont}) \tag{2.31}$$

$$(\epsilon_z - \epsilon_{z,cont})_{fuel} = (\epsilon_z - \epsilon_{z,cont})_{clad} \tag{2.32}$$

In addition to their primary roles in coupling the fuel pellet and cladding, the application of both the interfacial pressure and axial friction have secondary coupling effects. These secondary effects result largely from conservation of volume. As a cylinder is compressed radially or axially, it must expand along the other axis to compensate for lost volume. The primary and secondary effects of applying interfacial pressure and compressive axial force are illustrated in Figure 2-16. When interfacial pressure and axial friction are applied together, these secondary effects can create feedback between the coupling criteria, thwarting attempts to solve for the state of the coupled system.

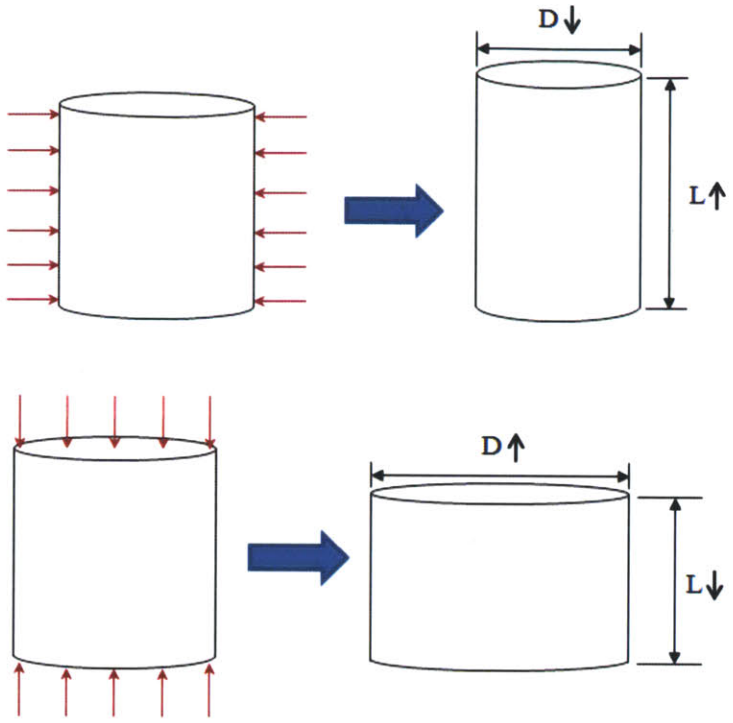

Figure 2-16: **Illustration of the primary and secondary effects of applying interfacial forces**

During hard contact, FRASP finds the appropriate values of interfacial pressure and axial friction to support the minimum gap size and axial locking conditions at each axial location. Initially, attempts were made to fully separate the solution processes for the interfacial pressure and axial friction values. In this process, FRASP attempted to satisfy the PCMI coupling criteria by adjusting the interfacial components based solely on their primary effects. These efforts failed because the secondary effects associated with both interfacial components proved to be substantial enough to cause violation of the coupling criteria.

In order to overcome the limitations of completely separating the solution of the interfacial pressure and axial friction, FRASP utilizes a solution scheme in which the coupling component values are found in an interrelated manner, but are still based only on their primary effects. In this partially separated scheme, illustrated in Figure 2-17, FRASP uses the current value of interfacial pressure along with a perturbed

value to extrapolate a new interfacial value via the Secant Method, discussed in Section 2.2, based on the current iteration of the friction state. This new interfacial pressure value is then used to perform a full iteration, again using the Secant Method, on the axial friction until the fuel pellet and cladding are successfully axially locked. After iterating on an appropriate axial friction, FRASP then finds another interfacial pressure value and the process is repeated until both coupling criteria are satisfied. It should be noted that neither step considers the coupling criteria of the other step in performing calculations. Experience running FRASP under a variety of conditions has shown this partially separated variable method to be both redundant and acceptably fast, thanks in part to the utilization of the Secant Method.

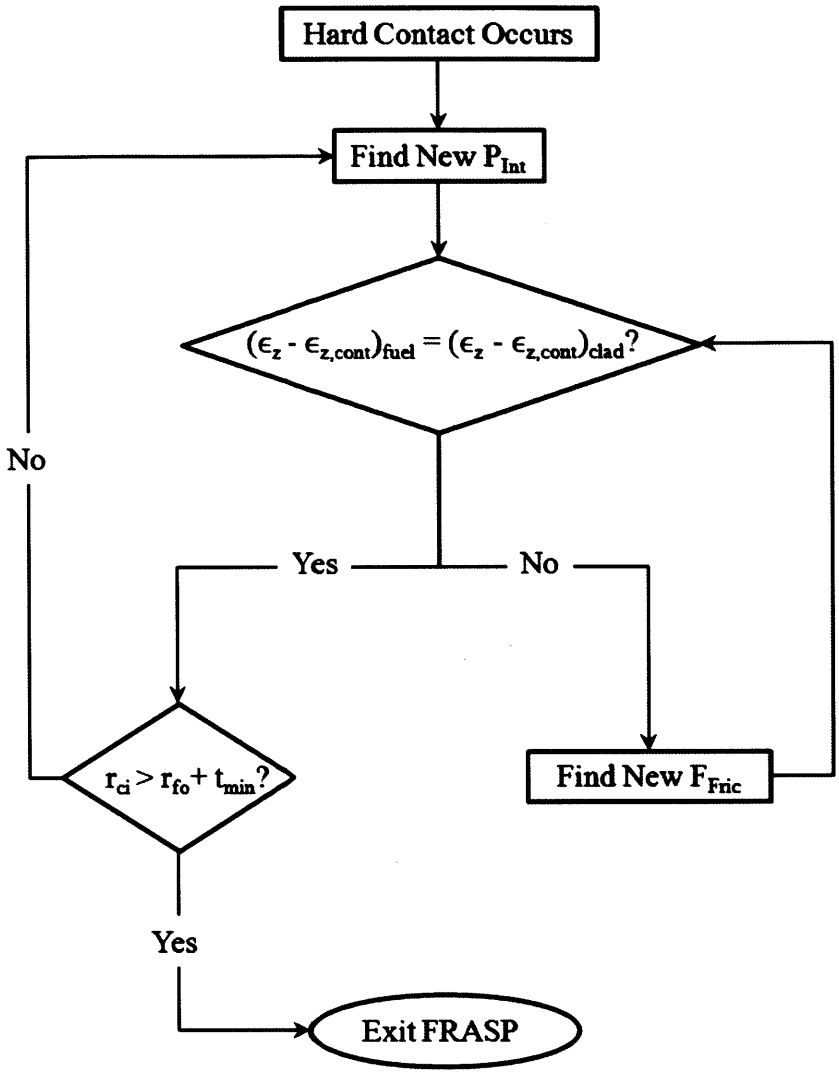

Figure 2-17: **Simplified flow chart of FRASP's partially separated PCMI solution process**

Because FRASP solves for PCMI conditions locally while incorporating axially communicated forces, it is important to perform structural state calculations in an axially descending manner along the fuel rod. As discussed in Section 2.2 FRASP assumes that the fuel rod is axially fixed at the base, which only allows for forces to be communicated in a downward direction. If FRASP is configured to solve for PCMI conditions, particularly the axial friction force, in an axially ascending manner,

it fails to recognize the axial coupling forces of the current time step that may exist above the axial location of interest. This leads to situations where axial friction is solved for using the previous time step friction values above the point of interest, which are themselves incorrect. As a result, the local friction values experience large oscillations which result in incorrect PCMI modeling and can even cause FRAPCON to crash. No such issues are experienced if the correct solution direction is utilized.

2.7 Incorporation of FRASP into FRAPCON

The driving purpose of FRASP's development was to replace the rigid pellet model in FRACAS-I for improved simulation of PCMI and introduce stress induced fuel pellet deformation. However, due to the dramatic differences between the thin shell and 1.5D structural mechanics models, FRASP proved unable to simply replace FRACAS-I's PCMI model alone. As a result, FRACAS-I was fully replaced within FRAPCON by FRASP. Figure 2-18 shows FRAPCON's code structure and illustrates where FRASP has been implemented to replace FRACAS-I.

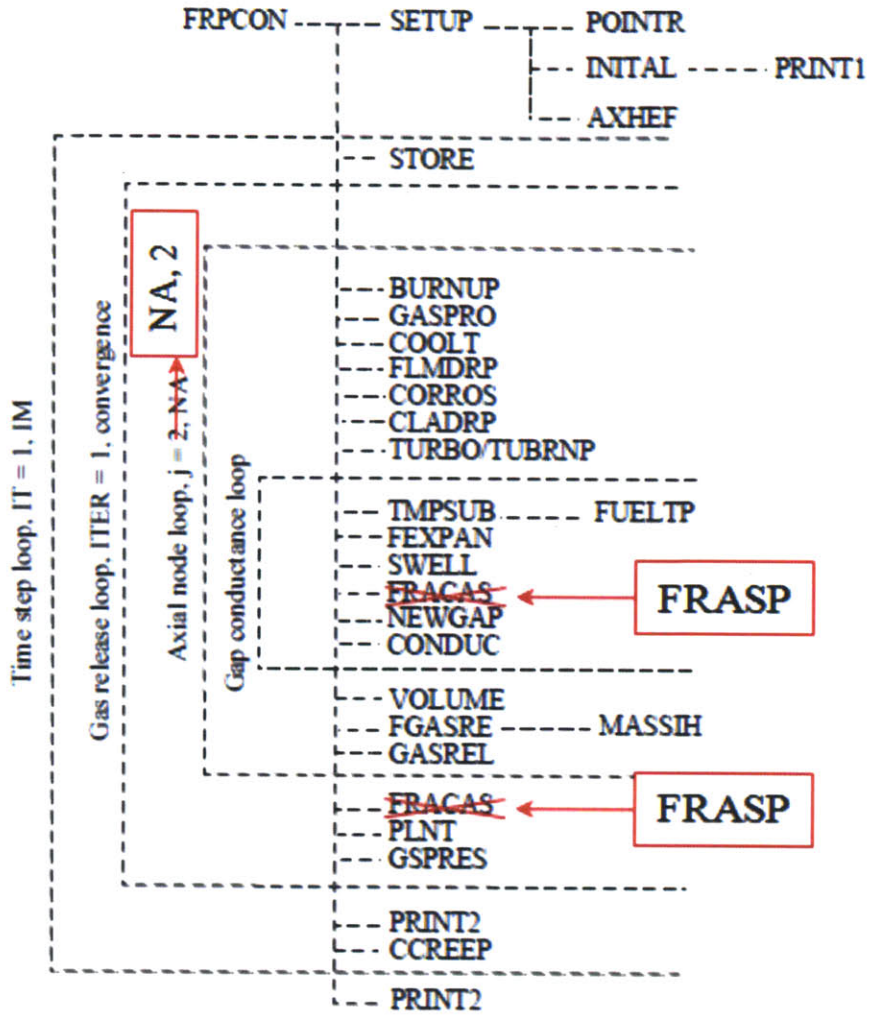

Figure 2-18: **Changes to the code structure of FRAPCON to incorporate FRASP**

In order to successfully replace FRACAS-I, FRASP needed to be constructed not only to provide the user with relevant structural information, but also to provide FRAPCON with data required to successfully perform its iterative calculations. Because of the intrinsically coupled behavior of fuel performance parameters, FRASP must be able to provide accurate values for use by FRAPCON or risk experiencing compounding feedback effects.

For FRAPCON's non-mechanical calculations, the most important information

needed from FRASP is the current fuel-cladding gap size, fuel and cladding nodal radii, and cladding length, as these parameters play critical roles in finding the fuel pellet temperatures and the state of interfacial gas. The size of the fuel-cladding gap is of particular importance because it directly affects the conductive heat transfer through the gas gap between the fuel external and cladding internal surfaces, which is a major component in finding the temperature drop across the fuel-cladding gap. As this temperature drop determine the surface temperature of the fuel pellet, which is the boundary condition for finding all fuel temperatures, its accuracy is of utmost importance.

The state of the interfacial gas, i.e. the molar composition and pressure, also effects the fuel-cladding gap temperature jump. While information from other subroutines provides the molar composition of the interfacial gas, the sizes of the fuel and cladding are required to find the free volume of the gas for pressure calculations. For these calculations, FRAPCON does make use of FRASP's calculated fuel and cladding radii and cladding axial elongation. However for the axial elongation of the fuel, FRAPCON continues to use a more simple method for finding the height of each radial node in the fuel pellet, as shown in Equation 1.1.

This simpler methodology for finding the axial elongation of the fuel is an artifact of FRAPCON prior to the implementation of FRASP. It was allowed to remain, however, due to the fact that FRASP does not account for variation in the axial strain within the fuel pellet. While conservation of volume makes this matter irrelevant with regard to total volume, FRAPCON applies the ideal gas law, Equation 2.33, to localized volumes of gas of varying temperature, which are summed according to Equation 2.34. If the uniform axial strain found by FRASP were applied to the fuel pellets for this purpose, an incorrect inter-pellet gas volume may result. Though this application uses different methodologies to finding the fuel pellet radius and height, which could prevent the conservation of volume, sensitivity studies have shown less than five percent difference in gas free volume between uniform and non-uniform axial strain applications.

$$PV = nRT \tag{2.33}$$

$$V_{total} = V_{plenum} + V_{gap} + V_{inter} \tag{2.34}$$

Prior to the implementation of FRASP, FRAPCON performed calculations in an axially ascending manner, starting at the base of the fuel pin. This solution method is in the same direction as coolant flow along the fuel pin, making FRAPCON's 1D single rod thermal hydraulic analysis, which is necessary to obtain cladding wall temperatures, simpler to implement. However, this ascending method does not account for mechanical coupling between axial nodes. As discussed in Section 2.6, this is counter to the solution direction required by FRASP. For the sake of the new mechanical model, FRAPCON was reversed to perform all calculations, with the exception of thermal hydraulics, in an axially descending manner, as shown in Figure 2-19.

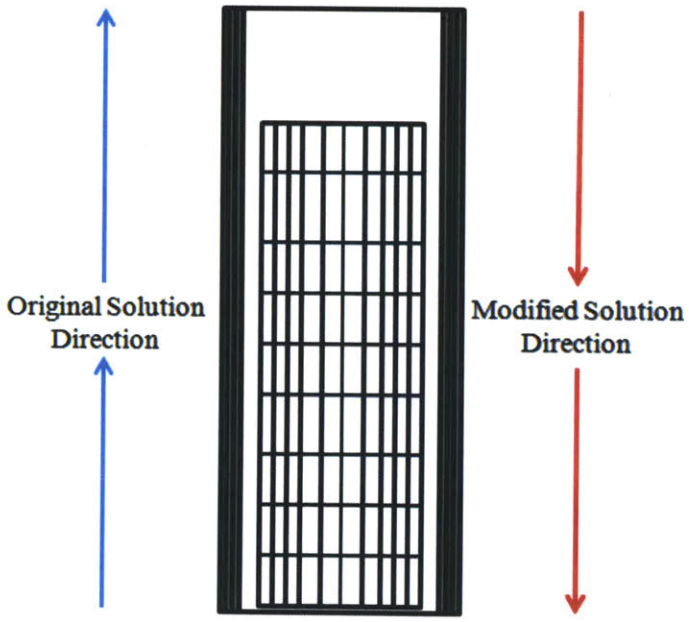

Figure 2-19: **Visualization of the modified solution direction for the implementation of FRASP**

Unlike FRACAS-I, FRASP considers cladding irradiation growth in evaluating the mechanical state. Incorporating cladding irradiation growth, especially axially, has effects on the stress levels in the cladding, which will affect creep behavior, and the amount of friction that must be applied to couple the fuel pellet and cladding. To account for the anisotropic growth and thermal expansion strains that are generated in Zircaloy (Luscher and Geelhood, 2011), FRASP allows for growth strains to be segmented by their axis of application.

In finding the fuel rod's structural state, FRASP makes use of existing correlations within FRAPCON for all needed material parameters. All of the correlations used to evaluate these parameters, such as the Young's Modulus and Poisson Ratio, already exist as functions and subroutines within FRAPCON. Rather than replicating the work that went into developing these functions and subroutines, FRASP is designed to access and utilize their outputs of material properties directly.

Because FRASP accounts for many more details of fuel rod structural mechanics, including fuel stresses, fuel cracking, radially dependent cladding stresses and strains, the radial stress component, and axial friction, significantly more structural information is available than in previous versions of FRAPCON. In order to provide information to the user in a relevant fashion, the majority of this new information is either modified to fit into FRAPCON's existing output files or not reported. Neither fuel stresses nor fuel cracking information are reported, as only the dimensional changes to the fuel, surface displacement and axial elongation, are relevant to fuel performance. An exception with regard to reporting is the axial friction values, which are made available in a separate output file created as part of FRASP's incorporation.

The values requiring the most modification for reporting in FRAPCON outputs are the cladding stresses and strains. In order to alter these values to be comparable to those calculated by FRACAS-I, the various stress and strain components are averaged on an area weighted basis, Equations 2.36 and 2.35. Figure 2-20 compares the nodally local cladding hoop stress values with the reported area weighted average when the cladding experiences 2.4 MPa of internal pressure, 15.5 MPa of coolant pressure, and no axial friction. While reporting different forms of these values may have relevance,

area weighted averages were chosen because they would be directly comparable to values provided by FRACAS-I and more applicable to experimental measurements.

$$\sigma_{Ave} = \frac{\int_A \sigma(r)\, dA}{\int_A dA} \approx \frac{\sum \sigma_i \times \left(r_i^2 - r_{i-1}^2\right)}{\left(r_N^2 - r_0^2\right)} \tag{2.35}$$

$$\epsilon_{Ave} = \frac{\int_A \epsilon(r)\, dA}{\int_A dA} \approx \frac{\sum \epsilon_i \times \left(r_i^2 - r_{i-1}^2\right)}{\left(r_N^2 - r_0^2\right)} \tag{2.36}$$

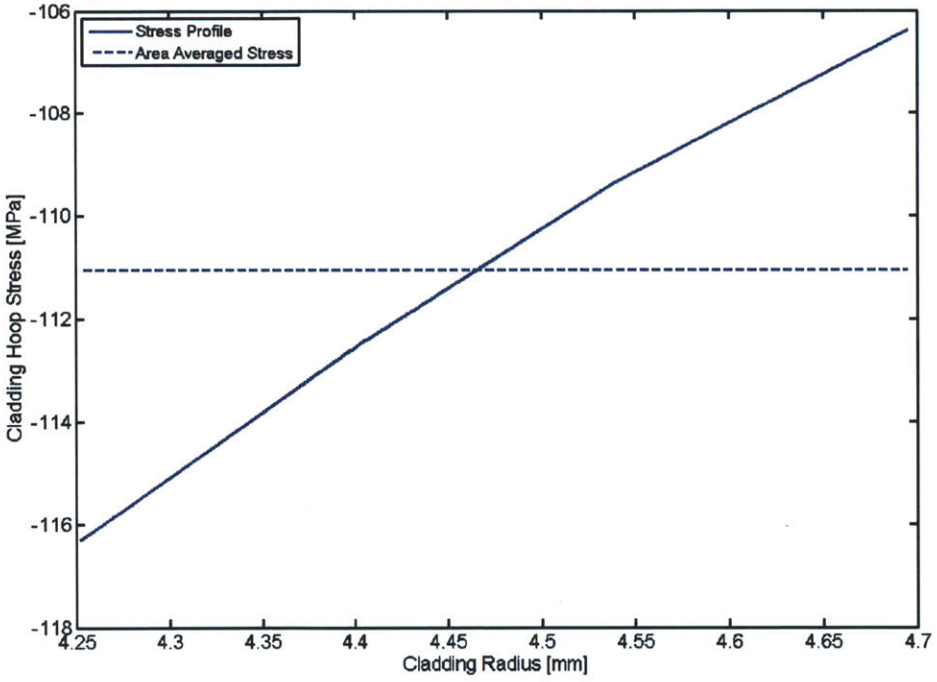

Figure 2-20: **Example of the differences in cladding local and average hoop stress**

2.8 SiC Cladding Model Changes

Because the use of Zr based alloys for fuel cladding is intrinsically incorporated into the structure of FRAPCON, evaluating SiC clad fuels requires changes to FRAPCON's cladding material properties. Previous work has focused on adapting FRAPCON-

3.3 to make use of SiC cladding. (Carpenter, 2006). These same changes have also been brought into the more advanced FRAPCON-EP (Xu and Kazimi, 2012).

While SiC is being actively investigated as a potential LWR cladding material [cite something], the exact form of the optimized SiC cladding structure has yet to be determined. Current designs favor a heterogeneous combination of monolithic and fiber-composite SiC layers, shown in Figure 2-21. Because both the design and exact material properties of SiC cladding for LWR environments remain uncertain, the entire thickness of the cladding is assumed to be homogeneous, high purity, high density fiber-composite SiC. While this assumption fails to capture the exact behavior of more complex designs, it does provide general insight into the behavior of SiC cladding. More detailed fuel performance investigation of specific SiC cladding designs may require further changes to material property correlations in FRAPCON.

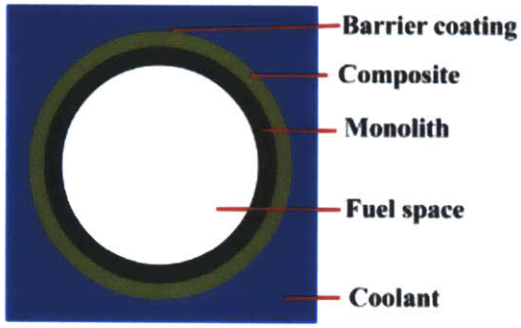

Figure 2-21: **Triplex SiC cladding design** (Carpenter et al., 2010)

For the SiC versions of FRAPCON, the majority of cladding material property models have been changed (Carpenter, 2006). The models changed include:

- Axial growths
- Creep
- Elastic modulus
- Emissivity
- Hardness
- Melting Point
- Oxidation
- Shear modulus
- Thermal conductivity
- Thermal expansion
- Ultimate stress

The changes made to transition from Zircaloy to SiC cladding are mainly isolated to cladding material property correlations. Within the structure of FRAPCON, these correlations are implemented within separate functions and subroutines, allowing for them to be modified in isolation from the higher level models which make use of their returned values. In following with this structured order, FRASP was designed to make use of available values, functions, and subroutines and only modify structural parameters. As such, incorporating FRASP into SiC versions of FRAPCON was essentially an identical process as its incorporation into the Zircaloy versions of FRAPCON, detailed in Section 2.7.

The incorporation of FRASP into SiC versions of FRAPCON did require one significant change to the structure of FRASP to accommodate the new cladding material. Because of its brittle nature, SiC is assumed to simply fail without yielding

and experiencing inelastic behavior. To incorporate this, cladding failure is assumed to occur at the ultimate stress, with purely elastic behavior up to that point. Since SiC plastic straining is wholly ignored, the cladding plastic strain relation within FRAPCON remained unmodified, utilizing the existing plastic strain correlations for Zircaloy. If FRASP were incorporated without modifying its method for finding the cladding yield stress, it would use a Zircaloy plastic strain relation with SiC elastic behavior, which would result in inaccurate treatment of cladding behavior.

To avoid potential issues in the treatment of plasticly deformed SiC, the methodology for finding the yield stress, discussed in Section 2.4.1, was replaced by simply applying the ultimate stress as the yield stress, given in Equation2.37(Carpenter, 2006).

$$\sigma_{ultimate}\,[Pa] = \sigma_{yield}\,[Pa] = 2.66 \times 10^4 T_{SiC}\,[K] + 2 \times 10^8 \tag{2.37}$$

Because this yield stress does not accommodate the previous permanent deformation of cladding, FRASP's application of instantaneous plastic strain to SiC does not relieve stress as effectively as it does for Zircaloy. In fact, during simulations requiring instantaneous plastic strain for SiC, FRASP fails to find an appropriate structural solution. This is acceptable, however, because the brittle nature of SiC dictates cladding failure beyond its yield stress, making any solution from FRASP for intact cladding fundamentally incorrect.

Experimental hoop strength tests of SiC cladding have resulted in the selection of a conservative 30 MPa internal pressure limit for SiC cladding (Carpenter et al., 2010), which is consistent with the predicted ultimate stress presented in Equation2.37. These experimental tests were performed under atmospheric conditions, implying that compressive external forces will act to alleviate the pressure gradient across the cladding. Because of this implicit support from the pressure of the coolant, approximately 15 MPa in a PWR, the operational maximum internal pressure for SiC cladding in a PWR environment can be assumed to increase to approximately 45 MPa.

This assumed increase in maximum internal pressure is heavily reliant on the presence of the coolant pressure and is therefore not valid for situations where it has been removed, such as Loss of Coolant Accidents (LOCAs). While the cladding may survive with 45 MPa of interfacial pressure under nominal conditions, the conservative limit of 30 MPa should be applied for all reactor operations, where a LOCA may occur unexpectedly at any time.

Because of the drastic differences between metal Ziracaloy and ceramic SiC claddings, many of the changed properties result in very different fuel performance characteristics. With the exception of brittle behavior, the modified creep and cladding swelling relations are the changes with the largest effect on fuel pin parameters.

Unlike Zircaloy, SiC does not effectively relieve internal stresses via creep straining at temperatures below 1000K. As this is much higher than temperatures which could be relevant to LWR operation, the creep strain rate is set to equal zero for all conditions within FRAPCON.

In Zircaloy clad fuel pins, the majority of fuel-cladding gap closure results from cladding creep down. The loss of this fuel-cladding gap closure mechanism results in a rather large temperature increase throughout the lifetime of the fuel pin. Maintaining this higher fuel temperature in turn increases the FGR which then, along with increased fuel thermal expansion, leads to an increase in plenum pressure within SiC clad fuel pins (Carpenter et al., 2010).

Also different than Zircaloy, SiC experiences isotropic irradiation swelling (Ishihara et al., 2002). Because Zircaloy only experiences axial swelling (Luscher and Geelhood, 2011), SiC irradiation swelling could not be directly implemented into FRACAS-I as a permanent strain. In order to successfully implement this into FRACAS-I, previous studies have modified the thermal expansion coefficients to include radial irradiation swelling, while leaving the axial swelling component to be applied as a simple strain outside of the mechanical model. The application of these strains are shown in Equations 2.38, 2.39, and 2.40 (Carpenter, 2006). This swelling component acts to increase the cladding radius, and thus the fuel-cladding gap size, through the life of the fuel pin causing higher fuel temperatures which results in higher

FGR and plenum pressure.

$$\left(\epsilon_{r,\theta}^{ThEx} + \epsilon_{r,\theta}^{s}\right) = \left(3 \times 10^{6} \left[\frac{1}{K}\right]\right) \times (T - 300\,[K]) + 0.0067 \times \left[1 - exp\left(\frac{-3\Phi\left[\frac{n}{cm^2}\right]}{10^{25}}\right)\right] \tag{2.38}$$

$$\epsilon_{z}^{ThEx} = \left(3 \times 10^{6} \left[\frac{1}{K}\right]\right) \times (T - 300\,[K]) \tag{2.39}$$

$$\epsilon_{z}^{s} = 0.0067 \times \left[1 - exp\left(\frac{-3\Phi\left[\frac{n}{cm^2}\right]}{10^{25}}\right)\right] \tag{2.40}$$

Unlike Zircaloy cases, FRASP and FRACAS-I treat the creep of SiC identically, i.e. as not existent. However, by incorporating the axial growth of the SiC cladding, which is neglected by FRACAS-I, FRASP is expected to provide a more accurate representation of the cladding's dimensional evolution through its evolution.

Because of the brittle nature of SiC, any deformation of the cladding caused by PCMI must remain elastic in nature. As the rigid pellet model simply forces the cladding to conform to the dimensional changes of the fuel, the cladding simply fails. By using the new PCMI model of FRASP and allowing for stress-induced fuel pellet deformation, FRAPCON is expected to provide usable solutions for some PCMI situations, which are currently beyond the capabilities of FRACAS-I.

Chapter 3

Preliminary Validation

In order to qualify the performance of FRASP, it was first validated against the previously incorporated mechanical model, FRACAS-I, for the case of an average rod under PWR conditions (Seabrook, 2007). The fundamental changes to the method of calculating fuel pellet and cladding dimensions by FRASP within FRAPCON have the potential to create unanticipated complications outside of the mechanical model. Because of the possible feedback effects, validating FRASP requires inspection of many non-structural parameters to demonstrate that any differences in the new model's calculations don't corrupt FRAPCON's other calculations.

Because the only changes that have been made to FRAPCON's calculations deal with the mechanical state of the fuel pin, all differences observed in this validation are the result of the incorporation of FRASP. Due to the complexity of fuel performance simulation, feedback effects from the mechanical calculations will exist in parameters that are not directly dependent on the structural state of the fuel and cladding, e.g. fission gas release. Therefore, in validating FRASP, it becomes important to evaluate changes throughout the fuel pin in assessing accuracy.

FRAPCON-3.3 was used for the validation of FRASP because it uses simpler models for many fuel performance parameters than FRAPCON-EP (Karahan et al., 2010). This is particularly true of fuel pellet swelling, which is simply linear with burnup in FRAPCON-3.3 (Luscher and Geelhood, 2011). The simplicity of the linear swelling model will be particularly helpful for demonstrating the occurrence of stress-

induced pellet deformation.

3.1 Validation Case

For the inspection of the models' differing results, a Zircaloy clad fuel rod with typical PWR design parameters, shown in Tables 3.1 and 3.2, was chosen with a very simple power history. This fuel rod was simulated to undergo three 20 month irradiation cycles at average power for the Seabrook Station Nuclear Power Plant prior to its 7% power uprate (Seabrook, 2007). The fuel rod, with this power history, achieved a final average burnup of 66.39 MWd/kgU, which is slightly higher than the NRC allowed peak rod burnup of 62 MWd/kgU (NRC, 2007; Geelhood et al., 2010).

Table 3.1: Fuel rod parameters for the preliminary validation of FRASP

Parameter	Units	Value
Fuel Rod Pitch	mm	12.59
Cladding Outer Diameter	mm	9.5
Cladding Thickness	mm	0.571
Fuel-Cladding Gap Thickness	μm	82.5
Active Fuel Height	m	3.66
Fuel Pellet Density	%	95.0
Initial U^{235} Enrichment	%	4.5
Plenum Height	m	0.254
Initial Cold Internal Helium Pressure	MPa	2.41

Table 3.2: **Reactor conditions for the preliminary validation of FRASP**

Parameter	Units	Value
Coolant Inlet Temperature	K	565
Coolant Pressure	MPa	15.5
Coolant Mass Flux	$kg/s - m^2$	3336
Core Average LHGR	kw/m	17.85

The axial power shape used for the validation case is assumed to be constant (O'Donnell et al., 2001), illustrated in Figure 3-1. This constant axial power shape was used rather than time and cycle dependent power shapes in order to minimize changes in local power levels. This is consistent with the goal of providing as simple of an irradiation history as possible for this fuel rod to help isolate the effects of incorporating FRASP into FRAPCON.

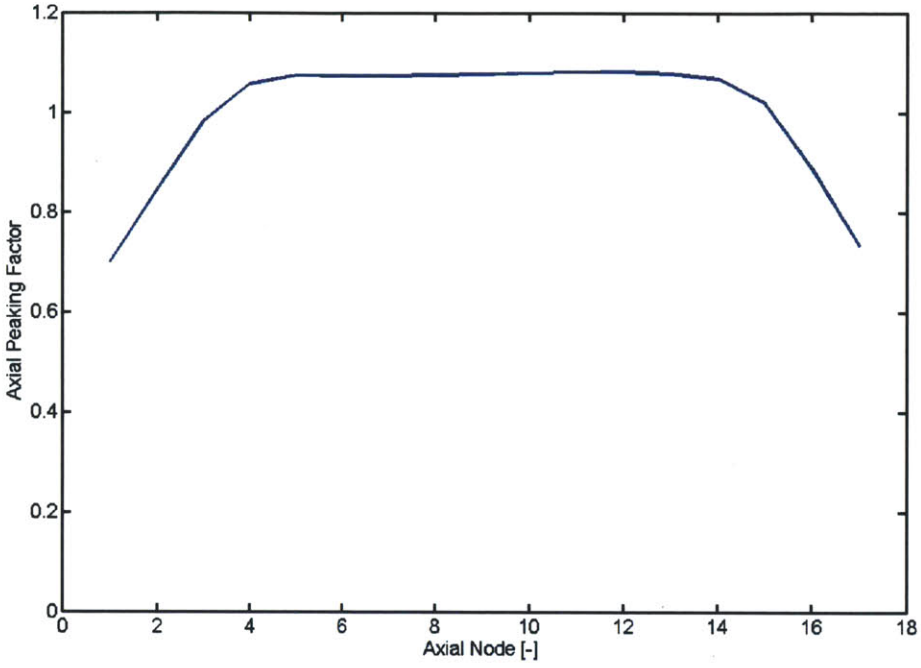

Figure 3-1: Axial peaking profile used in the preliminary validation

The power history used in this test case is admittedly overly simplified. This was done intentionally in order to allow for the differentiation of mechanical effects between the two models. By using a constant power history, rather than a more realistic varying power level, temperatures throughout the fuel stack will only change due to the evolution of the fuel rod, rather than changes in power levels. Though this evolution will generally cause the fuel temperature to increase, thereby increasing thermal expansion, fuel pellet swelling is expected to be the primary radial growth driver. Because the fuel swelling used by both models is linearly dependent on only burnup, any deviation in the radial growth rate can be taken as evidence of stress-induced pellet deformation.

By using the higher system pressure environment of a PWR for the validation case, the fuel-cladding gap will close much faster than in a BWR. This is preferable for validation, as it is more stressful for the cladding creep and PCMI models while

limiting temperature changes associated with fuel-cladding gap closure to very early in the lifetime of the fuel pin.

The time frame chosen for the fuel pin's life is longer than the typical 18 month cycles of the Seabrook Station Nuclear Power Plant **(Dobisesky, 2011)** and gives a fuel pin average burnup that is outside of NRC licensing limits. This was done purposefully to assure that the analyzed fuel rod to be a conservatively limiting case. The higher final burnup assures a large amount of fuel pellet swelling without exceeding the model's applicable range. Likewise, cladding oxidation is largely dependent on the residence time in the reactor, allowing for it to be well captured in this longer case.

3.2 Validation Results

The first parameters investigated for validation of FRASP are the fuel pellet outer and cladding inner radii. Despite the radical differences in the two methods used to calculate these radii, FRASP and FRACAS-I agree very well, as illustrated in Figures 3-2 and 3-3 for the axial peak power node.

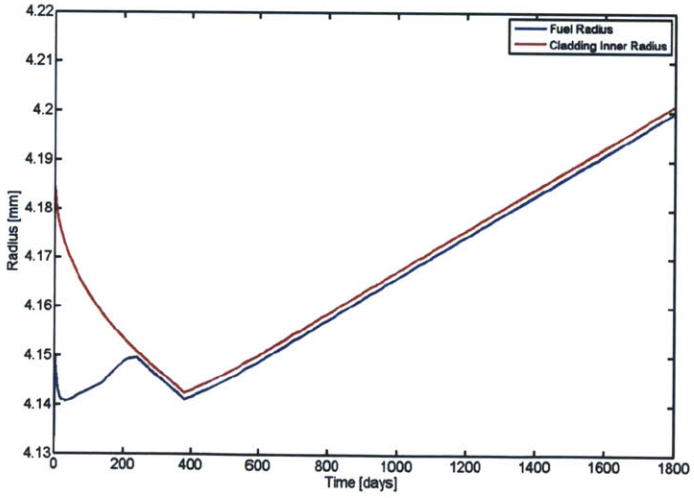

Figure 3-2: **Fuel pellet outer and cladding inner radii predicted by FRASP for the peak LHGR axial node**

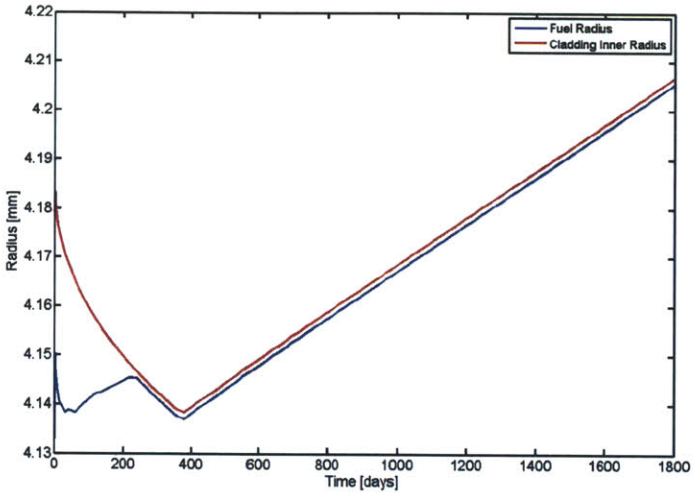

Figure 3-3: **Fuel pellet outer and cladding inner radii predicted by FRACAS-I for the peak LHGR axial node**

By observing the fuel pellet outer and cladding inner radii, the presence of several important fuel pin behavior trends can be observed. These trends can be isolated into three separate regions, as shown in Figure 3-4.

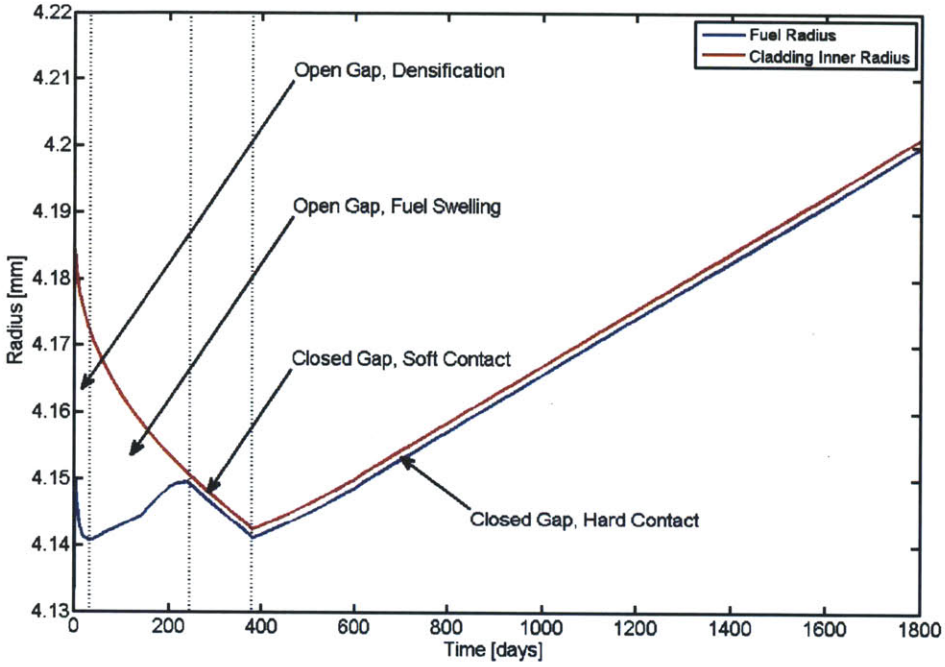

Figure 3-4: **Labeled description of fuel-cladding gap behavior over the fuel rod's lifetime**

The first labeled region shows the densification process on the fuel pellet due to the sintering of UO_2. As the fuel pellet density increases, the volume of the pellet decreases, as evidenced by a reduction in the fuel pellet radius. Since the densification of the fuel pellet is limited to early in the lifetime of the pin, the slope of the fuel pellet outer radius flattens towards the end of this first region as the fuel pellet swelling begins to dominate fuel pellet behavior.

In the second region, soft contact begins to occur between the fuel pellet and cladding. As this soft contact occurs, the outer radius of the fuel pellet is dictated by the inner radius of the cladding as relocation strain is recovered. This recovery process, as discussed in Section 2.3, physically represents a reduction in free space between the fuel pellet fragments.

With regard to the cladding, both the first and second labeled regions represent the period of cladding creep down. During this period, the core system pressure is

significantly higher than the gas pressure acting on the interior surface of the cladding. This pressure difference in turn causes the cladding to deform in an effort to relieve internal stresses.

In the final labeled region, the growth of the fuel pellet associated with swelling dictates the structural state of the cladding. At this point, half of the relocation strain of the fuel pellet has been recovered and the fuel pellet and cladding are now in hard contact. As the fuel pellet grows, the cladding is deformed so as to maintain a minimum fuel-cladding gap size.

It is in this final region that stress-induced fuel pellet deformation will be observed. Under these conditions, FRACAS-I uses the fuel pellet outer radius, via the rigid pellet model, to dictate the dimensions of the cladding. Alternatively, FRASP uses interfacial pressure and axial friction to couple the mechanics of the fuel pellet and cladding, as described in Section 2.6.

During the fuel pin's lifetime, the maximum temperature in the fuel pellet evolves, as shown in Figure 3-5 for the axial peak power pin. Early in the fuel pin's life, the differences between FRASP and FRACAS-I result in slightly different temperatures during the open gap regime. However, after the fuel pellet and cladding come into contact, the temperature differences between FRASP and FRACAS-I effectively disappear.

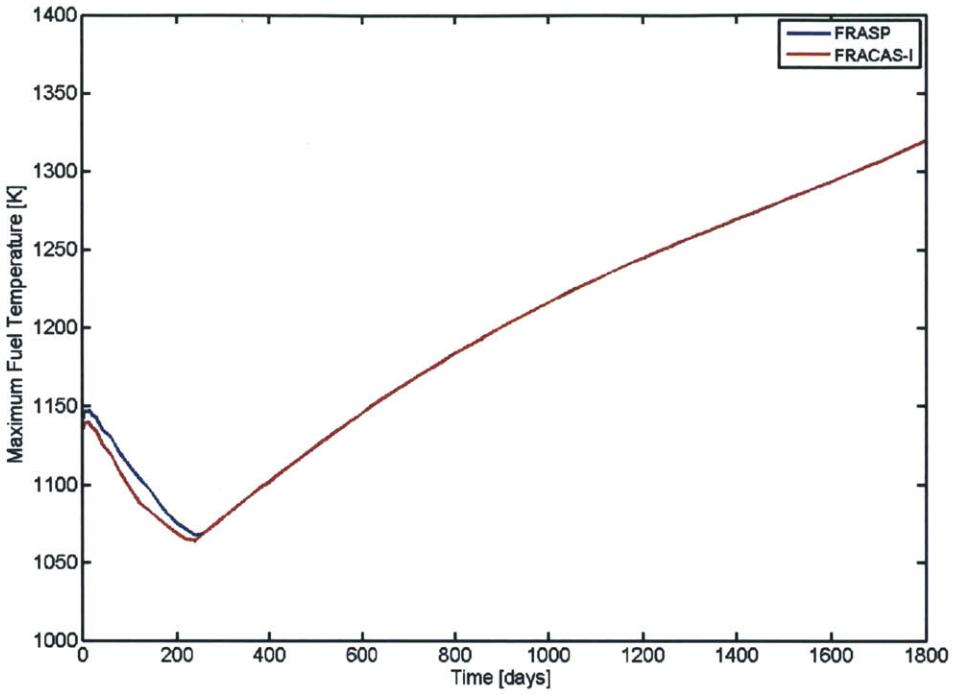

Figure 3-5: **Maximum fuel pellet temperature of the peak LHGR axial node**

As the fuel temperature between the two models is identical, shown in Figure 3-5, the thermal expansion of the fuel pellet will also be identical in the third region. Likewise, the burnup used by both models is the same. This translates to both models making use of the same fuel swelling strain, which is linearly dependent on burnup in FRAPCON-3.3. Because both FRASP and FRACAS-I are using the same strains, any differences in the growth rate of the fuel pellet will be evidence of stress-induced fuel pellet deformation.

Visual inspection of the radial growth rate of the cladding hoop strain after the onset of hard contact, illustrated in Figure 3-6, clearly shows FRASP to predict slower radial growth than FRACAS-I. This reduction in growth rate confirms the occurrence of stress-induced fuel pellet deformation. For this comparison, the cladding hoop strain was chosen rather than the fuel surface displacement largely for ease of extraction from FRAPCON output files as well as providing visual reference for the

onset of PCMI.

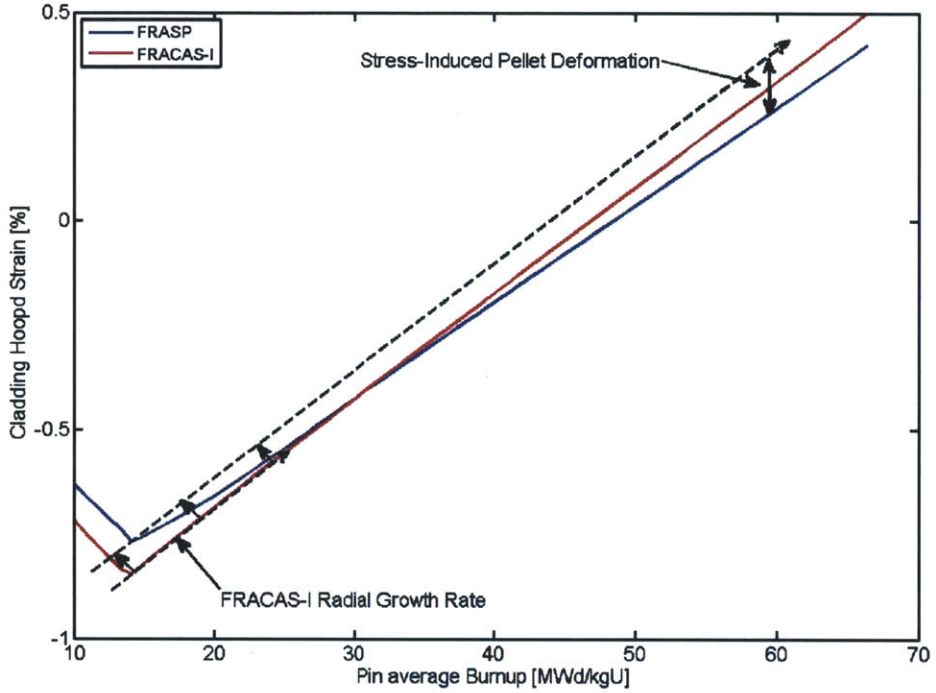

Figure 3-6: **Illustration of stress-induced fuel pellet deformation predicted by FRASP**

Figure 3-7 shows the maximum and minimum differences in the total cladding strain components over entire irradiation time. These differences are evaluated at the same axial location for each time step. Also shown is the average difference of each component over both the fuel rod's length and irradiation time. It should be noted that the values reported in Figure 3-7 do not correspond to the same locations or time steps. While disagreement exists between the two models, particularly in regard to axial and radial strain, these differences are within acceptable bounds, especially given the drastically different structural models.

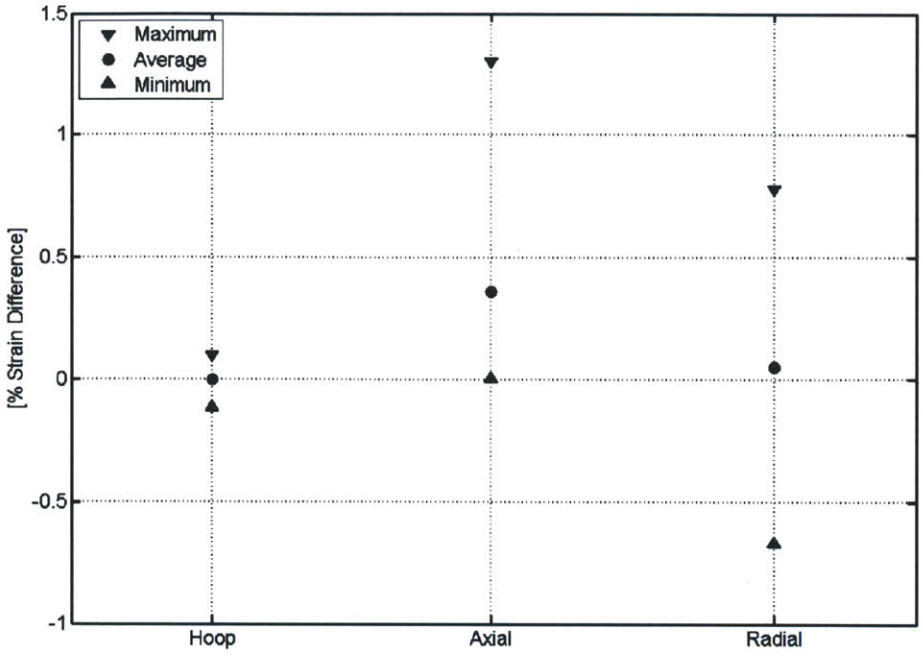

Figure 3-7: **Difference in the calculated total cladding strain components by FRASP and FRACAS-I**

At the end of irradiation in the reactor, the fuel pin will retain the permanent strains incurred during operation. Figure 3-8 shows the differences in calculations of these strain components between the two mechanical models. Similar to Figure 3-7, the permanent strains are within acceptable bounds of FRACAS-I.

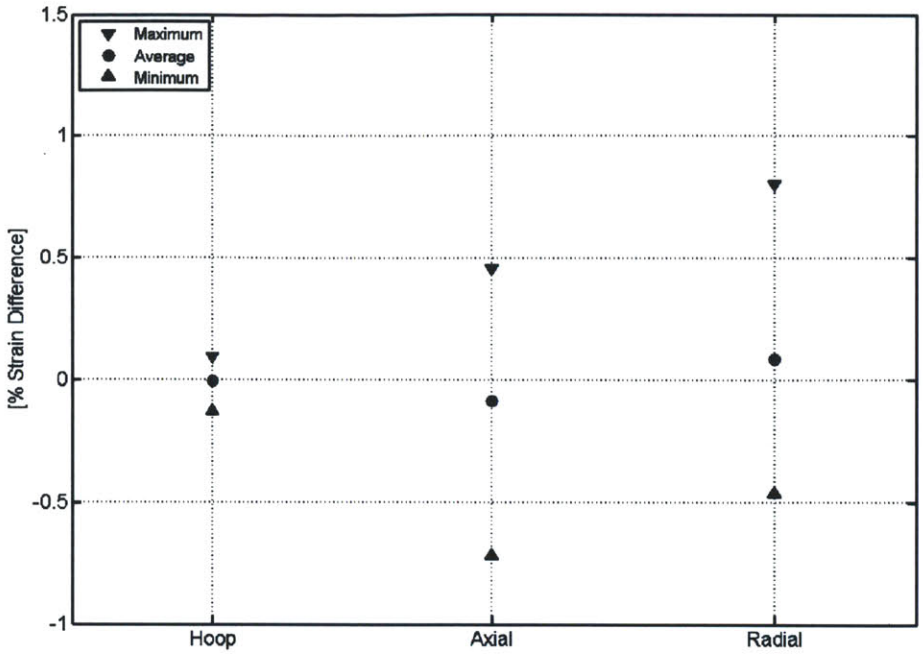

Figure 3-8: **Difference in the calculated permanent cladding strain components by FRASP and FRACAS-I**

Unlike the other two components, the hoop strain values, both total and permanent, found by FRASP and FRACAS-I are in very close agreement with one another. This is especially encouraging, as the cladding hoop strain is considered to be a primary criterion for limiting fuel pin lifetime (NRC, 2007).

The relatively larger differences observed in the axial and radial strain components between the two models are due to FRASP's incorporation of axial coupling via interfacial friction, use of cladding irradiation growth as a permanent strain, and the treatment of radial stress.

The effect of axial coupling is particularly evident in Figure 3-9, near the bottom most axial nodes of the fuel pin at the occurrence of pin-wide hard contact. Near the top of the rod, little difference exists between FRASP and FRACAS-I, as both models axial lock the fuel pellet and cladding and there are relatively small forces being communicated from non-local nodes above. However, at the bottom of the rod

all the friction applied to couple the fuel pellets and cladding above is experienced locally, causing higher axial strains.

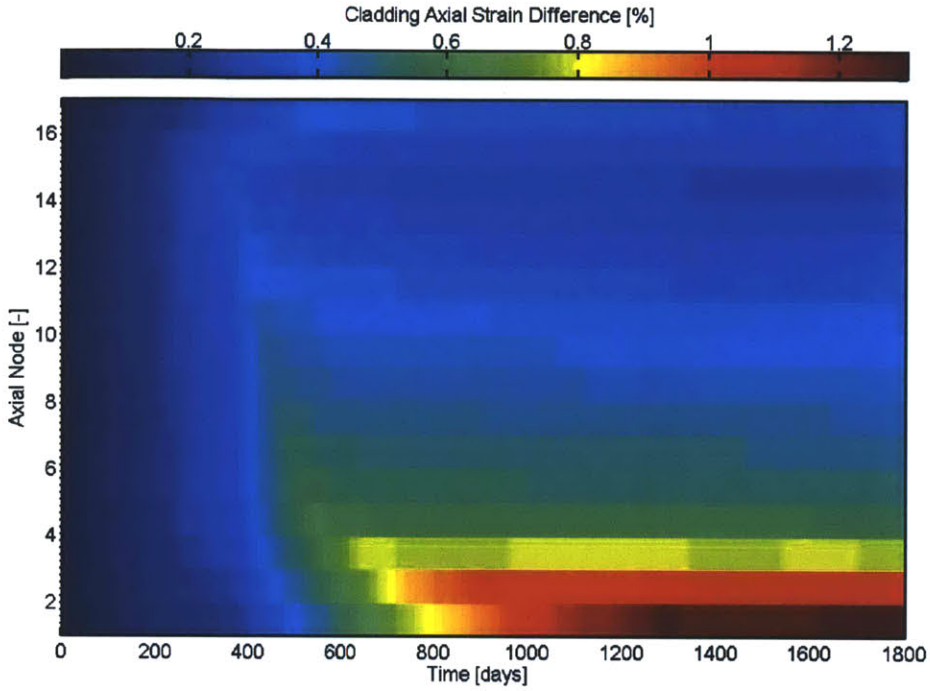

Figure 3-9: **Difference in calculated cladding axial strains between FRASP and FRACAS-I**

Nowhere in the fuel pin is the axial strain calculated by FRASP less than that found by FRACAS-I. This is simply due to the fact that FRACAS-I does not treat the irradiation induced axial growth of the cladding as a permanent strain in its structural calculations. Rather, FRACAS-I simply applies this axial growth to the total length of the cladding after the application of structural mechanics. Alternatively, FRASP treats the axial growth of the cladding as an anisotropic swelling strain within its structural calculations.

Lastly, the incorporation of radial stress, which is neglected by FRACAS-I, into FRASP directly affects the axial creep down of the cladding, as illustrated by Figure 3-10. Note that the permanent axial strain shown in Figure 3-10 has had the axial growth component subtracted in order to be compatible with the outputs of

FRAPCON. The difference in axial creep prior to hard contact results from the conservation of volume, applied via the Prandtl-Reuss Flow Rule, accommodating lower radial creep strains, as seen in Figure 3-11.

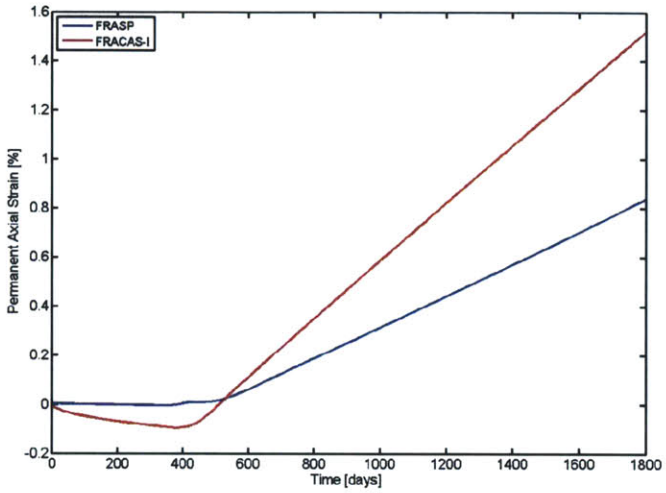

Figure 3-10: **Permanent cladding axial strain calculated for the peak LHGR axial node**

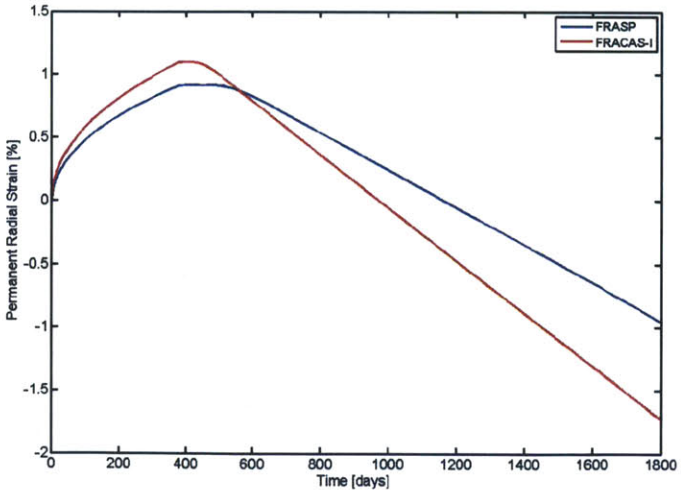

Figure 3-11: **Permanent cladding radial strain calculated for the peak LHGR axial node**

Figure 3-12 shows the differences in radial strain to be almost the inverse of the differences in axial strain observed in Figure 3-9. These differences result from the lower axial strain at the top of the fuel pin and inclusion of cladding axial growth as a swelling term within FRASP.

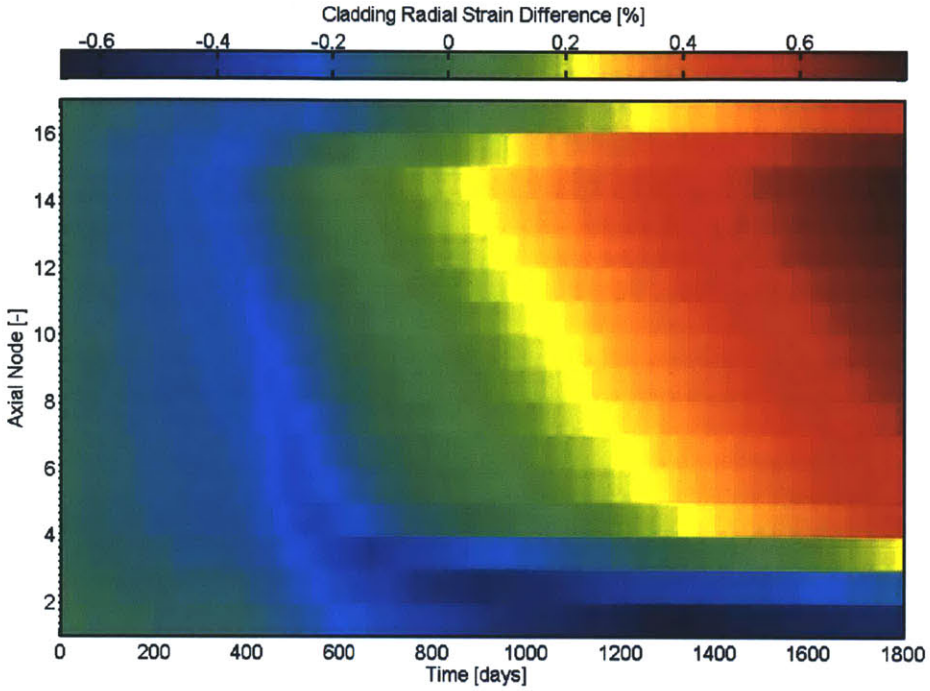

Figure 3-12: **Difference in calculated cladding axial strains between FRASP and FRACAS-I**

Because the axial growth is included in the axial strains, axial locking of the fuel pellet and cladding tends to require lower axial stress in FRASP, illustrated in Figure 3-13, which in turn leads to less axial permanent straining via creep. Due to the conservation of volume, less permanent axial straining due to lower axial stresses directly translates to increased permanent radial strain, assuming constant permanent hoop strain. This is evident after the onset of hard contact in Figures 3-10 and 3-11, and explains the trends of Figure 3-12. Along with FRASP's treatment of radial stresses, the treatment of irradiation growth within the structural model leads to lower stresses which affect how permanent strains are allocated.

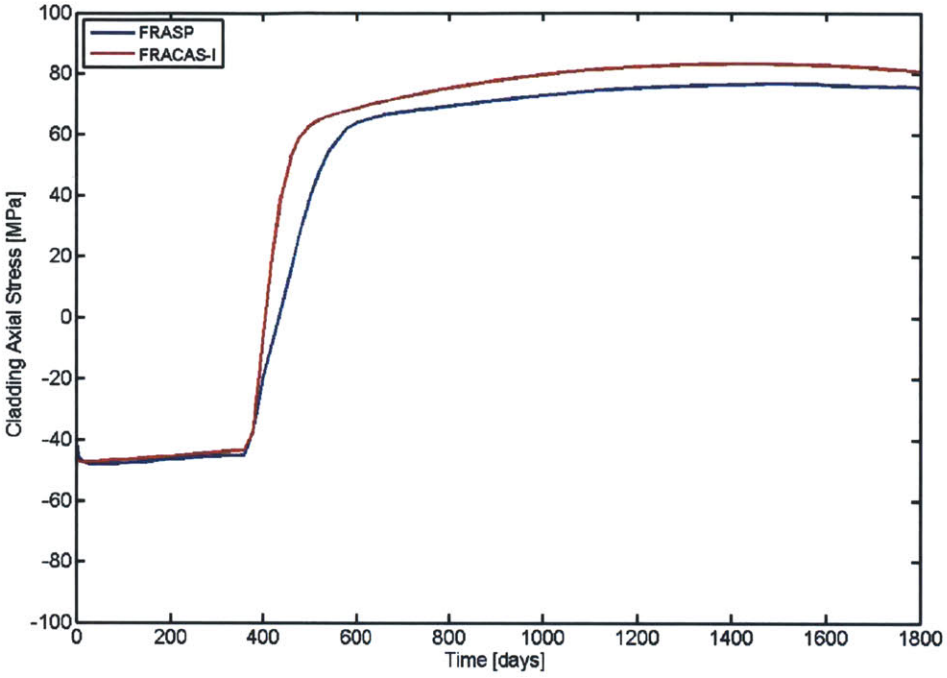

Figure 3-13: **Average cladding axial stress observed for the peak LHGR axial node**

Unlike the axial stress, FRASP generally predicts a higher hoop stress within the cladding, as seen for the peak axial node in Figure 3-14. The exception to this is in the vicinity of the initial onset of hard contact, during which the two models disagree on the appropriate amount of applied interfacial pressure, illustrated for the same node in Figure 3-15.

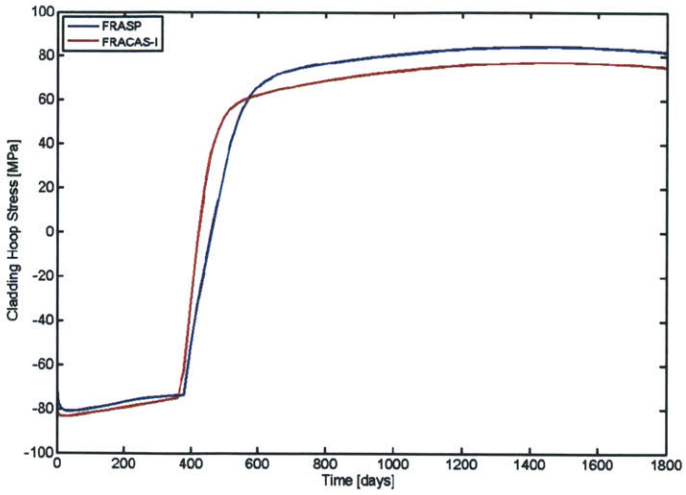

Figure 3-14: **Average cladding hoop stress observed for the peak LHGR axial node**

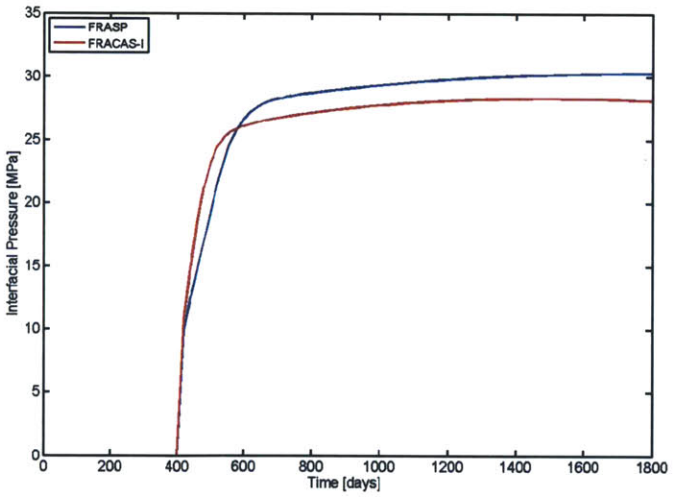

Figure 3-15: **Interfacial pressure observed for the peak LHGR axial node**

The higher interfacial pressure experienced by FRASP than FRACAS-I is further evidence of stress-induced fuel pellet deformation. Because the fuel pellet and cladding behaviors are directly coupled via interfacial forces, as opposed to calculating the interfacial pressure based on rigid pellet imposed cladding deformation, the

fuel pellet also experiences structural effects from PCMI. The deformation of the fuel pellet will absorb some portion of the interfacial pressure, which is primarily absorbed in deformation of the cladding, accounting for the higher interfacial pressure predicted by FRASP.

The largest stress difference between FRASP and FRACAS-I can be observed in the treatment of radial stress. As previously mentioned, FRASP differs from FRACAS in that it does not neglect radial stress within the cladding, shown in Figure 3-16. This difference primarily affects the allocation of permanent strain via the Prandt-Reuss Flow Rule, as has been discussed.

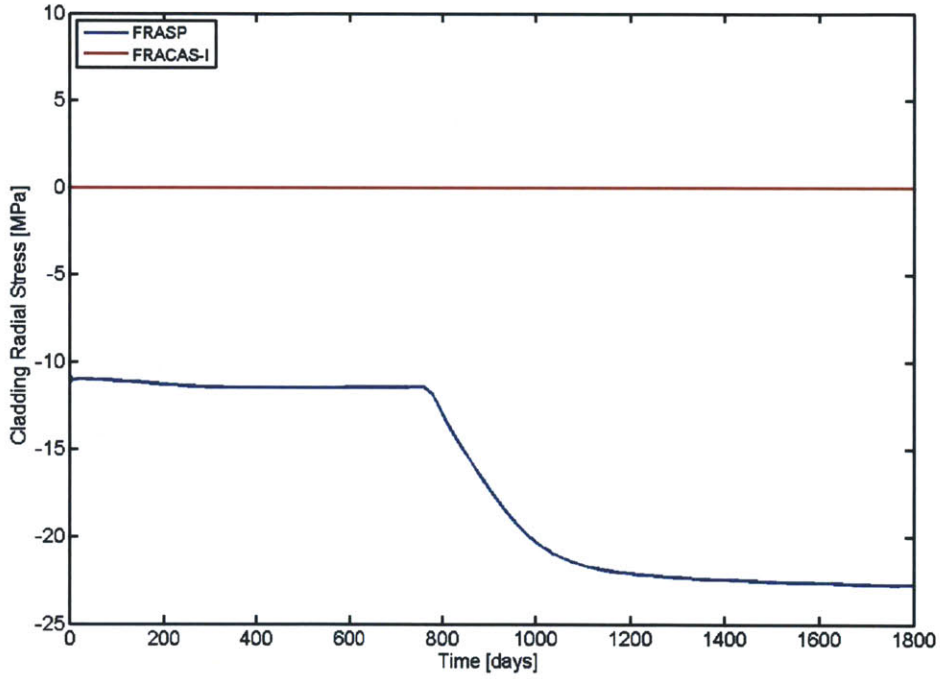

Figure 3-16: Average cladding radial stress observed for the peak LHGR axial node

In evaluating fuel pin design, the axial elongation of the cladding is important in avoiding fuel bowing. Therefore, it is critical that FRASP provides accurate predictions to fuel designers for this parameter. Figure 3-17 illustrates the different pre-

dicted cladding axial elongations between FRASP and FRACAS-I. The higher values found by FRASP are largely the manifestation of previously discussed elements, such as creep down and axial coupling, which have a cumulative effect. FRASP also predicts larger cladding axial extension at all points in the fuel pin's lifetime which at least ensures conservatism.

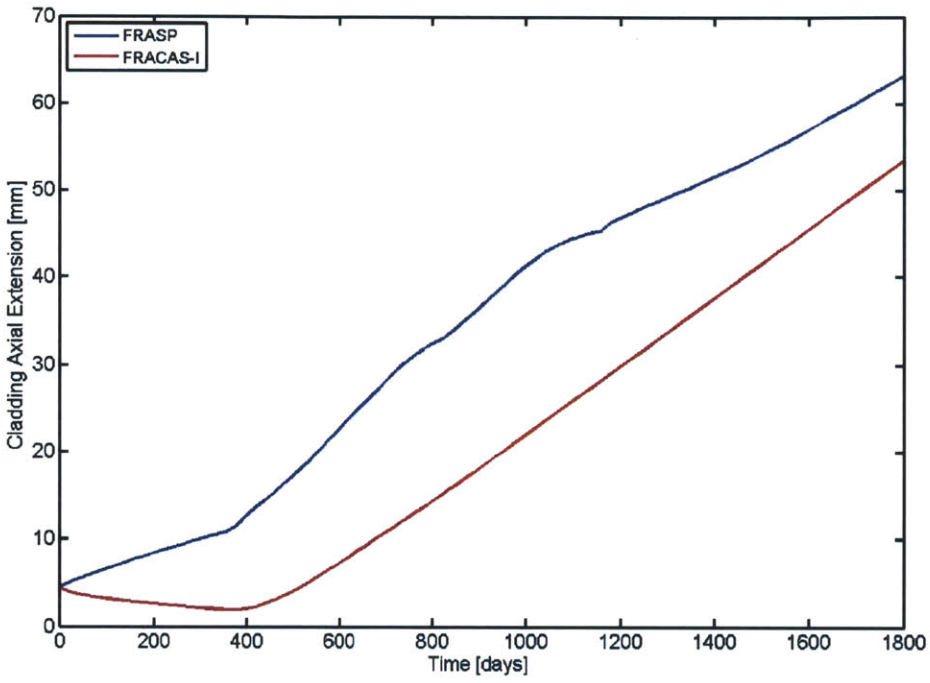

Figure 3-17: **Total observed cladding axial elongation throughout the fuel rod lifetime**

Also of interest in designing nuclear fuel is the plenum pressure within the fuel pin cladding. The plenum pressure, along with the gas composition, plays a large role in finding the thermal conductivity of the fuel-cladding gap, and thus the temperature of the fuel pellet. The plenum pressure must also be considered in evaluating the long term storage of spent fuel pins. The values for this parameter found by FRASP and FRACAS-I are shown in Figure 3-18. The differences seen in Figure 3-18 largely result from differences in the available gas volume in the fuel pin, shown in Figure 3-19, which are in turn related directly to values calculated by the structural models.

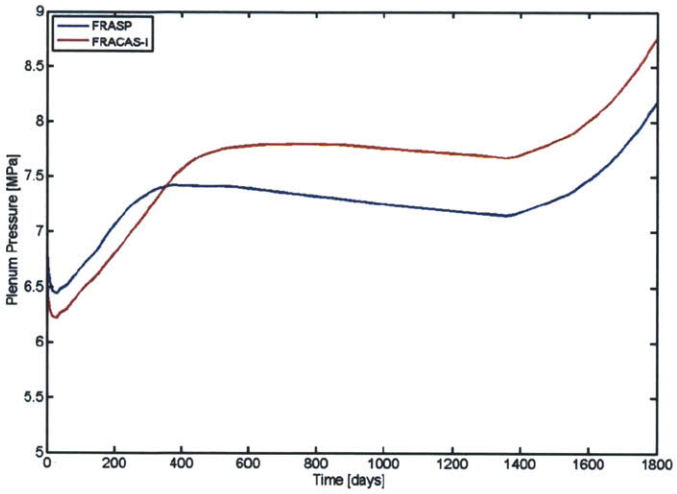

Figure 3-18: **Plenum pressure observed throughout the fuel rod lifetime**

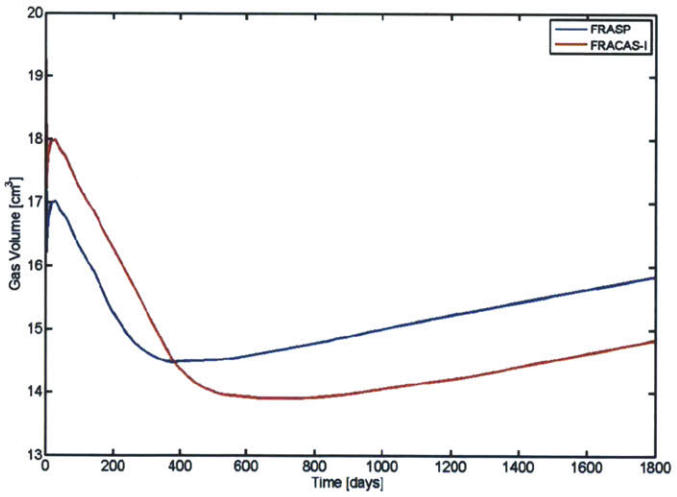

Figure 3-19: **Void volume observed throughout the fuel rod lifetime**

As previously mentioned, many parameters throughout the fuel pin, FGR etc., are directly related to the fuel pellet temperature. Figure 3-5 illustrated the differences that existed between the fuel temperatures found by using FRASP and FRACAS-I are minimal and effectively disappear after the fuel-cladding gap closes. These differences in fuel centerline temperature between the two codes largely result from the difference

in the fuel-cladding gap size. This can be seen by directly comparing the difference in calculated gap sizes and fuel maximum temperatures across the fuel pin's length and lifetime, shown in Figures 3-20 and 3-21 below.

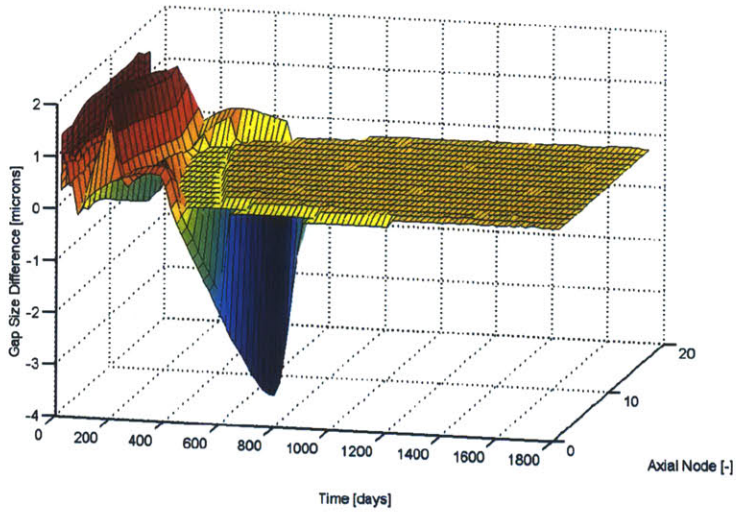

Figure 3-20: **Difference in the size of the fuel-cladding gap size observed between FRASP and FRACAS-I**

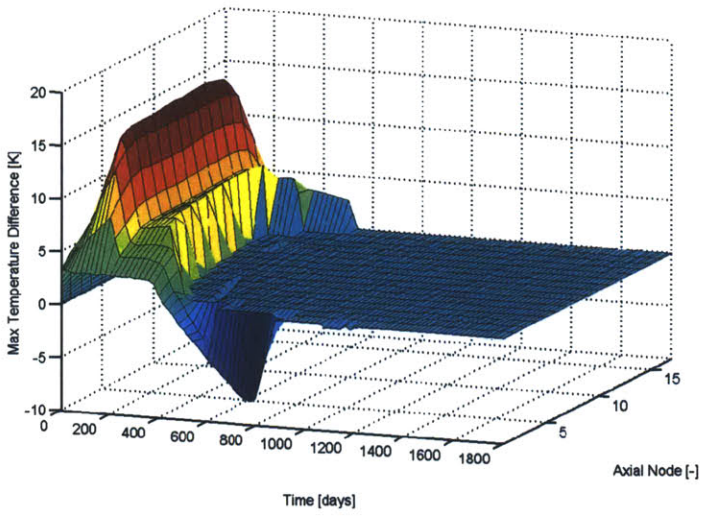

Figure 3-21: Difference in the maximum fuel pellet temperature observed between FRASP and FRACAS-I

It is in these differences that the incorporation of FRASP into FRAPCON plays a role in many non-structural parameters. The rather minimal maximum fuel temperature difference of 15.4K between the two models implies that few of these parameters will be affected solely by the implementation of FRASP.

Preliminary validation of FRASP within the framework of FRAPCON-3.3 has shown that the new PCMI model does, in fact, allow for the prediction of stress-induced fuel pellet swelling. As expected, some mechanical predictions can be observed to disagree between FRASP and FRACAS-I, though the majority of these differences are directly attributable to FRASP's improved models. The application of the new model has also proven to introduce minimal feedback effects on non-mechanical fuel rod parameters. While this validation has been limited to average PWR conditions, it has not revealed FRASP to exhibit any dramatically unexpected behavior or general performance concerns.

Chapter 4

Analyses of SiC Clad Fuel Rods Using FRAPCON-EP

To evaluate the effect of FRASP's implementation on the fuel performance predictions for SiC clad fuel rods in a PWR environment, FRAPCON-EP and FRAPCON-3.3 were both used to assess four limiting cases. While SiC cladding potentially provides the ability for fuel rods to reach much higher burnups than Zircaloy (Carpenter et al., 2010), this study focuses on peak fuel pin burnups close to what is currently practiced in the American commercial reactor fleet. This was done in an attempt to show the fuel performance implications of immediate adoption of SiC in a PWR reactor, taking as a reference the Seabrook Station Nuclear Power Plant.

The conditions used for the validation of FRASP in Section 3.1, were representative of the Seabrook reactor prior to its recent 7% uprate in operating power. The conditions associated with the current core design of the Seabrook reactor are presented in Table 4.1.

Table 4.1: **Current Seabrook core conditions**

Core Parameter	Units	Value
Coolant Inlet Temperature	K	565
Coolant Pressure	MPa	15.5
Coolant Mass Flux	kg/s-m^2	3336
Core Average LHGR	kW/m	19.16

Three test cases were selected as being reasonable applications of SiC cladding in commercial reactors under current operational practices. All cases analyze the peak discharge burnup fuel rod, which is presumed to be the core limiting rod. An initial case using Zircaloy cladding will provide a baseline for comparison of SiC fuel performance to current cladding under identical conditions. The first test case represents the replacement of Zircaloy cladding with SiC without further changes to the fuel rod. The second test case expands on the first case by introducing a central void to the fuel, decreasing the total fuel pellet volume by approximately 10%. The final test case includes both the SiC and annular fuel pellet along with a hypothetical 10% increase in the power of the analyzed rod. Relevant parameters for each case are listed in Table 4.2.

Table 4.2: **Description of cases to be analyzed**

	Cladding Type	Fuel Pellet Type	Total Core Power
Case #1	Zircaloy	Solid	3659 MW_t
Case #2	SiC	Solid	3659 MW_t
Case #3	SiC	Annular	3659 MW_t
Case #4	SiC	Annular	4025 MW_t

All of the cases were evaluated with FRAPCON-3.3 using FRACAS-I and FRAPCON-EP using FRASP. The initial Zircaloy clad case was also evaluated with FRAPCON-3.4 using its new FEA model. This model uses more sophisticated structural mechanics methods than FRACAS-I and FRASP along with updated Zircaloy material properties. As of this writing, however, the FEA model in FRAPCON-3.4 has not

been modified for the simulation of SiC clad fuel rods. For this reason, FRAPCON-3.4 is not included in the analysis of the SiC clad cases.

None of these three SiC cases are new applications of SiC cladding in PWR environments (Carpenter et al., 2010). Novel from other studies, however, is the application of the improved fuel behavior and mechanical models of FRAPCON-EP with FRASP. The primary purpose of evaluating these cases is to compare and contrast the predicted fuel rod behavior between the new and old fuel performance codes.

The input file for each of the evaluated cases can be found in Appendix A.

4.1 Power History Evaluation

Previous PWR fuel performance studies, for both Zircaloy and SiC cladding, have evaluated peak burnup fuel rods using simple power profiles (Carpenter et al., 2010; O'Donnell et al., 2001). These power profiles assumed the rod to be at a constant peak power level for a length of time, followed by a period in which the rod power is linearly decreased with time to an EOL power, Shown in Figure 4-1.

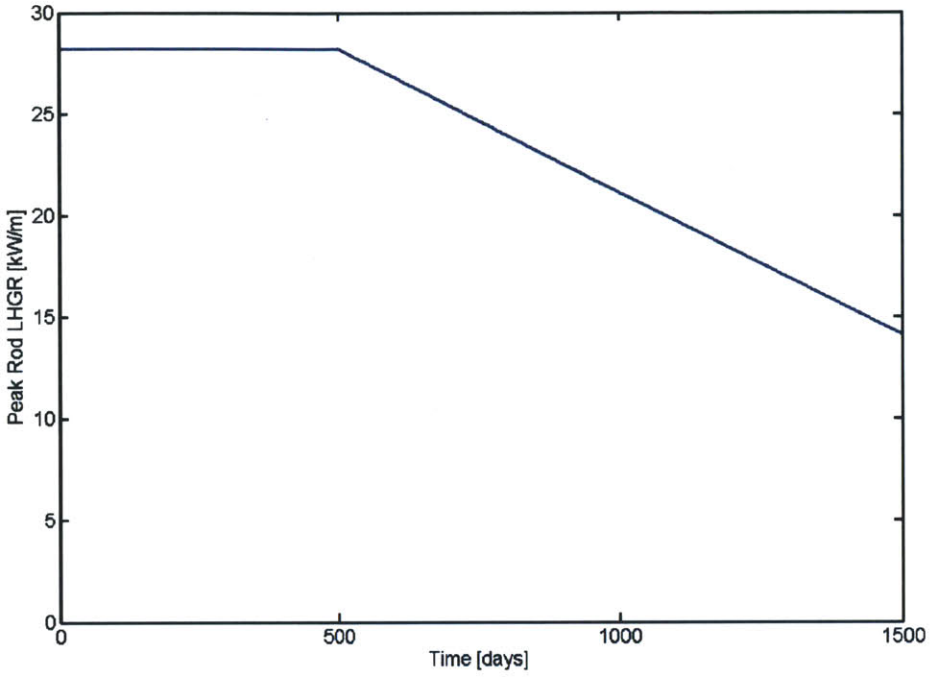

Figure 4-1: **Power history characteristic of those used in previous studies**

The simple power histories assumed in these studies are the result of lack of information on core peaking for a single fuel rod throughout its lifetime. However, thanks to information from recent full core simulations using SIMULATE (Dobisesky, 2011), this study is able to make use of more sophisticated power histories.

Current PWR operation practices utilize 18 month cycles with batch burnups of approximately 20 MWd/kgU. In this arrangement, no fuel assembly is exposed to more than three cycles in the core. Using SIMULATE, these typical operational conditions were evaluated for the operating conditions at the Seabrook reactor in an equilibrium cycle. The SIMULATE outputs were used to backtrack the previous locations of the assembly containing the peak burnup fuel rod as it is cycled through the core. Once the location of the assembly is known for each of the three cycles it resided in the reactor, the peaking factors for each location over the course of a cycle can be extracted and combined into a single assembly history. The peaking factor of the assembly containing the peak burnup rod as it was cycled through the core is

illustrated in Figure 4-2. Note that the burnup reported along the horizontal axis of Figure 4-2 represents the core average burnup, not that of the peak burnup rod.

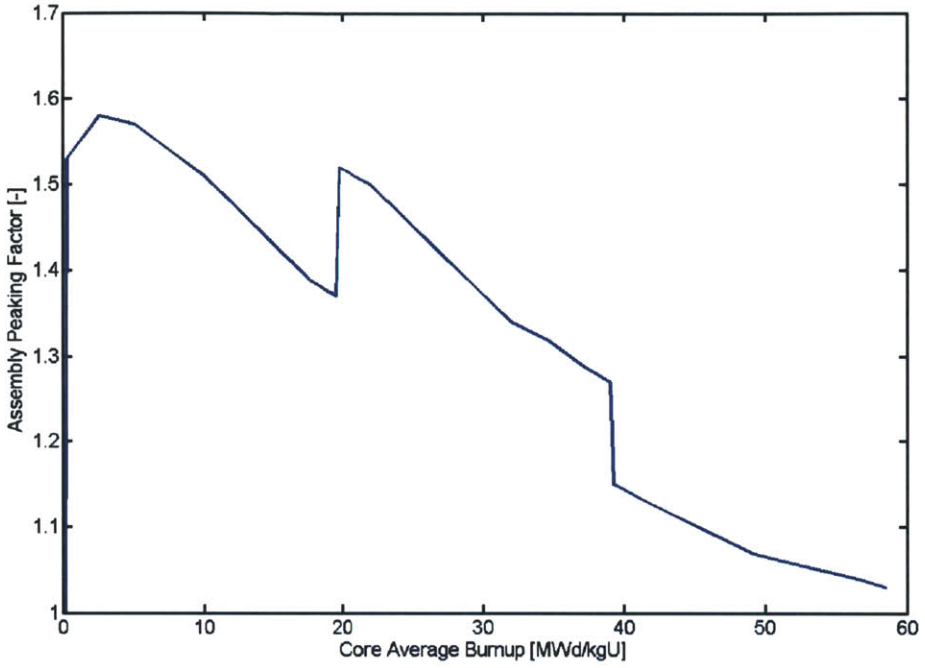

Figure 4-2: **Peaking factor history of the peak burnup assembly from SIMULATE results**

The LHGR associated with this reconstructed history was then evaluated by simply multiplying the core average LHGR of 5.84 kW/ft (19.16 kW/m) by the peaking factor. The core average burnup was converted to Effective Full Power Days (EFPDs) using Equation 4.1. Note that for the purposes of this study, normal days will be synonymous for EFPDs.The power history profile associated with this assembly peaking factor is shown in Figure 4-3 .

$$BU_{Core} = \frac{\dot{Q}_{core} \times t}{m_U} \tag{4.1}$$

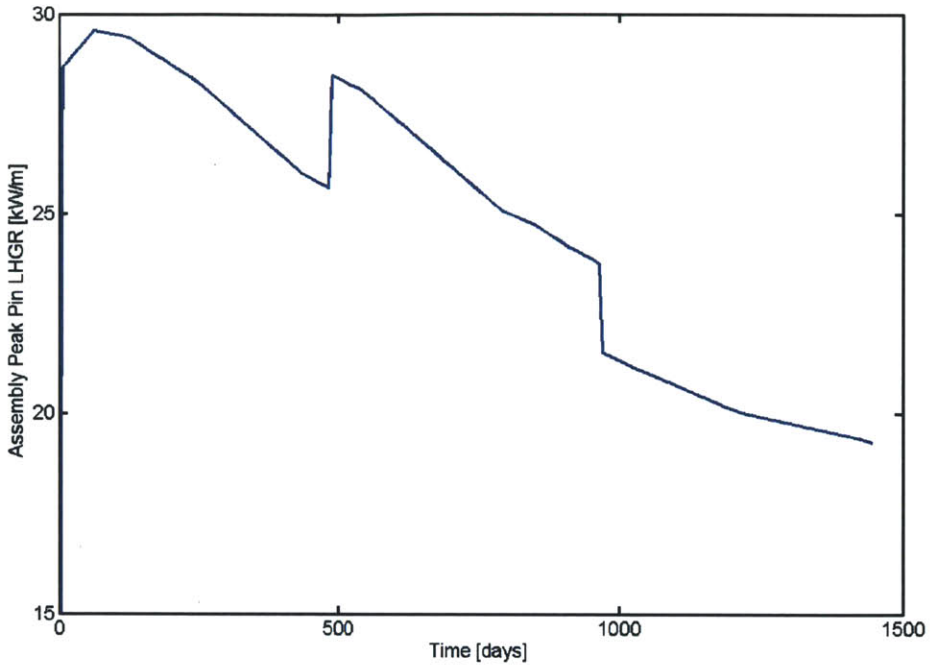

Figure 4-3: **Power history of the peak burnup assembly**

As an individual assembly is irradiated in a reactor, the location of the peak assembly rod migrates to various fuel rod locations based on build up and depletion of fissile isotopes. Because of this, the power profile reported in Figure 4-3 is not representative of the actual peak burnup fuel rod, and depicts an overly-conservative peak rod burnup of 74.03 MWd/kgU, as opposed to the reported value of 66.8 MWd/kgU. To accommodate the uncertainty of the varying location of the peak rod within the assembly of interest, the power levels in each of the three cycles were reduced by 10% and averaged to a constant value for each cycle, shown in Figure 4-4. This resulted in a final peak rod burnup of 66.63 MWd/kgU which is acceptably close to the reported value.

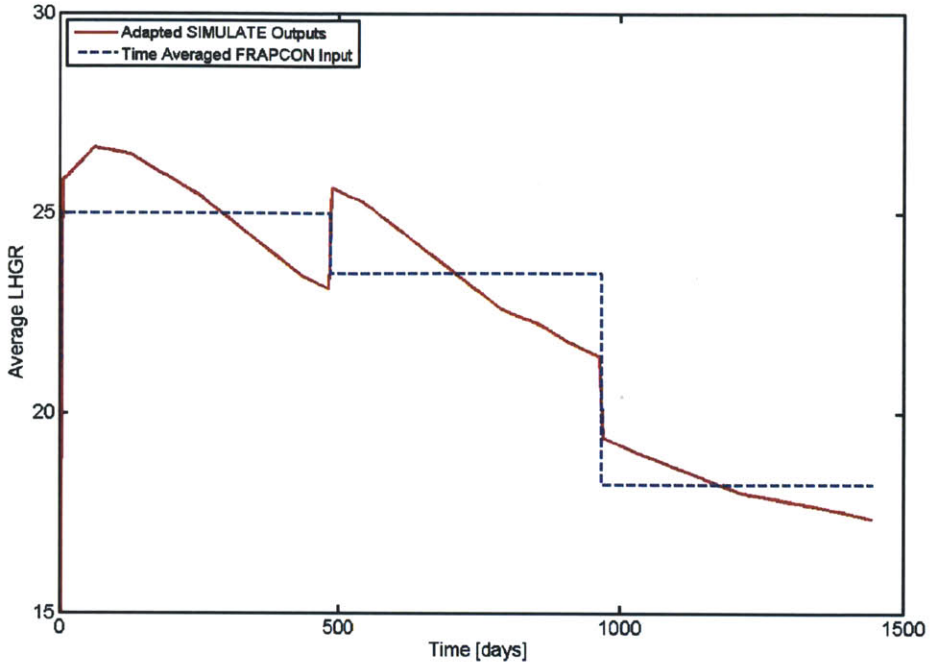

Figure 4-4: **Adapted power histories of the peak burnup fuel rod**

Through its irradiation over multiple cycles in the reactor, the axial power shape of a fuel pin changes, again due to fissile isotope build up and depletion. For this evaluation, it is assumed that these axial peaking factor changes have no effect on the total power produced by a single fuel pin, only on the location of power generation within the pin. In order to incorporate these changes, axial power shapes provided in the Seabrook UFSAR were utilized. These power shapes were given for the Beginning-of-Life (BOL) and End-of-Life (EOL) of fresh, once-burned and twice-burned fuel pins. An intermediate Middle-of-Life (MOL) axial power shape was simply interpolated for each cycle to help prevent dramatic axial power changes between transitions. Figures 4-5, 4-6, and 4-7 depict the evolving axial power shape for each of the three cycles.

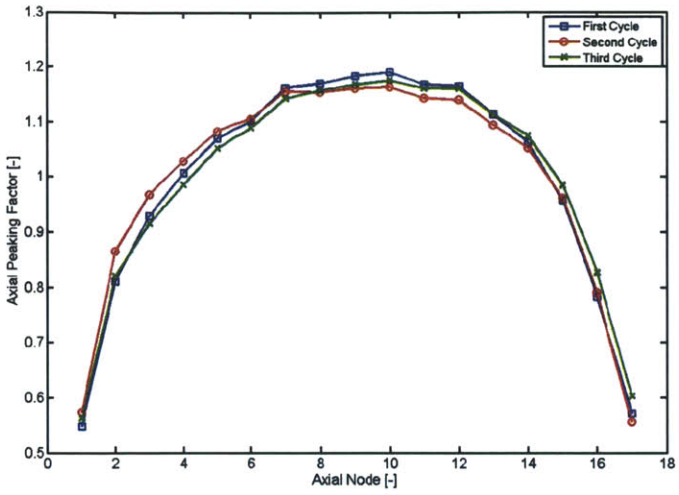

Figure 4-5: **BOL axial power shape associated with each irradiation cycle**

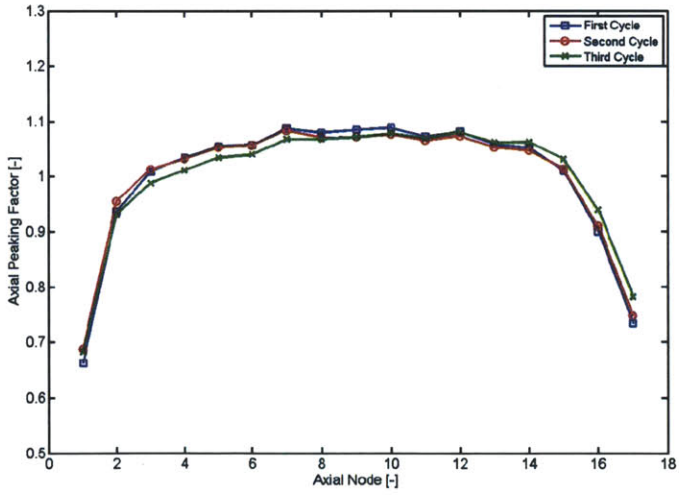

Figure 4-6: **MOL axial power shape associated with each irradiation cycle**

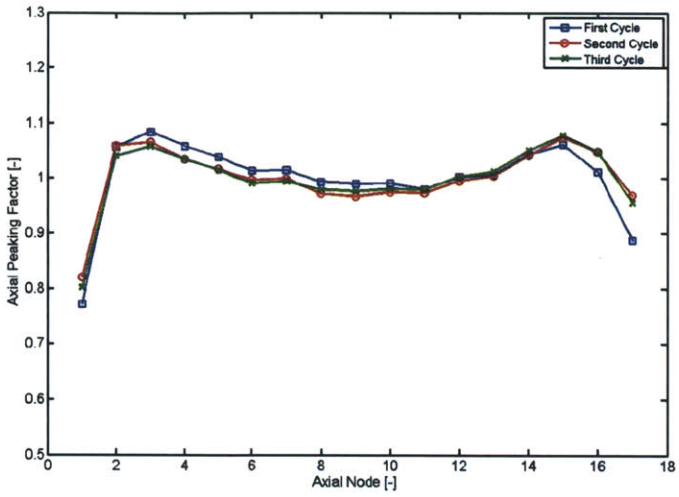

Figure 4-7: **EOL axial power shape associated with each irradiation cycle**

Each power cycle, which is assumed to have constant fuel pin power, experiences three different axial power shapes for equal amounts of time. By applying these changes, the fuel pin experiences a more realistic dynamic power history, as shown in Figure 4-8. The power history for the axial nodes of the fuel pin's BOL and EOL peak power locations are depicted in Figure 4-9.

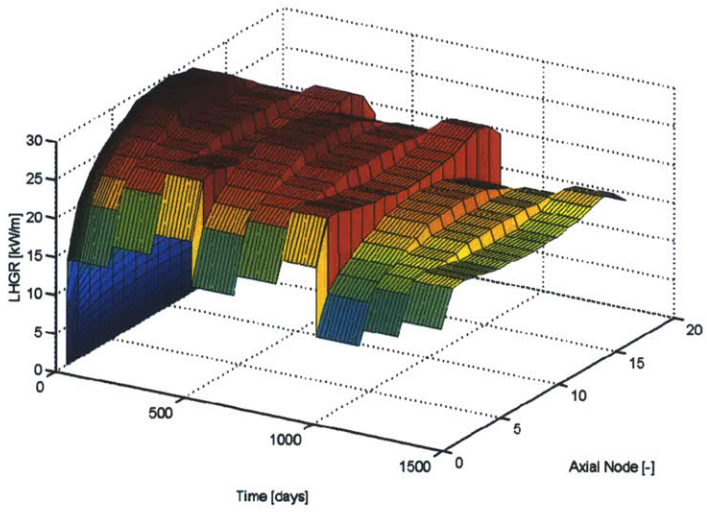

Figure 4-8: **Axial LHGR distribution throughout the fuel rod lifetime**

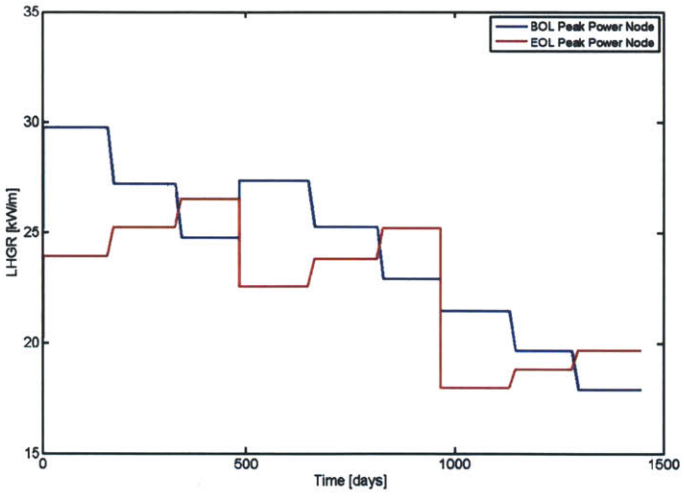

Figure 4-9: **Power histories of the BOL and EOL peak LHGR nodes**

4.2 Base Zircaloy-Clad Case

The first case evaluated is simply that of a Zircaloy clad fuel rod identical to those evaluated in the SIMULATE modeling presented in Section 4.1. This case is intended to provide a comparison between FRAPCON-EP, FRAPCON-3.3 and FRAPCON-3.4 for current PWR operation. It will also provide a baseline for the evaluation of SiC cladding.

While the final average burnup achieved by this fuel pin, 66.63 MWd/kgU, is beyond the NRC accepted limit of 62 MWd/kg, it is assumed to be appropriate for the purposes of this study. The as-fabricated fuel pin parameters are listed in Table 4.3.

Table 4.3: **Solid pellet fuel rod parameters**

Parameter	Units	Value
Fuel Rod Pitch	mm	12.59
Cladding Outer Diameter	mm	9.5
Cladding Thickness	mm	0.571
Fuel-Cladding Gap Thickness	μm	82.5
Fuel Pellet Outer Diameter	mm	8.19
Fuel Pellet Void Radius	mm	0.0
Active Fuel Height	m	3.66
Fuel Pellet Density	%	95.0
Initial U^{235} Enrichment	%	4.5
Mass of Uranium in Rod	kgU	1.784
Plenum Height	m	0.254
Initial Cold Internal Helium Pressure	MPa	2.41

Because of the updated fuel swelling models and the method of their application to the fuel pellet, Figure 4-10 shows the fuel pellet outer radius predicted by FRAPCON-EP to have a different shape from the two other codes immediately after the onset of hard contact. The fuel pellet radius predicted by FRAPCON-3.4 agrees well with FRAPCON-3.3 for the first cycle, but is closer to FRAPCON-EP for the second and third cycles. While Section 3.2 showed some effect of the implementation of FRASP on the shape of the fuel pellet outer radius, it is relatively minor. Therefore, the major changes seen in Figure 4-10 between FRAPCON-EP and FRAPCON-3.3 are much more likely the result of the more sophisticated fuel swelling models applied to FRAPCON-EP. While FRAPCON-3.4 makes use of similar fuel swelling models to FRAPCON-3.3, the more intricate FEA model predicts the fuel outer radius to behave more like that of FRAPCON-EP, especially towards EOL. This may be coincidence, but in fact FRAPCON-EP's fuel models do allow for shrinkage of the original porosity when fuel pellet is subjected to higher pressures, and the FRAPCON-3.4 swelling is somewhat retarded by the contact with the cladding

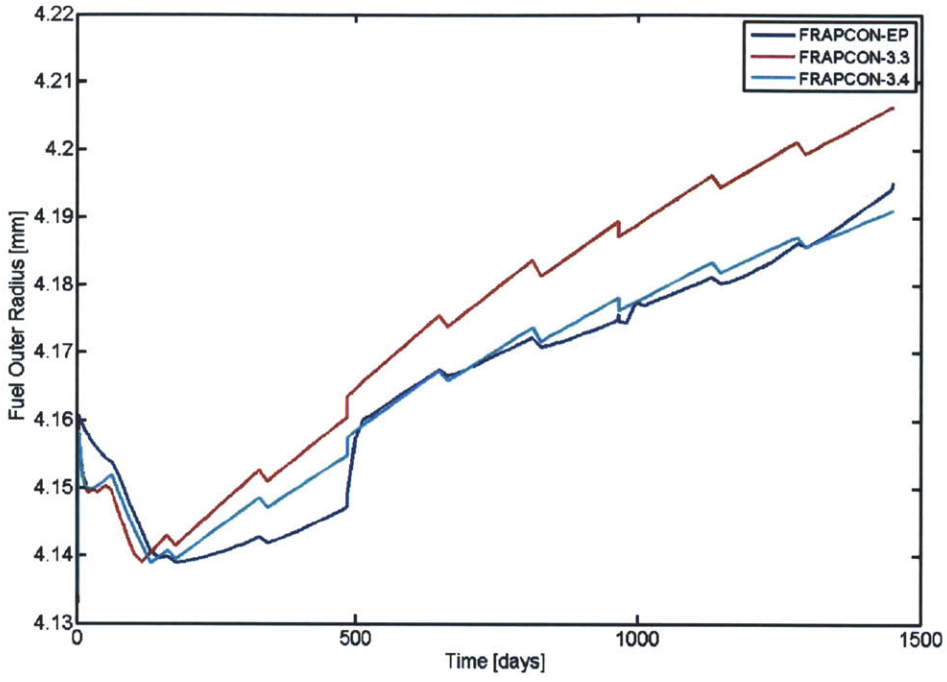

Figure 4-10: **Fuel pellet radius of the axial node with the BOL peak LHGR**

Similarly, the cladding inner radius is compared between the three models in Figure 4-11. Prior to hard contact, around 150-200 days, all three models experience cladding creep down with slightly varying rates. After the onset of hard contact, the cladding inner radius is largely dictated by a response to the growth of the fuel pellet, and the observed differences in the cladding radius result from the differing fuel behavior models and any stress-induced fuel pellet deformation allowed by the mechanical model. However, due to the differing fuel growth models, stress-induced fuel pellet deformation cannot be directly compared among these predictions.

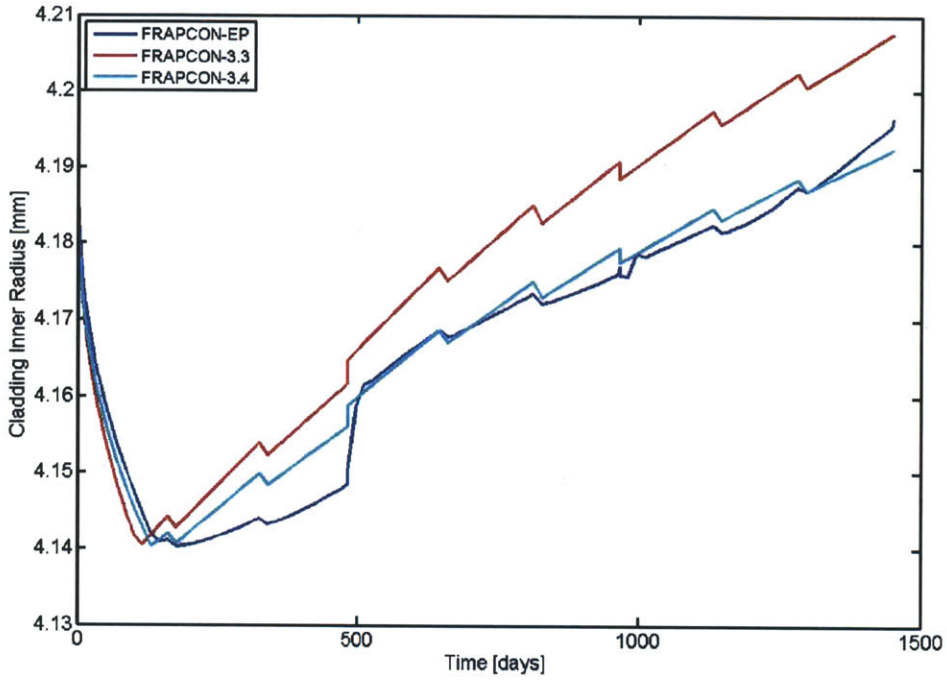

Figure 4-11: **Cladding inner radius of the axial node with the BOL peak LHGR**

The size of the fuel-cladding gap, shown in Figure 4-12, can give more relevant information for fuel performance because the fuel temperature is much more sensitive to the size of the fuel-cladding gap than it is to the independent dimensions of the fuel and cladding. Despite the different behaviors of the fuel outer and cladding inner radii, the gap size varies only slightly between the three models up to the onset of soft contact. After that point, the gap size is at the same minimum value for FRAPCON-EP, FRAPCON-3.3, and FRAPCON-3.4.

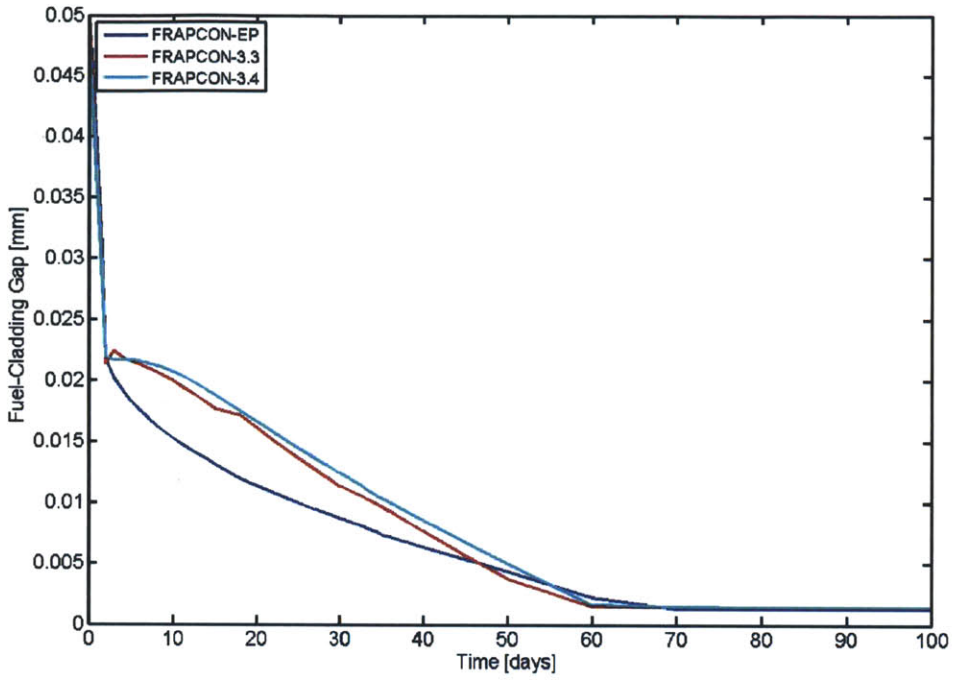

Figure 4-12: **Gap thickness of the axial node with the BOL peak LHGR**

From a regulatory point of view, the most important implication of the new structural models in FRAPCON-EP's simulation of steady-state operations is the EOL cladding hoop strain. This value often limits the fuel lifetime due to cladding strain beyond the NRC established maximum of 1%. Figure 4-13 compares the EOL hoop strain predictions between FRAPCON-EP, FRAPCON-3.3 and FRAPCON-3.4. All three fuel performance codes predict EOL cladding hoop strains which are well within NRC limits. As expected, due to the good agreement observed in the cladding inner radius, FRAPCON-EP and FRAPCON-3.4 agree very well for EOL hoop strain, with FRAPCON-3.3 predicting higher hoop strains across all of the axial nodes.

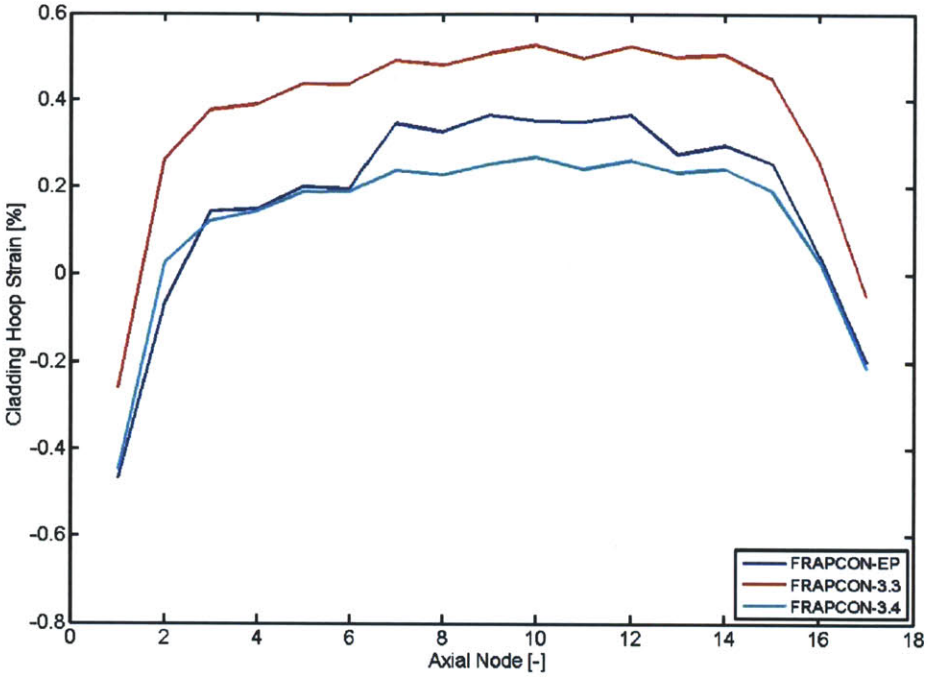

Figure 4-13: **Cladding hoop strain at EOL for the Zircaloy clad fuel rod**

The overall cladding elongation is illustrated for all three models in Figure 4-14. For this parameter, FRAPCON-3.4 can be seen to drastically under predict both FRAPCON-EP and FRAPCON-3.3. This is largely due to the application of an axial slip condition between the fuel pellet and cladding in the FEA model and differing cladding growth models. FRAPCON-EP's predicted overall cladding axial elongation differs from the nearly linear growth predicted by FRAPCON-3.3, largely due to its more intricate treatment of fuel swelling, which drives axial elongation during PCMI via axial locking. While this results in some disagreement between the two models, the final EOL elongation value is very similar for both FRAPCON-EP and FRAPCON-3.3.

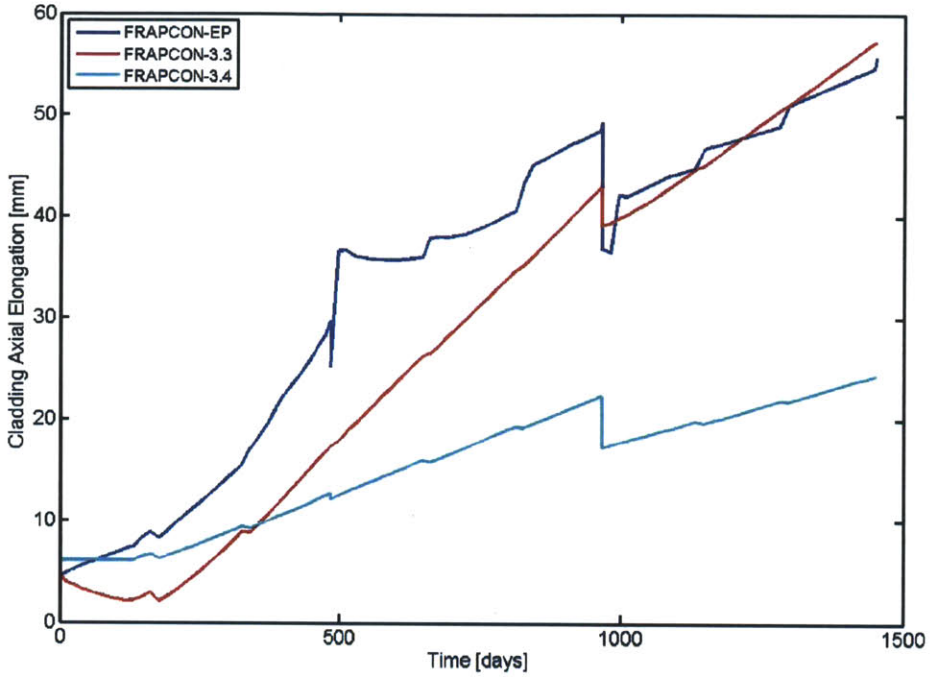

Figure 4-14: **Total axial cladding elongation of the Zircaloy clad fuel rod**

Aside from structural parameters, the implementation of the new mechanical model in FRAPCON-EP has feedback effects on non-structural fuel performance parameters. These feedback effects are primarily a function of temperature differences introduced in the fuel pellets. While a radially varying temperature profile exists at each axial level, the differences between maximum fuel temperatures, shown in Figure 4-15 and Figure 4-16, provide a good measure of how the different models affect fuel temperatures in general. The maximum temperature differences experienced between FRAPCON-EP and both of the other codes can be observed to be very similar, owing largely to the similar fuel properties of FRAPCON-3.3 and FRAPCON-3.4.

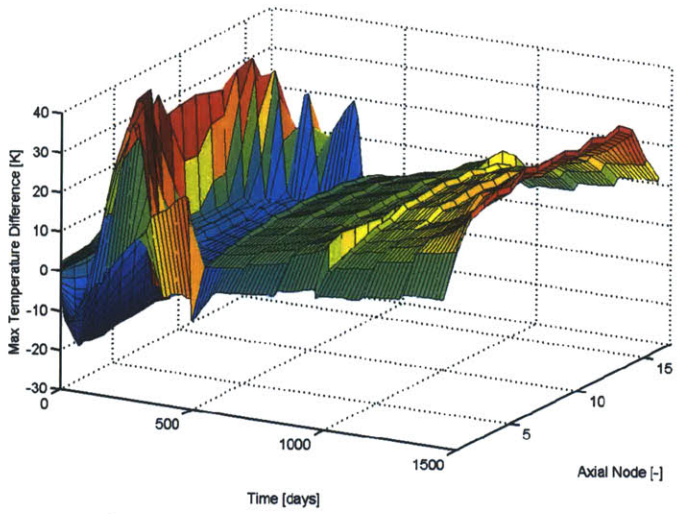

Figure 4-15: **Difference in maximum fuel temperature between FRAPCON-EP and FRAPCON-3.3 throughout the lifetime of the Zircaloy clad fuel rod**

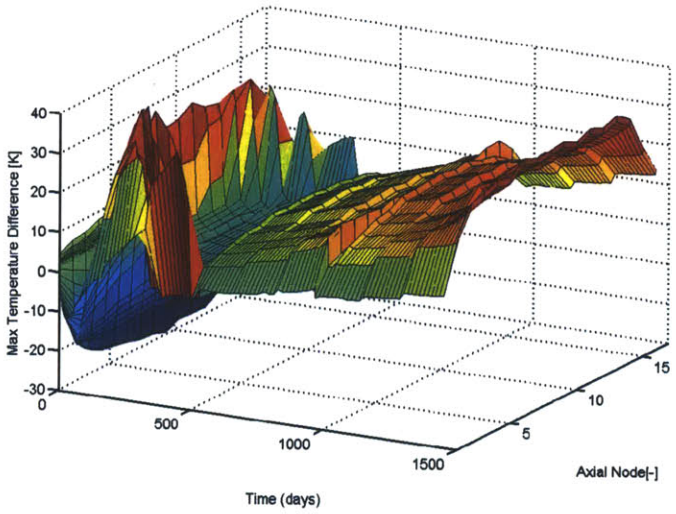

Figure 4-16: **Difference in maximum fuel temperature between FRAPCON-EP and FRAPCON-3.4 throughout the lifetime of the Zircaloy clad fuel rod**

Inspection of the differences between the maximum predicted fuel temperatures reveals that the maximum difference occurs immediately prior to the closure of the fuel-cladding gap. This is largely due to the vastly improved heat conduction across the fuel-cladding gap once the two components come into physical contact in association with the differing gap closure times observed in each model. The steadily increasing observed maximum temperature difference over the last two irradiation cycles is primarily due to the deteriorating fuel pellet conductivity with burnup which is accounted for in FRAPCON-EP's improved fuel behavior models. While the models do not agree perfectly, it is worth noting that the maximum observed difference is less than 40K, while the predicted maximum temperatures are on the order of approximately 1200K.

Another good measure for the behavior of the non-mechanical parameters is the average fuel temperature of the entire fuel stack in the rod, shown for all three codes in Figure 4-17. The average fuel temperature captures variation in the radial temperature profile that could be missed by only focusing on the maximum temperature. This allows for inferring into potential feedback effects resulting from differing structural predictions. As expected, due to their similar maximum fuel temperatures, FRAPCON-3.3 and FRAPCON-3.4 predict nearly identical average fuel temperatures. Prior to the second cycle, the difference in average fuel temperature between FRAPCON-EP and the other two models goes to zero as the gap closes and the fuel pellet and cladding come into contact. However, beyond the first cycle, the temperature difference steadily increases due to the aforementioned feedback effects.

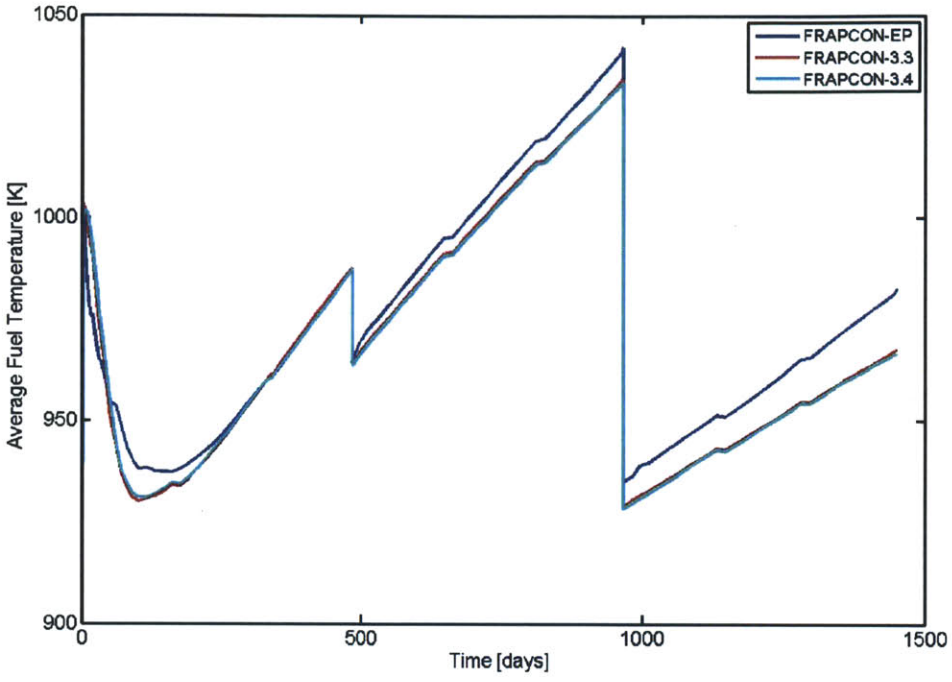

Figure 4-17: **Average temperature of the the fuel stack throughout the lifetime of the Zircaloy clad fuel rod**

The observed increases in the average fuel temperature are very slight during the second cycle, approximately 15K. Half-way through the second cycle, however, this slightly increased average temperature leads to increases in the FGR of FRAPCON-EP relative to that observed by both FRAPCON-3.3 and FRAPCON-3.4, as shown in Figure 4-18. Because the fuel temperatures are the same, the FGR differences between FRACPON-3.3 and FRAPCON-3.4 are likely attributable to changes in the FGR model and not structural or thermal feedback effects.

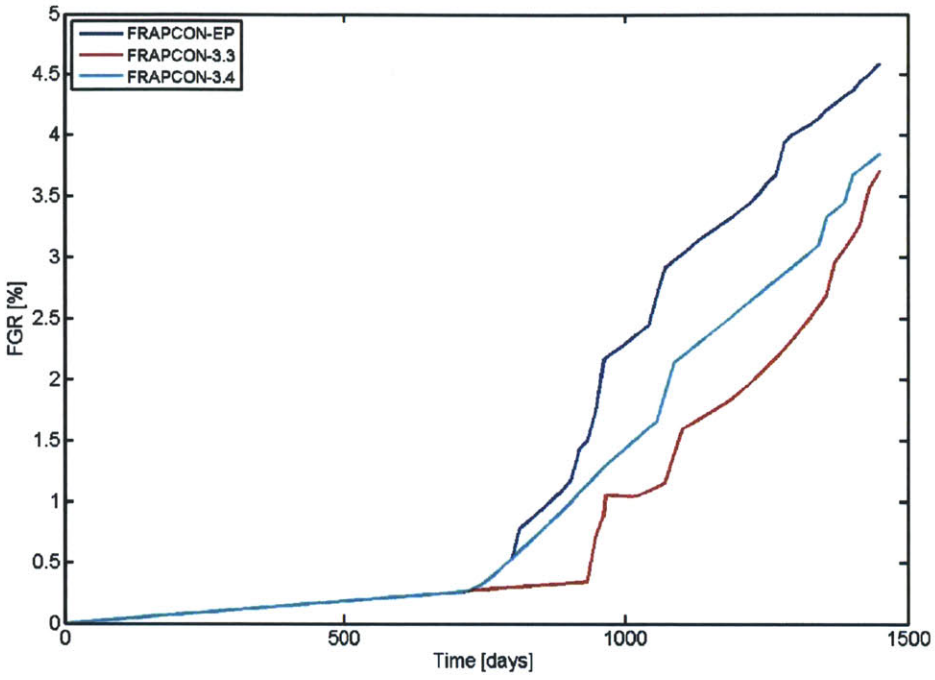

Figure 4-18: **Observed FGR throughout the lifetime of the Zircaloy clad fuel rod**

Figure 4-19 illustrates how, beginning midway through the second cycle, this increased rate of FGR corresponds to faster increases in the plenum pressure of the fuel rod. Ultimately this results in higher EOL plenum pressures predicted by FRAPCON-EP and FRAPCON-3.4 than FRAPCON-3.3. The good agreement in EOL plenum pressure by FRAPCON-EP and FRAPCON-3.4 is largely due to the better agreement on FGR and the similar structural parameters, which determine the available gas volume.

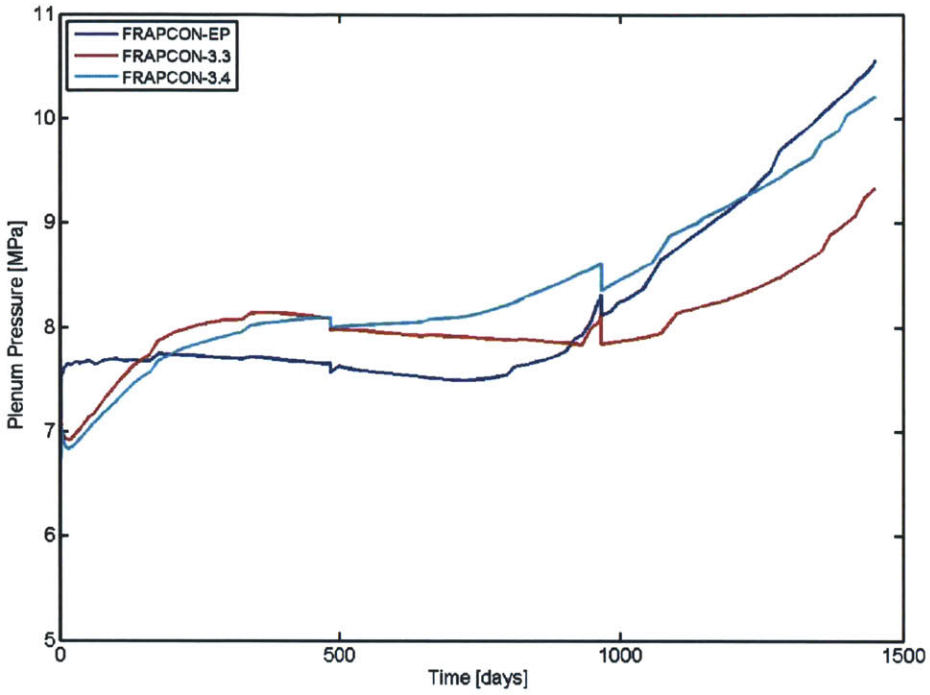

Figure 4-19: **Observed plenum pressure throughout the lifetime of the Zircaloy clad fuel rod**

4.3 SiC-Clad Solid Pellet Case

The first SiC clad fuel rod evaluated simply replaces the Zircaloy cladding without further changes to fuel pellet geometry or rod power history. This case is intended to be representative of conditions which would be experienced if SiC cladding were immediately adopted for use in PWR reactors for current commercial operations. Because the FEA model in FRAPCON-3.4 has not yet been modified to accommodate SiC cladding, it was not used for any of the cases using SiC.

The as-fabricated parameters of fuel pin, power history, and axial power shapes utilized by this case are identical to those presented in Section 4.2.

Because SiC cladding does not creep at the temperatures experienced during LWR operation, the cladding inner radius does not decrease during any phase of the fuel pin

lifetime. Also unlike Zircaloy cladding, SiC cladding does experience radial swelling during its initial irradiation. The effect of these two mechanisms on the cladding inner radius can be observed in Figure 4-20. While both FRAPCON-EP and FRAPCON-3.3 predict early increases in the cladding inner radius, FRAPCON-EP predicts this growth to occur at faster rate than FRAPCON-3.3. This difference is likely the result of FRASP accounting for the axial swelling of the SiC within the mechanical model rather than neglecting it, as it is treated within FRACAS-I. This cladding behavior is seen in all three SiC clad fuel rod cases.

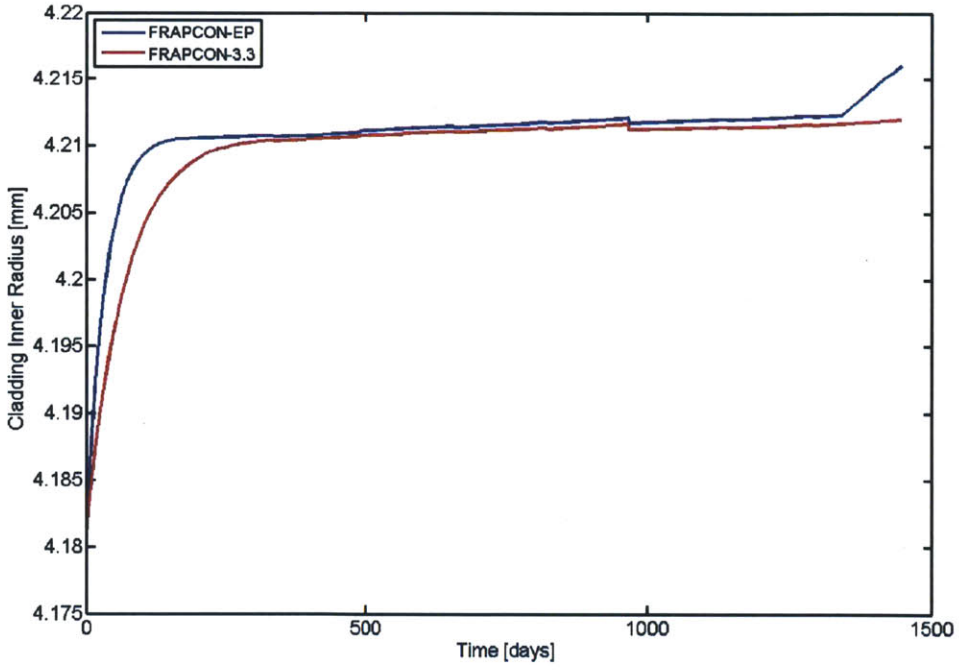

Figure 4-20: **Inner cladding radius of the axial node with the BOL peak LHGR for the SiC clad solid pellet case**

As a result of the near constant cladding inner radius, the only mechanism driving the closure of the fuel-cladding gap, shown for the BOL peak axial node in Figure 4-21, is the evolution of the fuel pellet size. Because the fuel pellet grows much slower than the Zircaloy creep down occurs, SiC clad fuel pins experience an open fuel-cladding gap for much longer periods of operation.

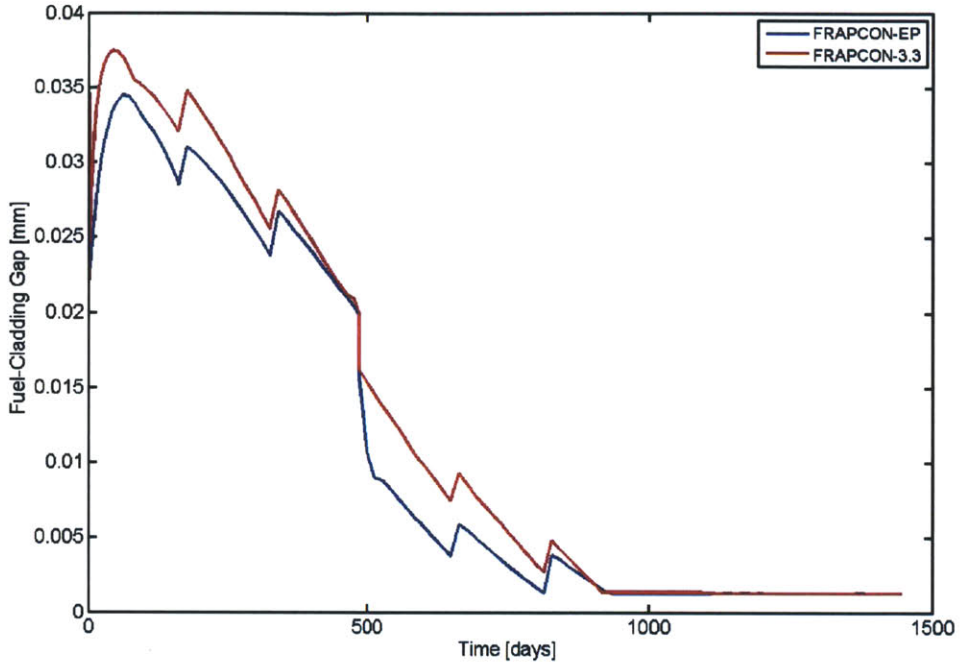

Figure 4-21: **Fuel-cladding thickness of the axial node with the BOL peak LHGR for the SiC clad solid pellet case**

Because the fuel-cladding gap is generally larger, the average fuel temperature of SiC clad fuel pins are higher than that of similar Zircaloy clad cases, as shown in Figure 4-22. While these average fuel temperatures are approximately 200K hotter than those observed in the Zircaloy clad case, FRAPCON-EP and FRAPCON-3.3 both predict values which are in good agreement with one another. As would be expected with the deterioration of the fuel conductivity with increased burnup, FRAPCON-EP does begin to predict increasingly higher average fuel temperatures later in life.

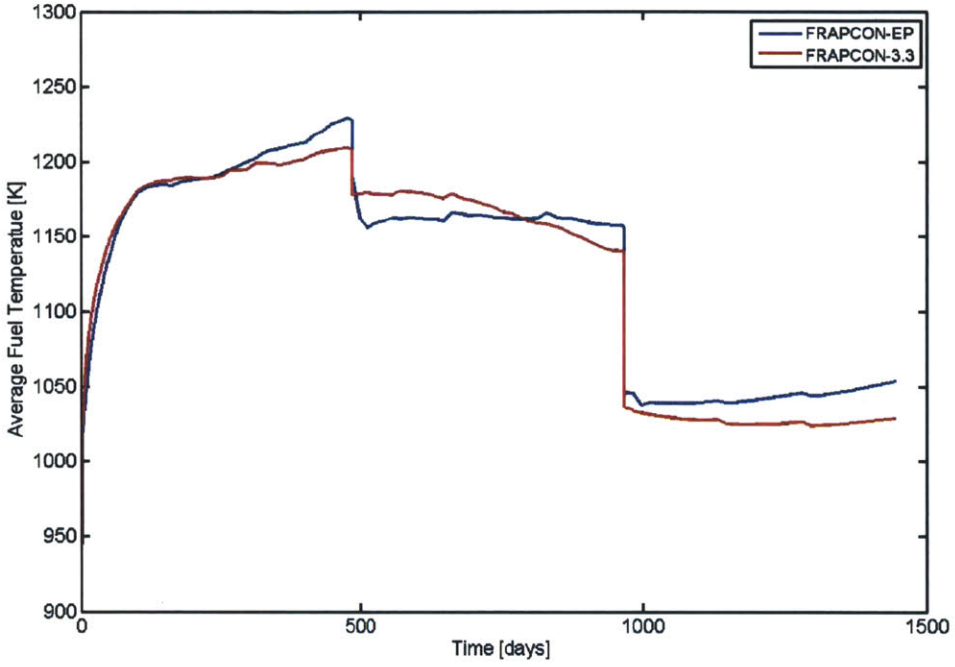

Figure 4-22: **Average temperature of the the fuel stack throughout the lifetime of the SiC clad solid pellet case**

While FRAPCON-EP does begin to diverge with FRAPCON-3.3 during the second irradiation cycle, as seen in Figure 4-23, the two codes' EOL FGR predictions are very similar. While the relative difference in the predicted FGR is approximately 20% towards the end of the second irradiation cycle, this is similar to the relative difference observed in Figure 4-18 for the Zircaloy case. The good agreement between the FGR predictions is largely attributable to the good agreement in average fuel temperature observed in Figure 4-22.

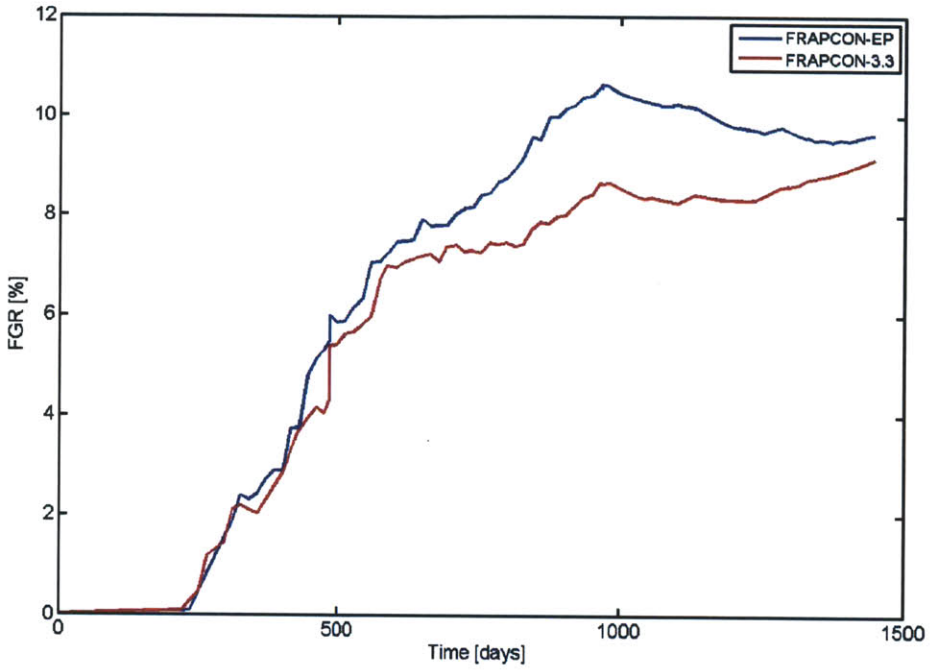

Figure 4-23: **Observed FGR throughout the lifetime of the SiC clad solid pellet case**

For the plenum pressure of the solid SiC clad fuel rod, FRAPCON-EP does predict higher values than FRAPCON-3.3, observed in Figure 4-24. While these differences are relatively close, less than 15%, they are likely result primarily from the elevated FGR predictions by FRAPCON-EP. The increased average fuel temperature also leads to increased thermal expansion of the fuel stack, which decreases the available gas volume, increasing plenum pressure.

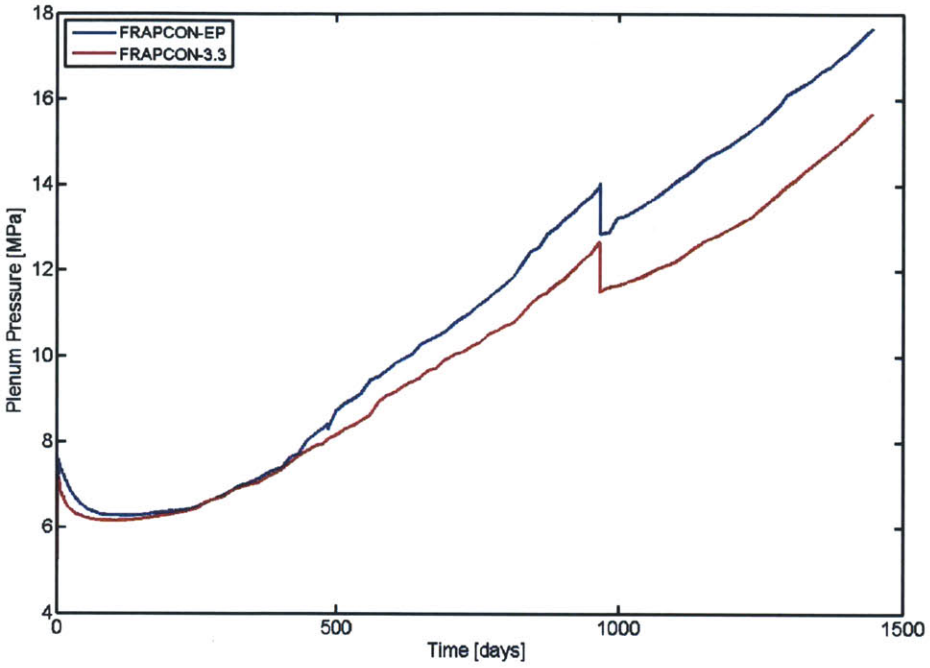

Figure 4-24: **Observed plenum pressure throughout the lifetime of the SiC clad solid pellet case**

Investigation of the total cladding axial elongation, illustrated in Figure 4-25, reveals dramatic differences between the predictions of FRAPCON-EP and FRAPCON-3.3. This difference is most likely the result of a simple mistake in writing the output of FRAPCON-3.3 made during the implementation of SiC material properties. If the maximum SiC irradiation growth strain of 0.67% is simply added, after being applied to an initial length of 3.66 meters, to the reported value of FRAPCON-3.3, the two models' predicted cladding elongation are seen to be within about a millimeter of one another. It can be observed from the asymptotic behavior of the cladding inner radius in Figure 4-20 that this maximum swelling value will be achieved relatively quickly.

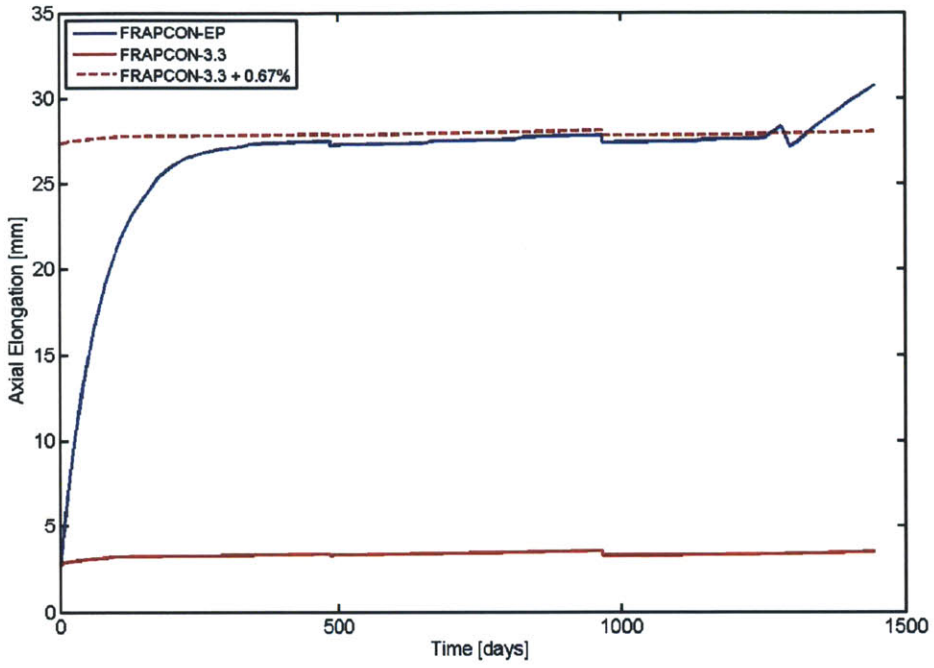

Figure 4-25: **Total axial cladding elongation of the SiC clad solid pellet case**

Unlike FRAPCON-3.3, FRAPCON-EP predicts the onset of hard contact in the SiC clad solid pellet case. Figure 4-26 shows the evolution of the maximum interfacial pressure experienced by the fuel and cladding during operation. It should be noted that this maximum interfacial pressure is a synthesis of information from multiple axial nodes rather than a single location and represents the maximum value throughout the fuel rod at any given time.

While the interfacial pressure predicted by FRAPCON-EP is relatively high, it remains below the effective interfacial pressure limit of 45 MPa. Because the interfacial pressure limit led to the development of the ultimate stress of the SiC cladding, it is not surprising that FRASP's predicted interfacial pressure values remain below that limit. However, the proximity of the interfacial pressure to this 45 MPa limit, in conjunction with the rate of increasing maximum interfacial pressure observed in Figure 4-26, raises concerns as to how much longer the cladding would survive under

these conditions. In fact, should the conservative limit of 30 MPa be adopted to avoid post-LOCA failure, the irradiation time may be limited to 1370 days.

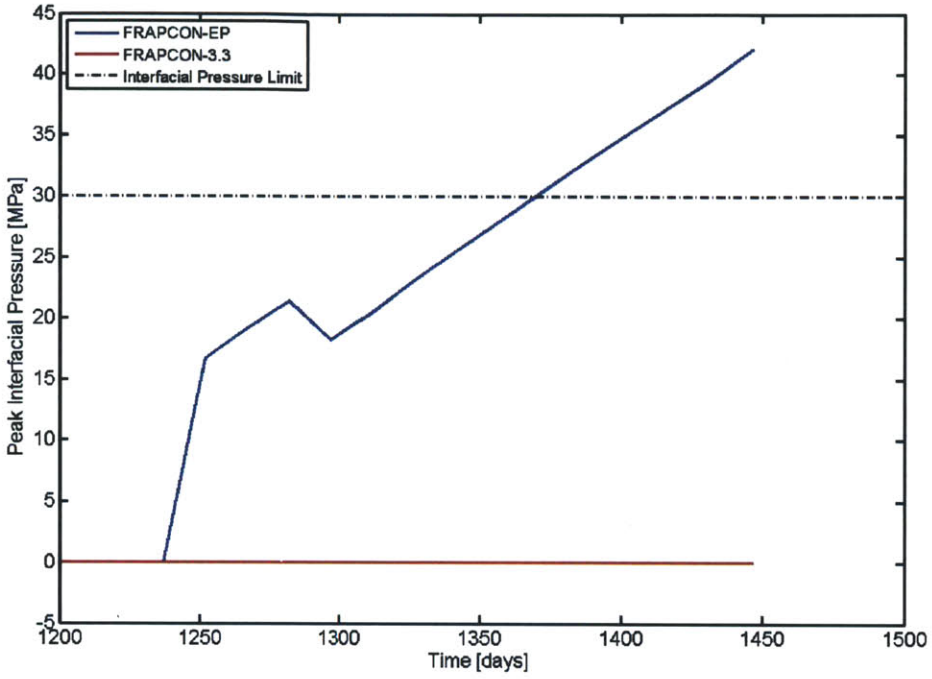

Figure 4-26: **Maximum interfacial pressure throughout the lifetime of the SiC clad solid pellet case**

If FRAPCON-3.3 had determined hard contact to occur, it would not be able to provide any interfacial pressure information, as the assumptions of the rigid pellet model would require plastic straining, and thus cladding failure. The prediction of PCMI between the fuel pellet and SiC cladding is a result of both the improved fuel pellet growth and structural mechanics models of FRAPCON-EP. Figure 4-27 and 4-28 relate the fuel pellet radius and predicted interfacial pressure of both models at the EOL for the fuel pin. These figures show that an increased fuel radius of 1.2 microns, or approximately 0.03% additional fuel swelling, results in the prediction of greater than 20 MPa of interfacial pressure due to the resulting application of PCMI behavior.

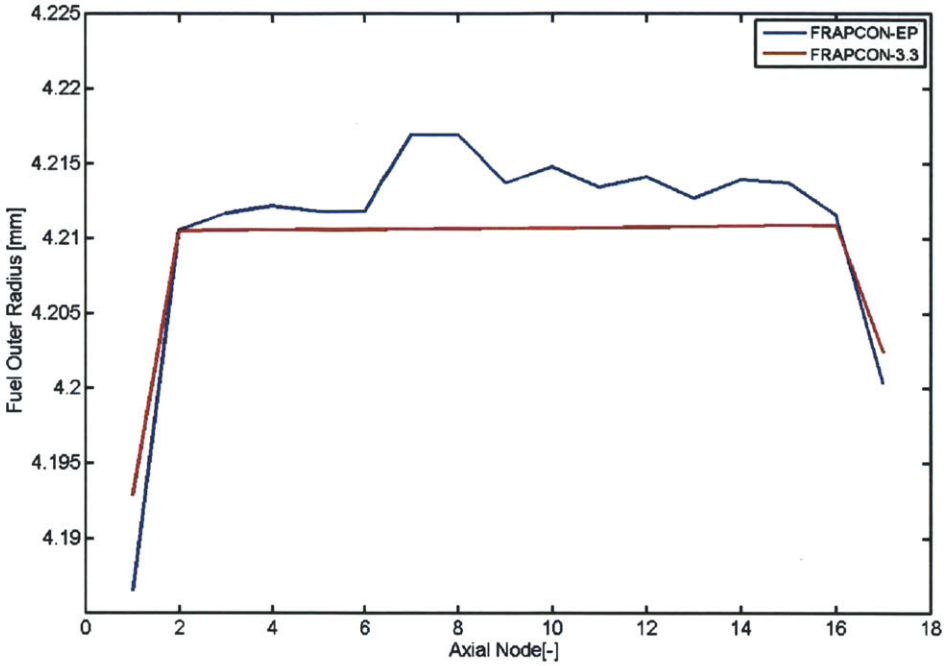

Figure 4-27: **Observed EOL fuel outer radii of the SiC clad solid pellet case**

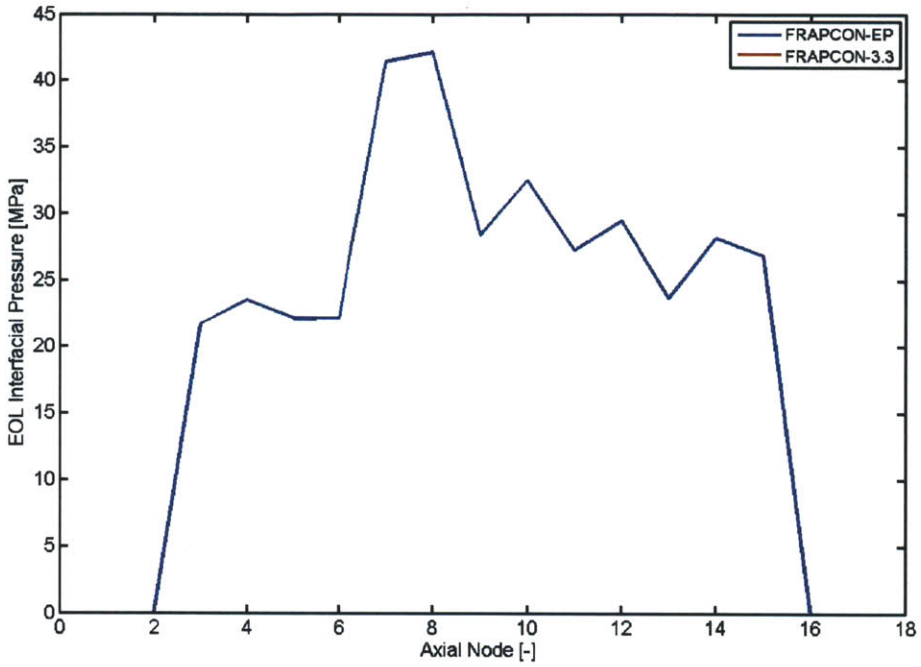

Figure 4-28: **Interfacial pressure observed at EOL of the SiC clad solid pellet case**

As a result of the hard contact between the fuel pellet and cladding, the EOL cladding hoop strain predicted by FRAPCON-EP is much larger than that of FRAPCON-3.3, as shown in Figure 4-29. Because the cladding experiences only elastic behavior, the hoop strains observed are directly proportional to the interfacial pressure.

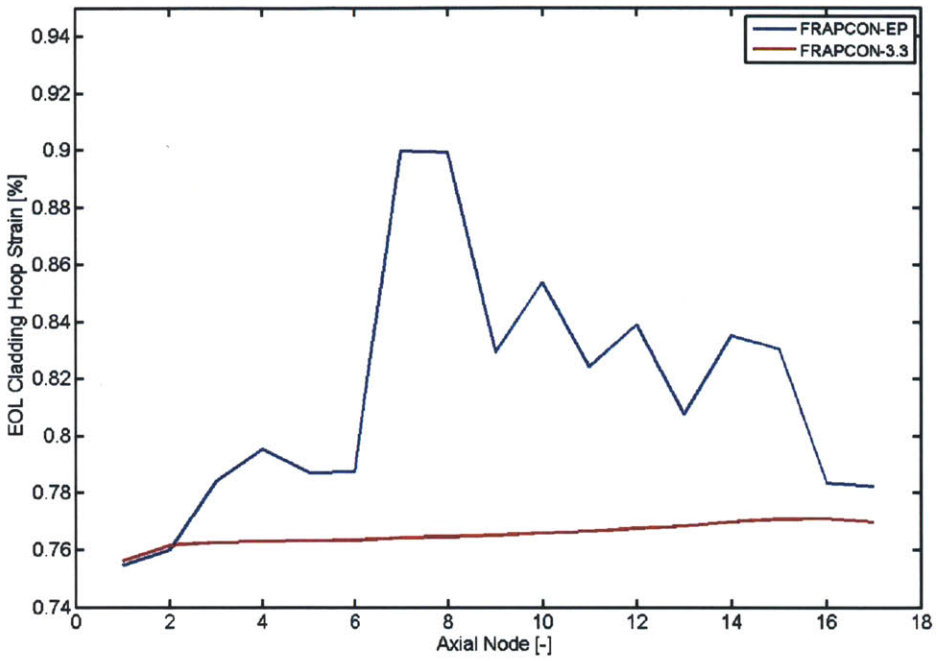

Figure 4-29: **Cladding hoop strain at EOL of the SiC clad solid pellet case**

Prior to hard contact, when the mechanisms dictating the cladding size were limited to irradiation growth and thermal expansion, the cladding hoop strains, illustrated in Figure 4-30, are much more comparable, within 0.015%, between the two models.

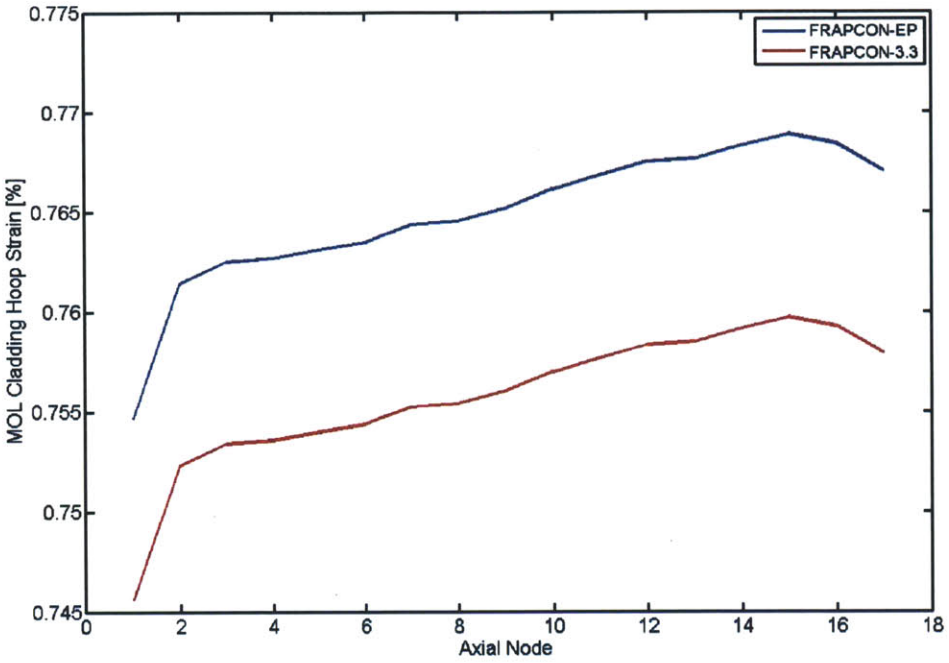

Figure 4-30: **Cladding hoop strain at MOL of the SiC clad solid pellet case**

Along with the interfacial pressure and cladding expansion associated with PCMI, the cladding also experiences axial elongation associated with the axial locking of the fuel pellet and cladding. Figure 4-31 provides a three dimensional view of how the application of friction and axial coupling provides differing axial strain predictions from FRAPCON-3.3. As seen in Section 3.2 this difference is particularly evident in the lower nodes, which are subjected to axially communicated friction from all the nodes above them.

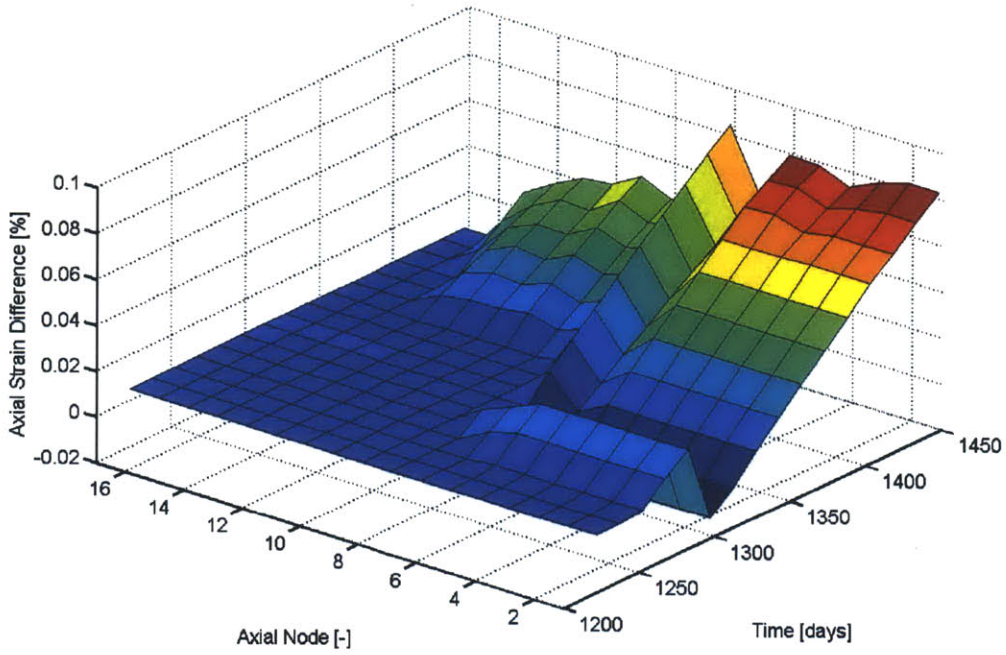

Figure 4-31: **Difference in predicted cladding axial strain observed by FRAPCON-EP and FRAPCON-3.3 for the SiC clad solid pellet case**

4.4 SiC-Clad Annular Pellet Case

In order to improve the general fuel performance of SiC, it has been proposed to introduce a central void to the fuel pellets within identical SiC cladding. By reducing the radial distance heat must travel from any point in the annular fuel pellet to the outer surface, temperatures throughout the fuel are reduced, along with feedback effects associated with high fuel temperatures, e.g. high FGR. This temperature reduction is intended to counteract the higher temperatures associated with the larger fuel-cladding gap resulting from the lack of creep down in SiC.

The introduced inner radius is based on a 10% reduction of the cross sectional area of the fuel pellet. This reduction in cross sectional area was intended to reduce total fuel pellet volume by 10%; however, due to dishing of the ends of each fuel pellet, the

total volume reduction was decreased to 9.3%. The void introduced into the center of the annular fuel pellet has an as-fabricated radius of 0.129 cm, and reduces the mass of uranium in the fuel rod to 1.62 kgU.

As this case is intended to illustrate the fuel performance benefits associated with introducing the central void to the fuel pellet, the same power history found in Section 4.1 was used. Because of the reduction in fuel mass associated with the central void, the fuel pin average burnup is increased by approximately 10%, resulting in a final burnup of 73.5 MWd/kgU, shown in Figure 4-32.

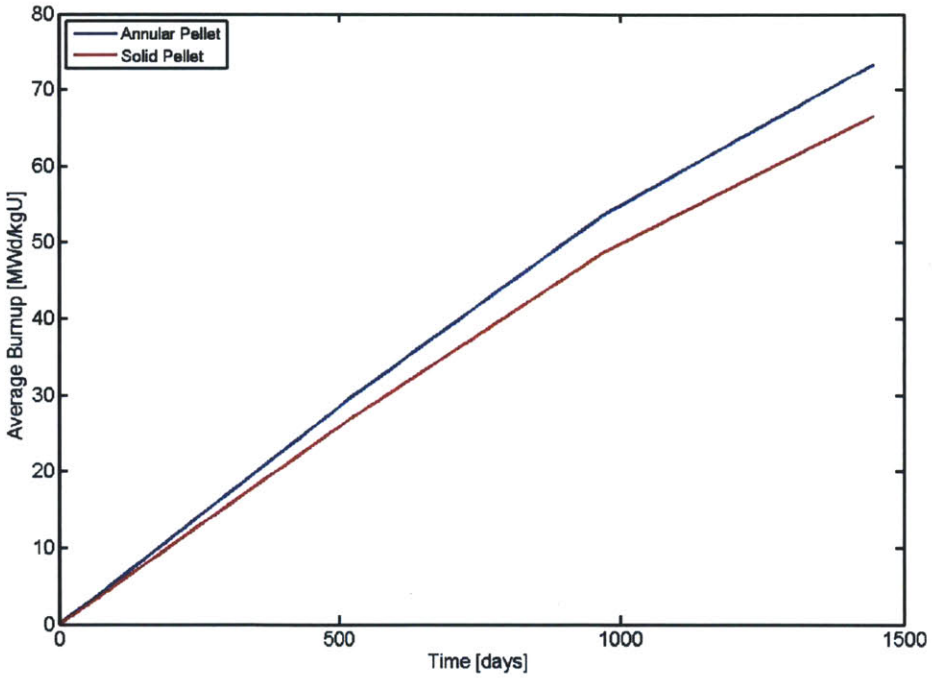

Figure 4-32: **Comparison of the burnup between the solid and annular pellet cases**

Because of the higher burnup of this case, a higher enrichment of the uranium is expected to be necessary. While this increased enrichment is expected to have economic implications, it has limited effects on fuel performance characteristics and is thus neglected.

For non-mechanical parameters, the introduction of the central void to the annular

fuel pellet improves general performance of the fuel. These parameters, quantified by the average fuel temperature, FGR, and plenum pressure, shown in Figures 4-33, 4-34, and 4-35, demonstrate good agreement between FRAPCON-EP and FRAPCON-3.3. For this particular case, FRAPCON-EP tends to return less conservative EOL values for all three of these parameters.

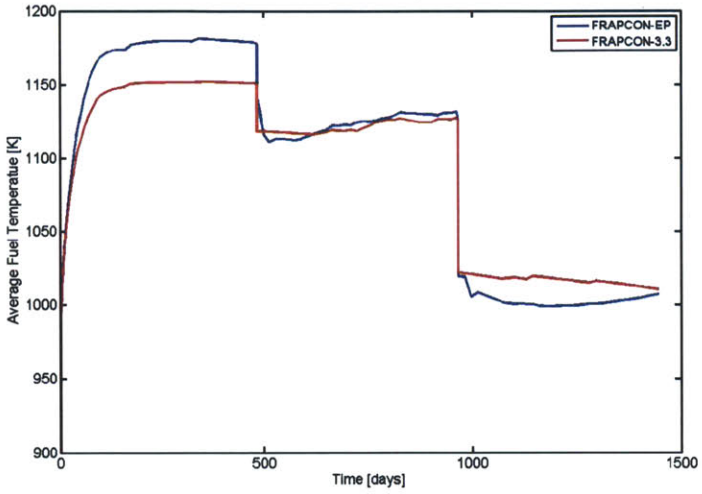

Figure 4-33: **Average temperature of the the fuel stack throughout the lifetime of the SiC clad annular pellet case**

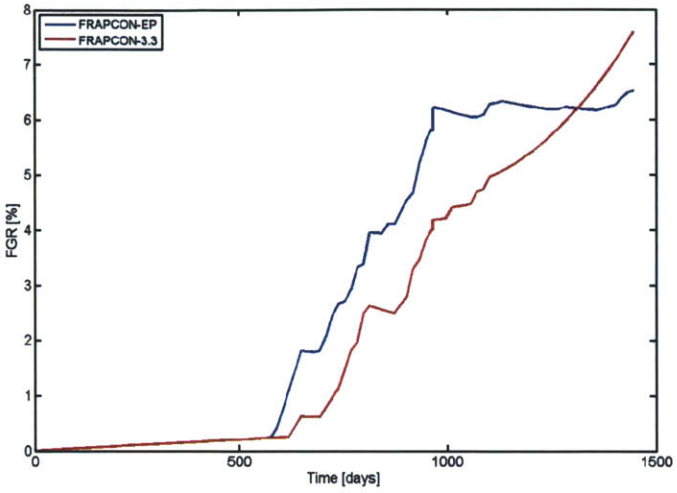

Figure 4-34: **Observed FGR throughout the lifetime of the SiC clad annular pellet case**

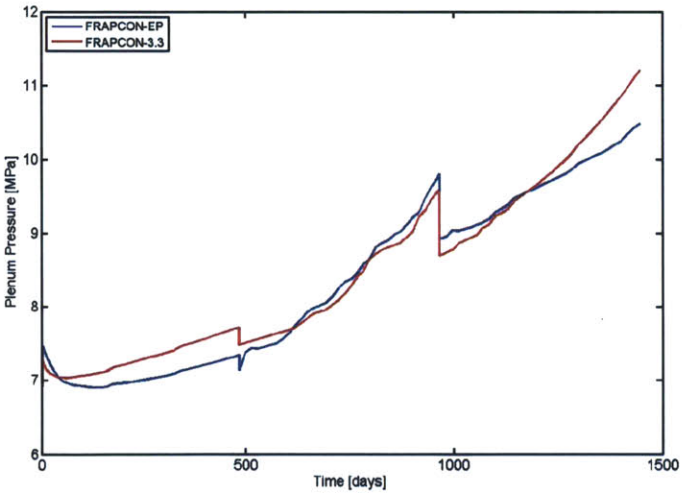

Figure 4-35: **Observed plenum pressure throughout the lifetime of the SiC clad annular pellet case**

Prior to the onset of hard contact between the fuel pellet and cladding, the inner cladding radius associated with the annular pellet case is identical to that of the solid pellet case. However, Figure 4-36 illustrates that the cladding does not behave

identically over the entire lifetime of the fuel pin due to an earlier onset of hard contact, which causes a larger EOL value due to elastic straining by the fuel pellet. Similar to the solid fuel pellet case, only FRAPCON-3.3 predicts that PCMI does not occur, contrary to FRAPCON-EP's predictions.

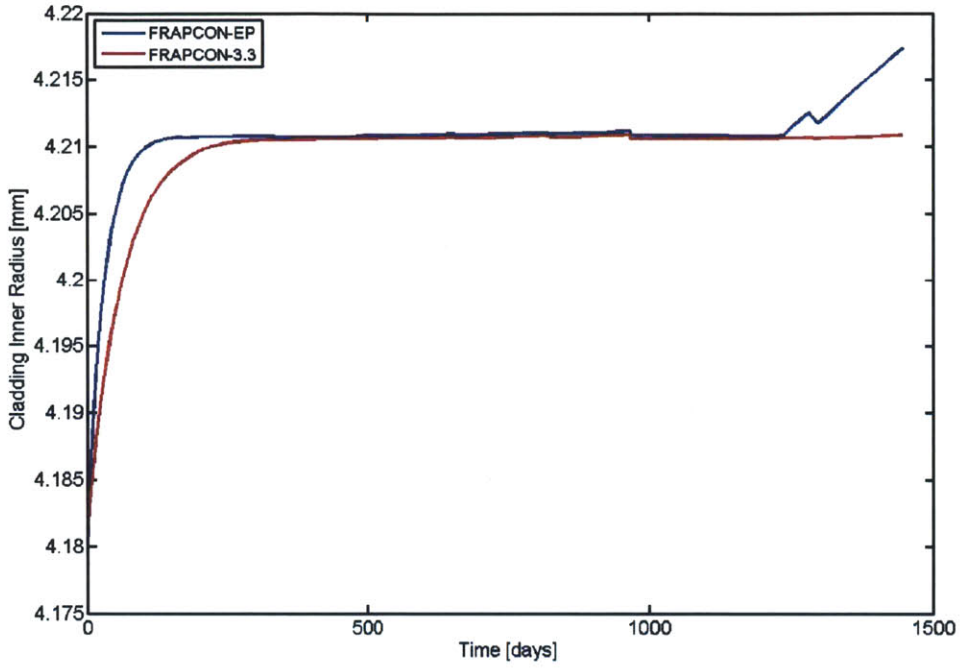

Figure 4-36: **Inner cladding radius of the axial node with the BOL peak LHGR for the SiC clad annular pellet case**

Evaluation of the EOL cladding hoop strain in Figure 4-37 shows that while the peak cladding hoop strain, 0.88%, is lower than that of the solid pellet case, 0.9%, the annular pellet case gives an identical average EOL hoop strain of 0.81%. As with the solid pellet case, the PCMI-induced cladding deformation is purely elastic, in accordance with the brittle nature of SiC.

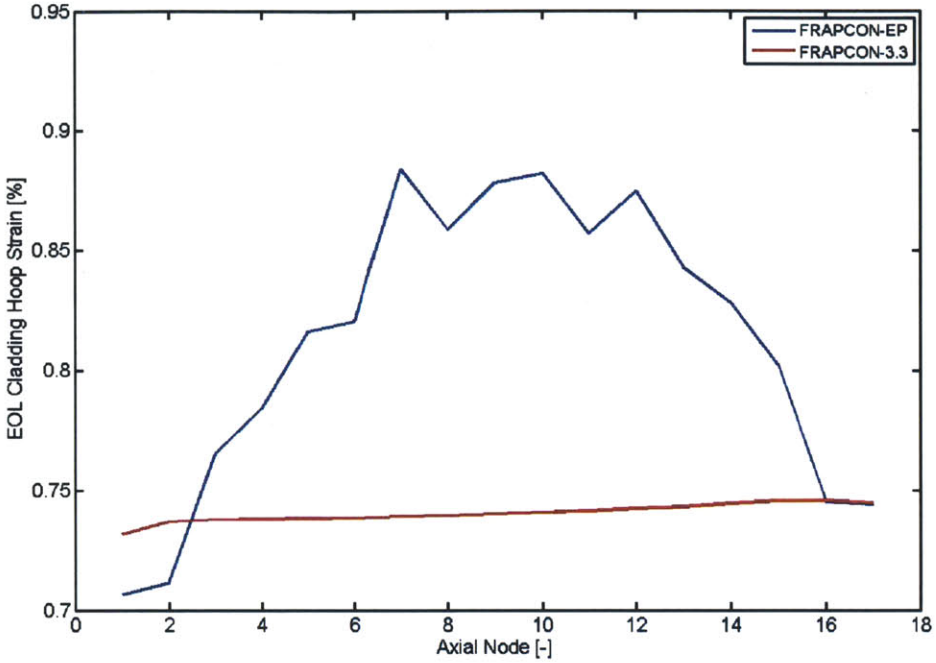

Figure 4-37: **Cladding hoop strain at EOL of the SiC clad annular pellet case**

As previously mentioned, the annular fuel pellet case does see a slightly earlier onset of hard contact between the fuel pellet and cladding. The peak interfacial pressure of the annular pellet case, shown in Figure 4-38, indicates PCMI will first occur after 1,222 days, while it is first experienced with a solid fuel pellet after 1,237 days. Perhaps more relevant than the time of PCMI occurrence is the burnup at which it occurs. For the solid and annular fuel pellet cases, FRAPCON-EP predicts PCMI occurrence at 58.6 MWd/kgU and 64.01MWd/kgU, respectively.

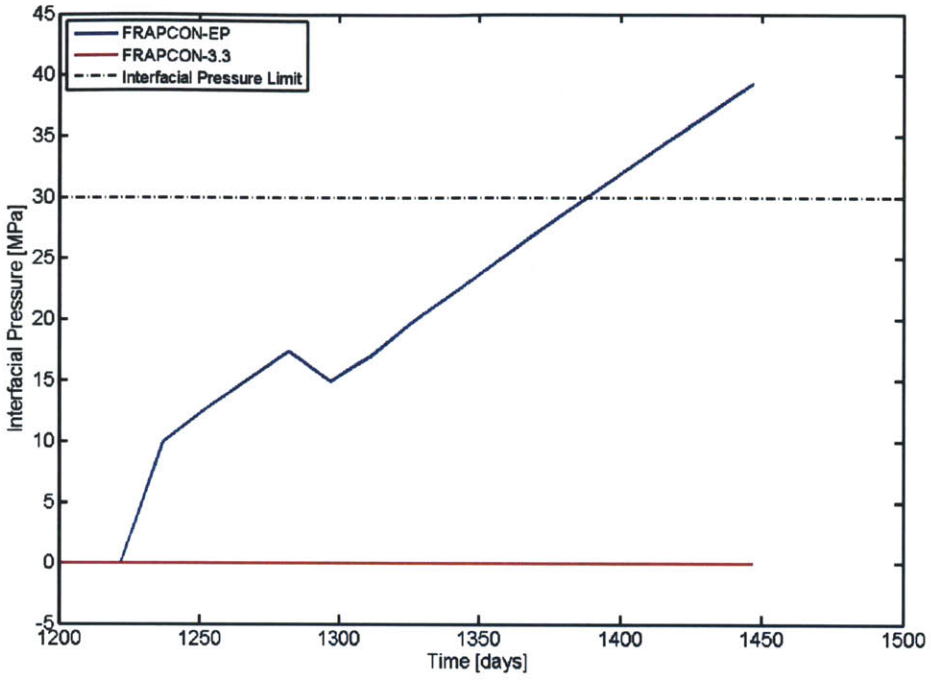

Figure 4-38: **Maximum interfacial pressure throughout the lifetime of the SiC clad annular pellet case**

It can also be observed from Figure 4-38 that the maximum interfacial pressure predicted by FRAPCON-EP remains below the 45 MPa limit. While the rate of maximum interfacial pressure increase is cause for concern over the survival of the brittle cladding, the margin to failure is improved from the solid fuel pellet case. However, with a maximum allowed interfacial pressure of 30 MPa, only slight improvement in available time is predicted.

The EOL SiC cladding axial elongation for the annular fuel case is predicted to be only 2.3 mm, or 0.06% total axial strain, larger than that of the solid pellet case. This difference results from the different PCMI conditions of the annular case and is otherwise predicted to behave identically to the solid pellet case. For these reasons, the cladding axial elongation associated with this case is not explicitly presented here.

While the PCMI behavior predicted by FRAPCON-EP is not wholly dictated by the fuel radius, as it is with the rigid pellet model in FRACAS-I, it does provide

the driving force for cladding deformation. Figure 4-39 shows the EOL difference in the fuel outer radius predicted by FRAPCON-EP and FRAPCON-3.3. On average, FRAPCON-EP predicts the fuel outer radius to be only 7.55 microns, or 0.04% radial strain, larger than FRAPCON-3.3.

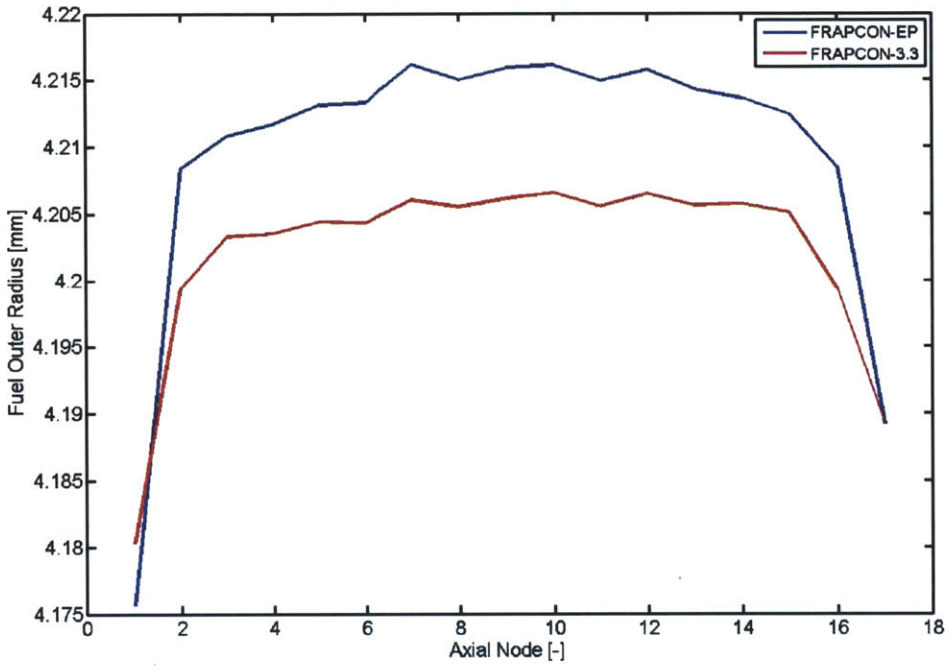

Figure 4-39: **Observed EOL fuel outer radii of the SiC clad annular pellet case**

The primary reason for the larger fuel outer radius predicted by FRAPCON-EP stems from FRASP's treatment of the fuel inner radius. Unlike FRACAS-I, FRASP applies the calculated radial displacements to the innermost radial fuel node boundary. By neglecting the radial displacement of the inner fuel node boundary, FRAPCON-3.3 does not capture the evolution of the fuel inner radius. It can be seen in Figure 4-40 that FRAPCON-EP predicts the fuel inner radius to experience increases up to 2.5% greater than its original value. This growth is largely due to the same mechanisms driving the total pellet growth.

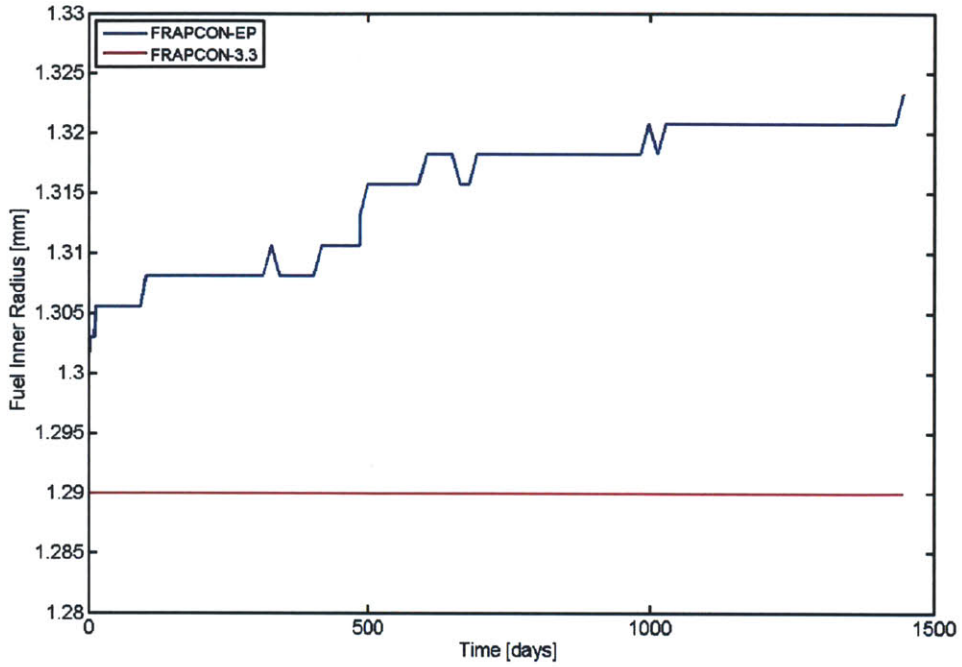

Figure 4-40: **Inner fuel pellet radius of the axial node with the BOL peak LHGR for the SiC clad annular pellet case**

At the EOL for the annular case, the fuel inner radius, shown in Figure 4-41, is predicted by FRAPCON-EP to be an average of 29.45 microns larger than that used by FRAPCON-3.3. If not for the increased size of the fuel inner radius, the fuel outer radius predicted by FRAPCON-EP would not be large enough to support the PCMI observed in the annular fuel case.

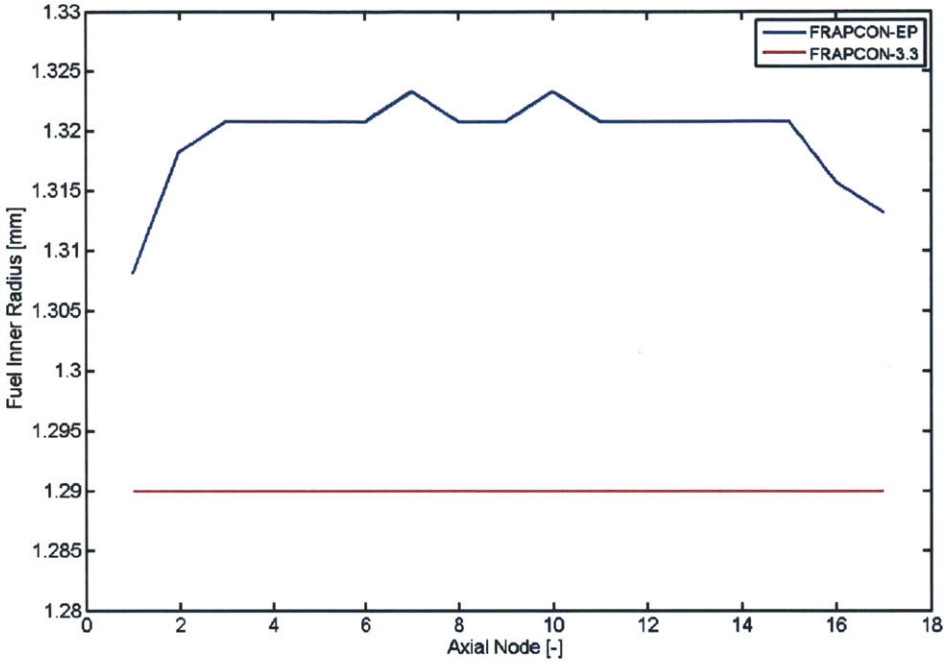

Figure 4-41: **Observed EOL fuel inner radii of the SiC clad annular pellet case**

More appropriately, if the same inner radial displacement utilized by FRASP were applied to the EOL fuel outer radius predicted by FRAPCON-3.3, visualized in Figure 4-42, the rigid pellet model in FRACAS-I would undoubtedly result in cladding failure. While the predictions calculated using the different fuel behavior models of FRAPCON-EP may not be directly applicable, it is comparable to what would be expected if FRACAS-I accounted for the evolution of the fuel pellet's inner radius.

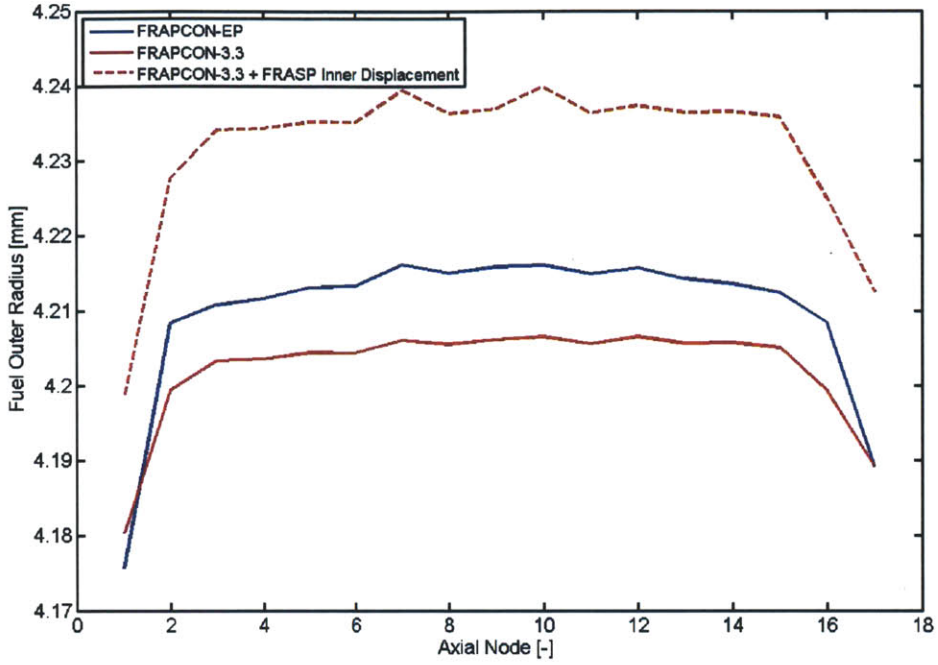

Figure 4-42: **Comparison of FRAPCON-EP and FRAPCON-3.3 EOL fuel outer radii with and without the addition of FRASP's predicted inner surface displacement for the SiC clad annular pellet case**

4.5 10% Uprated SiC-Clad Annular Pellet Case

To take further advantage of the improved fuel performance related to the introduction of a central void to the fuel pellet of SiC clad fuels, a case was evaluated with a 10% increase in core power. This uprate in core power has been suggested and analyzed in previous studies of the application of SiC cladding (Carpenter et al., 2010; Dobisesky, 2011) and is primarily intended to provide an economic incentive for electric utilities to adopt SiC cladding.

The conditions for a 10% increase in core power of the Seabrook reactor are listed in Table 4.4. To accommodate the core power increase without increasing the core outlet temperature, the coolant mass flux is also increased by 10%. The as-fabricated

fuel rod parameters, however, remained unchanged from the original annular fuel pellet case.

Table 4.4: **10% Uprated Seabrook core conditions**

Core Parameter	Units	Value
Coolant Inlet Temperature	K	565
Coolant Pressure	MPa	15.5
Coolant Mass Flux	kg/s-m^2	3670
Core Average LHGR	kW/m	21.08

For application of the new core power to the fuel pin, the power history used in previous cases was uniformly increased by 10% without altering the length of each reactor cycle beyond 18 months, illustrated in Figure 4-43. This uprated power history essentially assumes that the increases to the LGHR associated with the peak burnup fuel rod directly scales with the uprate to total core power. In reality this is likely not the case, as total core uprates may be achieved by increasing the power of the average fuel rod while decreasing the peaking factor of the peak rod to avoid increases in peak LHGR. However, this proportionally increased power history was assumed in order to provide a conservatively limited case.

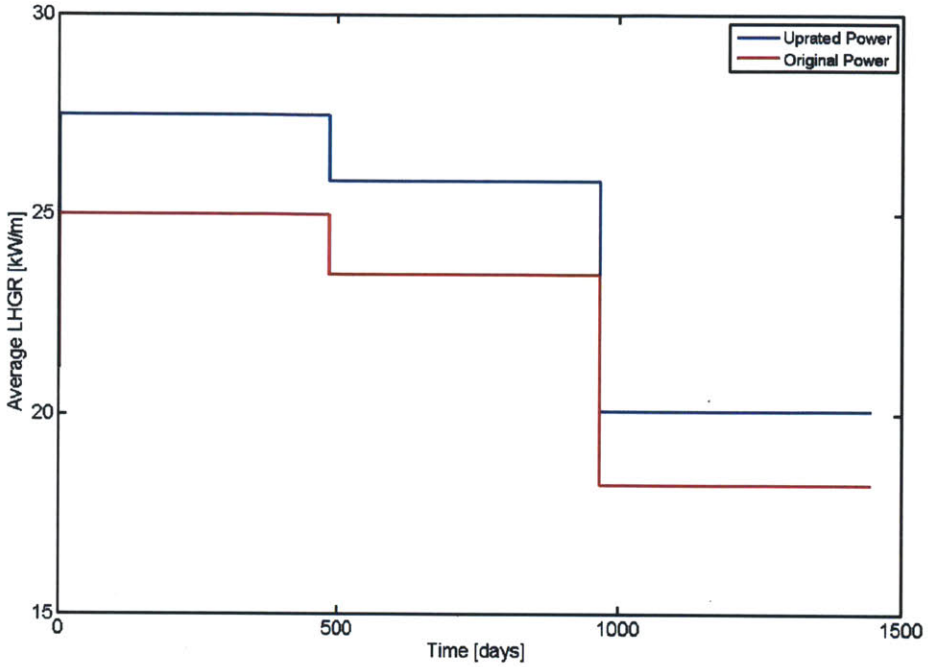

Figure 4-43: **Comparison of initial and uprated average fuel rod power histories**

For this uprated case, FRAPCON-3.3 predicts no cladding failure up to the planned EOL burnup of 80.85 MWd/kgU. However, given the predictions of FRAPCON-EP, it comes as little surprise that the newer fuel performance code predicts failure of the SiC cladding, surviving to an average pin burnup of 72.47 MWd/kgU. Figure 4-44 shows a comparison of the original, planned, and achieved average fuel pin burnups.

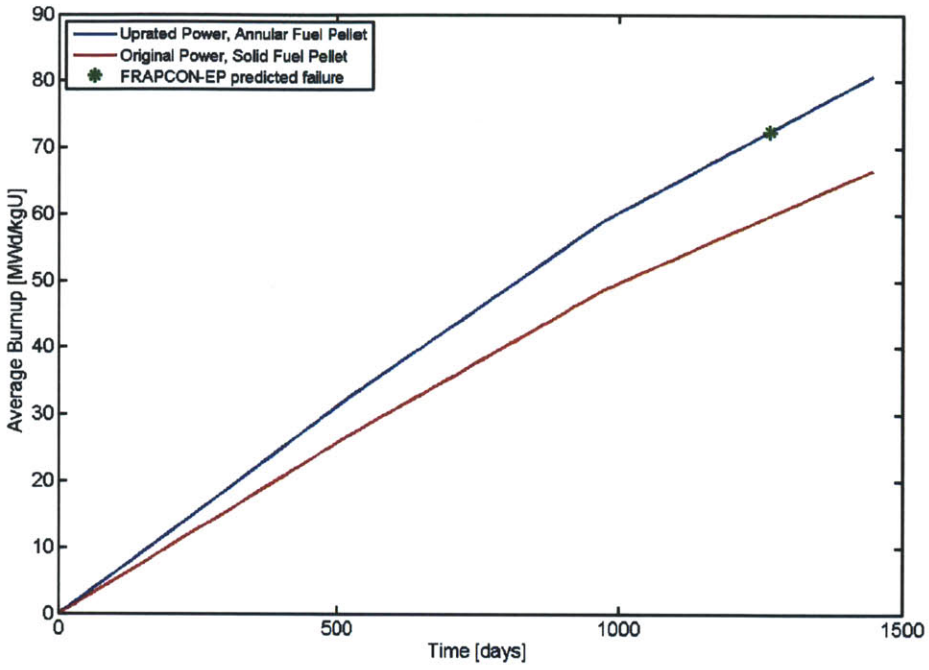

Figure 4-44: **Comparison of the burnup between the solid and uprated annular pellet cases with the FRAPCON-EP's last point of expected cladding survival marked**

Because FRAPCON-EP predicts mechanical failure of the cladding, comparison of non-mechanical parameters is largely immaterial and they are therefore not investigated here. A comparison of the EOL cladding hoop strain predictions of FRAPCON-EP and FRAPCON-3.3, shown in Figure 4-45, reflect results similar to those observed in the previous SiC clad cases. Note that for the predictions of FRAPCON-EP for this uprated case, EOL will refer to the final achieved burnup, 72.47 MWd/kgU, at which the cladding is predicted to not experience failure.

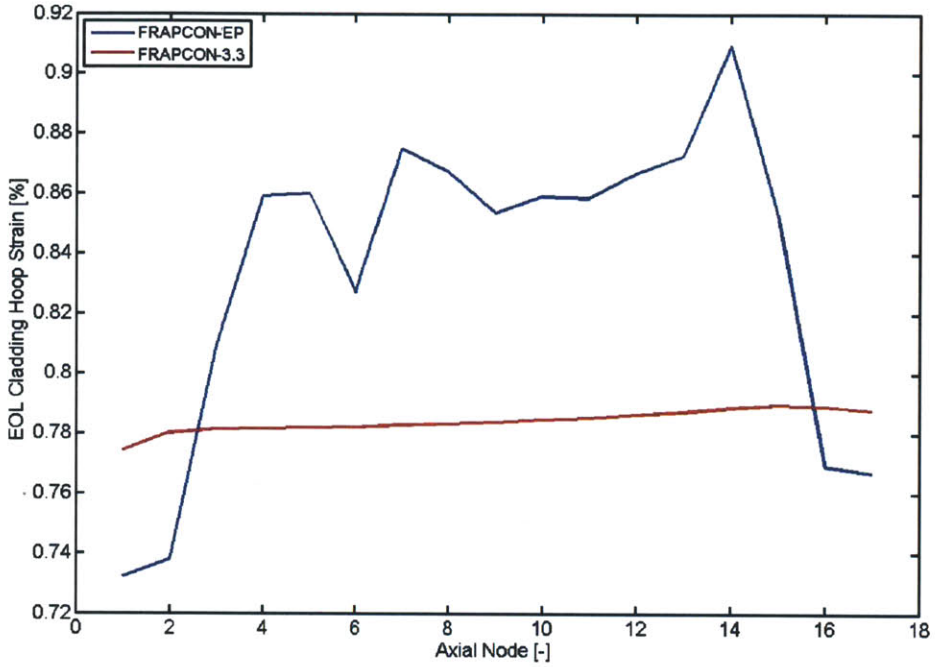

Figure 4-45: **Cladding hoop strain at EOL of the uprated case**

Similar to the annular pellet case at the original core power, the difference in predicting cladding failure between FRAPCON-3.3 and FRAPCON-EP is largely a result of the treatment of the inner cladding radius, observed in Figure 4-46. The addition of the difference in the predicted final fuel inner radius between the two models again shows that if FRAPCON-3.3 were to include the inner fuel displacement, it too would more than likely predict failure of the brittle cladding.

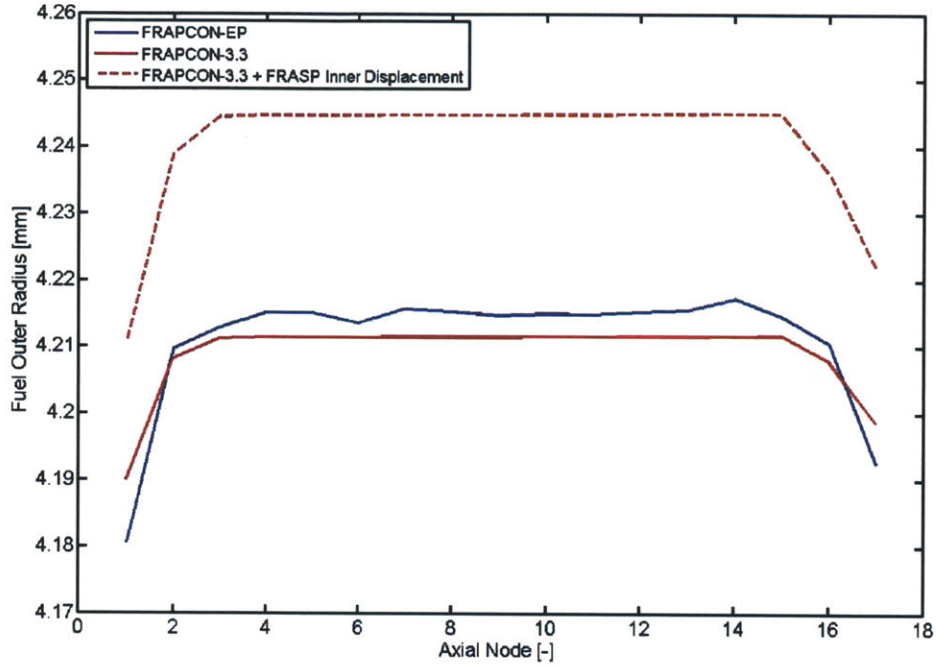

Figure 4-46: **Comparison of FRAPCON-EP and FRAPCON-3.3 EOL fuel outer radii with and without the addition of FRASP's predicted inner surface displacement for the uprated case**

The fact that FRAPCON-EP predicts failure for the uprated annular pellet case at a lower burnup than is achieved with annular fuel at the original power level is due entirely to the higher fuel temperatures resulting in larger thermal expansion of the fuel pellet. This increased thermal expansion also results in higher peak interfacial pressure occurring earlier, as shown in Figure 4-47. An investigation of the predicted EOL interfacial pressure in Figure 4-48 reveals that FRAPCON-EP continues to predict only values below the tolerable maximum of 45 MPa for elastic behavior.

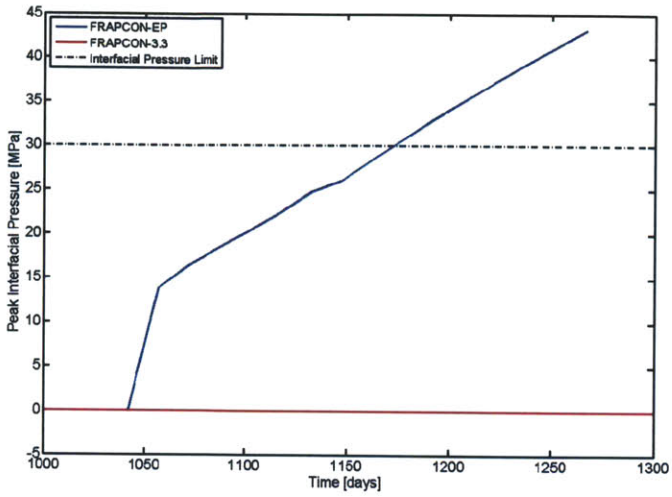

Figure 4-47: **Maximum interfacial pressure throughout the lifetime of the uprated case**

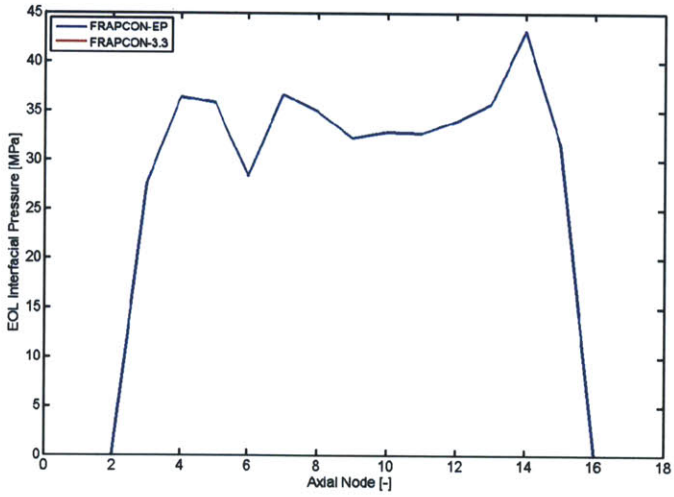

Figure 4-48: **Interfacial pressure observed at EOL of the uprated case**

4.6 Discussion of SiC Clad PWR Fuel Designs

After applying the improved models of FRAPCON-EP to three limiting SiC clad fuel rod designs, it can be observed that the structural predictions of FRAPCON-3.3 are not as conservative as previously assumed. All three cases result in PCMI, and the final uprated case is not predicted to survive three full cycles in a PWR.

Investigation of the mechanisms leading to these results show that generally higher fuel temperatures for the solid pellet and the FRASP's treatment of the fuel inner radius for annular fuel cases to be primarily responsible. The second point of fuel inner radius treatment is of particular concern, as FRAPCON-3.3's approach of wholly neglecting its evolution is responsible for the prediction of cladding survival. While changes in this dimension are relatively small, a maximum of approximately 2.5% the total change in fuel radius, they can have dramatic effects on the less ductile SiC cladding.

While FRAPCON-EP does not predict cladding failure for either the solid fuel pellet or annular fuel pellet cases before the planned EOL, both experience interfacial pressures which are approaching the maximum tolerable limit for SiC cladding. These predictions are acceptable for the steady state operations of the reactor, especially given that these are the peak burnup pins, but may not be able to survive a transient. Given their proximity to the failure criteria, these pins are likely to experience failure should such a stressful situation occur. Transient analysis of SiC clad fuel pins is outside the realm of this study and will be left as future work.

Unlike Zircaloy, which has a long and well documented operational history, few effective benchmarks exist for comparing SiC clad fuel rod simulations to real world operation. To compound the issue, no regulatory limits are in place to provide effective guidelines for the acceptable fuel performance criteria associated with SiC clad fuel rods. While these are broad concerns, they should be considered by future fuel designers when evaluating the use of SiC cladding.

This study suggests that it may not be appropriate to simply replace the Zircaloy cladding of current PWR fuel pin designs with SiC, much less do so with an up-

rated core power. This does not disqualify the use of SiC as a potential cladding material, but rather implies that its incorporation has dramatic implications on fuel performance which must be accounted for appropriately. Oversimplification of the mechanisms driving these behaviors, exemplified by the treatment of the cladding inner radius in FRAPCON-3.3, may result in predictions which fail to capture potentially critical behavior, like PCMI.

Chapter 5

Summary and Recommendations for Future Work

This work focused on developing and applying a new model, FRASP, for modeling PCMI conditions in FRAPCON-EP. The implementation of this new model is intended to replace the constraints associated with the rigid pellet and thin shell models in FRACAS-I with coupled 1.5D structural mechanics for the fuel pellet and cladding in FRASP. Incorporating this more advanced model into FRAPCON will allow fuel rod analysts to better predict conditions which could potentially lead to PCMI failure.

5.1 Summary of FRASP Development and Preliminary Validation

Unlike FRASP, FRACAS-I makes use of a simplistic model without detailed structural mechanics for fuel growth and the thin shell approximation for the mechanical behavior of the cladding. Because these models are incompatible with the PCMI for relatively slow transients (such as powering up the core) and for ceramic cladding, coupling the behavior of the fuel pellet and cladding required a complete replacement of FRACAS-I with FRASP in FRAPCON. This new mechanical model applies 1.5D

structural mechanics to two concentric annular cylinders representing the fuel pellet and cladding. These new models include provisions for both the brittle fracture of the fuel pellet and inelastic straining, both instantaneous and time dependent, of the cladding.

The incorporation of FRASP into FRAPCON was done in such a way such that it provides a new framework for determining the fuel rod's structural state using non-mechanical and material property parameters calculated by independent models within FRAPCON. Because of its use of existing models, FRASP is highly versatile and can be incorporated into any modified version of FRAPCON which uses a code structure similar to FRAPCON-3.3. This versatility gives FRASP the ability to improve FRAPCON's mechanical analysis regardless of the governing fuel and cladding behaviors.

In order to preliminarily validate FRASP, an average fuel rod under typical PWR conditions was evaluated. For this validation, FRAPCON-3.3 was used in two separate flavors, one using FRASP and one using FRACAS-I. While some variations existed between the results of the two fuel performance codes, they were generally slight and attributable to FRASP's improved treatment of several phenomena. Investigation of non-mechanical parameters showed that these observed variations didn't cause radical feedback effects in general fuel performance predictions. Most importantly, this validation showed that the PCMI model within FRASP does allow for a degree of stress-induced fuel pellet deformation.

5.2 Summary of FRAPCON-EP Analysis of SiC Clad Fuel Rods

Because of FRASP's ability to better evaluate PCMI, it was decided to evaluate three cases representative of the application of SiC cladding under current PWR operational practices, which has previously proven to be a challenge to FRACAS-I. This analysis was performed to evaluate the potentially differing predictions of

FRAPCON-EP with FRASP and FRAPCON-3.3 with FRACAS-I. Both codes were modified to include the material properties of SiC cladding into their respective mechanical models. These cases also took advantage of improvements in the simulation of the Seabrook reactor core to make use of significantly more realistic power histories than had been used in previous studies.

Due to the new fuel behavior and mechanical models in FRAPCON-EP, it predicted more limiting fuel performance results for SiC clad fuel rods than had previously been estimated using FRAPCON-3.3. This included relatively longer periods of time in which PCMI was expected to be occurring. The fuel rods operated at current reactor power levels were expected to survive up to 77 MWd/kgU, though with interfacial pressures that exceed the accepted operational limit. However, the case operating at a 10% uprated power level predicted failure at burnups slightly beyond 72 MWd/kgU. In contrast, FRAPCON-3.3 fails to predict hard contact between the fuel and cladding, and thus PCMI, for any of the analyzed cases.

Investigation into the cause of these differences revealed two mechanisms driving them. The first, most applicable to the solid pellet case, is FRAPCON-EP's more sophisticated treatment of fuel pellet swelling, which leads to a slightly larger fuel pellet. The second, and more serious difference, is observed only in the cases involving annular fuel pellets. For these cases, the differing results seem to result from the mechanical models' treatment of the inner fuel pellet radius. While FRACAS-I treats this value as constant, FRASP predicts it to grow and evolve throughout the life of the fuel rod, leading to a significantly larger fuel pellet and the failure of the cladding. This treatment of the inner fuel pellet radius as constant by FRACAS-I presents serious questions about previously analyzed annular fuel rod cases. The FRASP model, however, has not been verified against experiments with annular pellets. Therefore, without further validation, it cannot be taken as certain either.

5.3 Recommendations for Future Uses of and Improvements to FRASP

The development of FRASP was intentionally oriented to allow its incorporation into multiple versions of FRAPCON-3 in order to facilitate the improved mechanical modeling of a wide range of fuel rod designs. The work performed in this study alone detailed the incorporation and use of FRASP into three separate versions of FRAPCON. As observed in the SiC clad cases, the use of FRASP's improved mechanical models may provide otherwise unobserved insights into the feasibility of fuel designs. Future work should be oriented to implement FRASP into other existing versions of FRAPCON, including those for a high content of plutonium oxide, as in the RBWR, uranium nitride fuel, and thorium fuel. The need for non-steady-state analysis of these innovative fuel rod designs may also create a desire to modify FRASP for use in FRAPTRAN, FRAPCON's equivalent for fast transient fuel rod analysis.

The work presented in this study focused only on a preliminary validation of FRASP and its potential benefits for evaluating innovative fuel rod designs. While this validation against FRACAS-I allows for the quantification of differing effects between the two models, a more rigorous validation against experimental data is needed to fully trust the results found by FRASP. These experimental validations should focus on commercial reactor operations, for both PWRs and BWRs, and power ramp experiments in test reactors. Comparisons with power ramp data is particularly relevant to the validation of FRASP's PCMI model.

The fuel pellet model within FRASP is highly dependent on the effects of the smeared cracking model. Within this model, FRASP could benefit from two distinct improvements. The first is to relax the limit of 10 cracks on the surface of the fuel pellet. This upper limit was implemented based on limited experience with the use of FRASP at high LHGRs. Future work should focus on better quantifying the non-physical effects of large amounts of cracking and perhaps look for a relation for a non-static maximum crack value. Likewise, crack healing should be further investigated for implementation into the fuel pellet model.

The friction model within FRASP would also benefit from the addition of a slip condition associated with a friction coefficient and the interfacial pressure. While this would likely have little effect on ductile materials like Zircaloy, it may well provide insight into improved PCMI performance for stiffer cladding materials, such as SiC.

By providing more detailed information about the stress and strain profiles throughout the fuel pellet and cladding, the use of FRASP opens the door for more sophisticated modeling of parameters in both components. This includes the potential incorporation of new models for cladding corrosion, fuel and cladding creep, and iodine assisted SCC PCI failure mechanisms. Likewise, FRASP would be able to make use of the improved material properties found by these more sophisticated models to provide improved mechanical performance analysis.

5.4 Recommendations for Future Analyses of SiC Clad Fuel Rods

The analyses of SiC clad fuel rods performed as part of this work using the improved FRAPCON-EP code suggest that it may not be feasible to simply replace Zircaloy cladding in a current PWR environment with SiC and achieve the same burnup, and is even less likely to be achievable with a 10% power uprate. While these cases were not focused on improving overall fuel performance, they did reveal that using current PWR fuel rod geometry, even with the introduction of a central void in the pellet, with current power histories is likely not to offer higher burnup potential.

This, however, does not disqualify the use of SiC as a cladding material. The use of SiC cladding may be driven more by the need to avoid catalytic oxidation of the cladding at high temperatures, and thus limiting the hydrogen generation under severe accidents. These results simply suggest that SiC is not direct replacement for Zircaloy in current fuel rod geometries and operations which are highly optimized for the use of Zircaloy. Future analysis of SiC clad fuel rods should focus on optimizing their design in conjunction with their operational conditions.

Currently, NRC operational criteria are directed entirely towards the regulation of Zircaloy clad fuel rods. In order to successfully deploy SiC clad fuel rods, quantifiable limits need to be established for their operation. The establishment of acceptable limits for normal operation will provide fuel designers with a better defined design space. Similar to the Zircaloy cladding limits, these limits will require further analysis of transient and accident scenarios.

Bibliography

Atkinson, K. and Han, W. (2004). *Elementary Numerical Analysis.* John Wiley & Sons.

Berna, G. A., Beyer, C., Davis, K. L., and Lanning, D. D. (1997). Frapcon-3: A computer code for the calculation of steady-state, thermal-mechanical behavior of oxide fuel rods for high burnup. Technical Report NUREG/CR-6534, Vol. 2, US Nuclear Regulatory Commission.

Bernaudat, C. (1995). Mechanical behaviour modeling of fractured nuclear fuel pellets. *Nuclear Engineering and Design*, 156:373–381.

Beyer, C., Hann, C., Lanning, D., Panisko, F., and Parchen, L. (1975). Gapcon-thermal-2: A computer program for calculating the thermal behavior of an oxide fuel rod. Technical Report BNWL-1898, US Nuclear Regulation Commission.

Callister, W. (2007). *Materials Science and Engineering an Introduction.* John Wiley & Sons, 7th ed edition.

Carpenter, D. (2006). Assessment of innovative fuel designs for high performance light water reactors. Master's thesis, Massachusetts Institute of Technology.

Carpenter, D., Kohse, G., and Kazimi, M. (2010). *An Assessment of Silicon Carbide as a Cladding Material for Light Water Reactors*, volume MIT-ANP-TR-132. Center for Advanced Nuclear Energy Systems.

Dangouleme, D., Inozemtsev, V., Kamimura, K., Kucuk, A., Novikov, V., Onufriev,

V., and Tayal, M. (2010). Iaea review of fuel failures in water cooled reactors. In *Proceedings of 2010 LWR Fuel Performance/TopFuel/WRFPM.*

Dobisesky, J. P. (2011). Reactor physics considerations for implementing silicon carbide cladding into a pwr environment. Master's thesis, Massachusetts Institute of Technology.

Geelhood, K., Beyer, C., and Luscher, W. (2008). Pnnl stress/strain correlation for zircaloy. Technical Report PNNL-17700, US Department of Energy.

Geelhood, K., Luscher, W., and Beyer, C. (2010). Frapcon-3.4: A computer code for the calculation of steady-state, thermal-mechanical behavior of oxide fuel rods for high burnup. Technical Report NUREG/CR-7022, Vol. 1, US Nuclear Regulatory Commission.

Herranz, L., Vallejo, I., Khvostov, G., Sercombe, J., and Zhou, G. (2011). Assessment of fuel rod performance codes under ramp scenarios investigated within the scip project. *Nuclear Engineering and Design*, 241:815–825.

Ishihara, M., Baba, S., Hoshiya, T., and Shikama, T. (2002). Irradiation effects on thermal expansion of sic/sic composite materials. *Journal of Nuclear Materials*, 307-311:1168–1172.

Jankus, V. and R.W., W. (1972). Life-ii - a computer analysis of fast-reactor fuel-element behavior as a function of reactor operating history. *Nuclear Engineering and Design*, 18:83–96.

Karahan, A. (2009). *Modeling of Thermo-Mechanical and Irradiation Behavior of Metallic and Oxide Fuels for Sodiun Fast Reactors.* Phd, Massachusetts Institute of Technology.

Karahan, A., Feng, B., and Kazimi, M. (2011). Analysis of mixed oxide fuel behavior under reduced moderation boiling water reactor conditions with frapcon-ep. In *Proceedings of ICAPP 2011.*

Karahan, A., Lerch, A., and Kazimi, M. (2010). Development of frapcon-ep for high burnup and high temperature fuel pellet behavior modeling. In *Proceedings of 2010 LWR Fuel Performance/TopFuel/WRFPM.*

Knief, R. (1992). *Nuclear Engineering.* Taylor & Francis, second edition edition.

Lanning, D., Beyer, C., and Berna, G. A. (1997). Frapcon-3: Integral assessment. Technical Report NUREG/CR-6534, Vol. 3, US Nuclear Regulatory Commission.

Lerch, A. (2010). Thermomechanical analysis of innovative nuclear fuel pin designs. Master's thesis, Massachusetts Institute of Technology.

Luscher, W. and Geelhood, K. (2011). Material property correlations: Comparisons between frapcon-3.4, fraptran 1.4, and matpro. Technical Report NUREG/CR-7024, Pacific Northwest National Laboratory.

Lustman, B. (1981). Development of the zircaloy-clad uo2 fuel element for shipping-port. *Journal of Nuclear Materials*, 100:72–77.

Marchal, N., Campos, C., and Garnier, C. (2009). Finite element simulation of pellet-cladding interaction (pci) in nuclear fuel rods. *Computational Materials Science*, 45:821–826.

Massih, A., Jernkvist, L., Lindbak, J., and Zhou, G. (2005). Analysis of pellet-clad interaction of lwr fuel rods during power ramps. In *18th International Conference on Structural Mechanics in Reactor Technology (SMiRT 18).*

NRC, U. (2007). Standard review plan for the review of safety analysis reports for nuclear power plants: Lwr edition: Reactor (nureg-0800, chapter 4). Technical Report NUREG-800, US Nuclear Regulatory Commission.

O'Donnell, G., Scott, H., and Meyer, R. (2001). A new comparative analysis of lwr fuel designs. Technical Report NUREG-1754, US Nuclear Regulatory Commission.

Olander, D. R. (1976). *Fundamental Aspects of Nuclear Reactor Fuel Elements.* US Department of Energy.

Rusch, C. (2008). Nuclear fuel performance: Trends, remedies, and challenges. *Journal of Nuclear Materials*, 383:41–44.

Seabrook (2007). Revision 11 to updated final safety analysis report, chapter 4. Technical report, US Nuclear Regulatory Commission.

Sercombe, J., Aubrun, I., and Nonon, C. (2012). Power ramped cladding stresses and strains in 3d simulations with burnup-dependent pellet-clad friction. *Nuclear Engineering and Design*, 242:164–181.

Sjoden, G. (2009). *Foundations in applied Nuclear Engineering Analysis.* World Scientific.

Thourvenin, G., Michel, B., Sercombe, J., and Planq, D. (2007). Multidimensional modeling of a ramp test with the pwr fuel performance code alcyone. In *Proceedings of the 2007 International LWR Fuel Performance Meeting.*

Todreas, N. and Kazimi, M. (1990). *Nuclear Systems I.* Taylor & Francis Group.

Williamson, R., Hales, J., Novascone, S., Tonks, M., Gatson, D., Permann, C., Andrs, D., and Martineau, R. (2012). Multidimensional multiphysics simulation of nuclear fuel behavior. *Journal of Nuclear Materials*, 423:149–163.

Xu, S. and Kazimi, M. (2012). Assessment of different fuel design options with sic cladding for light water reactors. In *Proceedings of ICAPP 2012.* Department of Nuclear Science and Engineering, MIT.

Appendix A: FRAPCON Inputs

Preliminary Validation Case

```
*************************************************************************
* frapcon3, steady-state fuel rod analysis code, version 3 *
*-------------------------------------------------------------------- *
* *
* CASE DESCRIPTION: Seabrook 6.5mil gap, constant power *
* *
*UNIT FILE DESCRIPTION *
*---- ------------------------------------------- *
* Output : *
* 6 STANDARD PRINTER OUTPUT *
* *
* Scratch: *
* 5 SCRATCH INPUT FILE FROM ECH01 *
* *
* Input: FRAPCON2 INPUT FILE (UNIT 55) *
* *
*************************************************************************
* GOESINS:
FILE05='nullfile', STATUS='scratch', FORM='FORMATTED',
CARRIAGE CONTROL='LIST'
*
* GOESOUTS:
FILE06='constant-33Zr-FRASP.out', STATUS='UNKNOWN', CARRIAGE CONTROL='LIST'
FILE66='constant-plot-33Zr-FRASP.out', STATUS='UNKNOWN', CARRIAGE CONTROL='LIST'
/*************************************************************************
43: Seabrook 6.5mil gap, constant power
$frpcn
im=107, na=17, ngasr=30, nr=25,
$end
$frpcon
nunits=0, pitch=1.259e-2, dco=9.5e-3, thkcld=5.71e-4, thkgap=8.25e-5,
hplt=9.83e-3, hdish=2.87e-4, dishsd=4.01e-3, den=95.0, enrch=4.5,
roughc=5.1e-7, roughf=7.6e-7, idxgas=1, fgpav=2.41e6, cpl=0.254,
totl=3.66, rc=0.0, rsntr=97.2, dspg=8.19e-3, dspgw=1.27e-3, vs=28,
icor=0, crdt=0.0, crdtr=0.0, iplant=-2, icm=4, nsp=0,
p2=15.5e6, tw=565.82, go=3336, nplot=1, iq=0, fa=1.0,
jn=1*14, jst=97*1, slim=0.05, jdlpr=0,
qf(1)= 0.629,0.839,0.957,1.032,1.065,1.078,1.075,1.085,1.078,1.061,1.031,
0.942,0.824,0.659,
x(1)= 0.000,0.311,0.483,0.630,0.758,0.941,1.252,2.49,2.826,3.020,3.118,
```

```
3.272,3.429,3.660,
ProblemTime= 0.0100,0.1090,0.2080,0.3070,0.4060
0.5050,0.6040,0.7030,0.8020,0.9010
1.0000,2.0000,4.0000,7.0000,10.0000
15.0000,20.0000,30.0000,40.0000,60.0000
80.0000,100.0000,120.0000,140.0000,160.0000
180.0000,200.0000,220.0000,240.0000,260.0000
280.0000,300.0000,320.0000,340.0000,360.0000
380.0000,400.0000,420.0000,440.0000,460.0000
480.0000,500.0000,520.0000,540.0000,560.0000
580.0000,600.0000,620.0000,640.0000,660.0000
680.0000,700.0000,720.0000,740.0000,760.0000
780.0000,800.0000,820.0000,840.0000,860.0000
880.0000,900.0000,920.0000,940.0000,960.0000
980.0000,1000.0000,1020.0000,1040.0000,1060.0000
1080.0000,1100.0000,1120.0000,1140.0000,1160.0000
1180.0000,1200.0000,1220.0000,1240.0000,1260.0000
1280.0000,1300.0000,1320.0000,1340.0000,1360.0000
1380.0000,1400.0000,1420.0000,1440.0000,1460.0000
1480.0000,1500.0000,1520.0000,1540.0000,1560.0000
1580.0000,1600.0000,1620.0000,1640.0000,1660.0000
1680.0000,1700.0000,1720.0000,1740.0000,1760.0000
1780.0000,1800.0000,
qmpy= 0.01,1.79,3.58,5.36,7.15
8.93,10.71,12.50,14.28,16.06
17.85,17.85,17.85,17.85,17.85
17.85,17.85,17.85,17.85,17.85
17.85,17.85,17.85,17.85,17.85
17.85,17.85,17.85,17.85,17.85
17.85,17.85,17.85,17.85,17.85
17.85,17.85,17.85,17.85,17.85
17.85,17.85,17.85,17.85,17.85
17.85,17.85,17.85,17.85,17.85
17.85,17.85,17.85,17.85,17.85
17.85,17.85,17.85,17.85,17.85
17.85,17.85,17.85,17.85,17.85
17.85,17.85,17.85,17.85,17.85
17.85,17.85,17.85,17.85,17.85
17.85,17.85,17.85,17.85,17.85
17.85,17.85,17.85,17.85,17.85
17.85,17.85,17.85,17.85,17.85
17.85,17.85,17.85,17.85,17.85
17.85,17.85,
$end
```

Seabrook Solid Pellet Case

```
*****************************************************************************
* frapcon3, steady-state fuel rod analysis code, version 3 *
*---------------------------------------------------------------------- *
* *
* CASE DESCRIPTION: Seabrook 6.5mil gap, constant power *
* *
*UNIT FILE DESCRIPTION *
*---- ------------------------------------------- *
* Output : *
* 6 STANDARD PRINTER OUTPUT *
* *
* Scratch: *
* 5 SCRATCH INPUT FILE FROM ECH01 *
* *
* Input: FRAPCON2 INPUT FILE (UNIT 55) *
* *
*****************************************************************************
* GOESINS:
FILE05='nullfile', STATUS='scratch', FORM='FORMATTED',
CARRIAGE CONTROL='LIST'
*
* GOESOUTS:
FILE06='solid-EPSiC-FRASP.out', STATUS='UNKNOWN', CARRIAGE CONTROL='LIST'
FILE66='solid-plot-EPSiC-FRASP.out', STATUS='UNKNOWN', CARRIAGE CONTROL='LIST'
/*****************************************************************************
43: Seabrook 6.5mil gap, constant power
$frpcn
im=136, na=17, ngasr=30, nr=25,
$end
$frpcon
nunits=0, pitch=1.259e-2, dco=9.5e-3, thkcld=5.71e-4, thkgap=8.25e-5,
hplt=9.83e-3, hdish=2.87e-4, dishsd=4.01e-3, den=95.0, enrch=4.5,
roughc=5.1e-7, roughf=7.6e-7, idxgas=1, fgpav=2.41e6, cpl=0.254,
totl=3.66, rc=0.0, rsntr=97.2, dspg=8.19e-3, dspgw=1.27e-3, vs=28,
icor=0, crdt=0.0, crdtr=0.0, iplant=-2, icm=4, nsp=0,
p2=15.5e6, tw=565.82, go=3336, nplot=1, iq=0, fa=1.0,
jn=9*26, jst=46*1,11*2,11*3,12*4,11*5,11*6,12*7,10*8,12*9, slim=0.05, jdlpr=0,
qf(1)=0.396,0.509,0.716,0.854,0.932,0.966,1.044,1.078,1.078,
1.139,1.173,1.173,1.165,1.199,1.199,1.156,1.182,1.165,1.122,
1.087,1.052,0.975,0.845,0.725,0.552,0.458,
qf(27)=0.477,0.608,0.847,0.959,1.000,0.996,1.037,1.042,1.025,
1.062,1.075,1.066,1.054,1.079,1.079,1.042,1.070,1.066,1.042,
1.037,1.037,1.008,0.930,0.847,0.707,0.630,
qf(53)=0.557,0.706,0.979,1.067,1.075,1.035,1.043,1.019,0.987,
1.003,0.995,0.979,0.963,0.979,0.979,0.947,0.979,0.987,0.979,
1.003,1.035,1.051,1.019,0.971,0.858,0.797,
qf(79)=0.389,0.526,0.776,0.906,0.970,0.994,1.059,1.092,1.083,
1.140,1.164,1.156,1.148,1.172,1.172,1.132,1.156,1.140,1.100,
1.075,1.043,0.978,0.857,0.729,0.534,0.427,
qf(105)=0.498,0.631,0.874,0.972,1.002,0.997,1.031,1.040,1.023,
1.061,1.070,1.057,1.040,1.065,1.065,1.036,1.061,1.057,1.036,
1.031,1.031,1.010,0.938,0.858,0.720,0.645,
```

```
qf(131)=0.629,0.758,0.996,1.060,1.051,1.014,1.014,0.996,0.968,
0.987,0.977,0.959,0.932,0.959,0.959,0.941,0.968,0.977,0.977,
0.996,1.032,1.060,1.041,1.014,0.941,0.901,
qf(157)=0.397,0.520,0.744,0.856,0.917,0.948,1.019,1.060,1.070,
1.121,1.151,1.162,1.151,1.182,1.182,1.151,1.172,1.162,1.121,
1.090,1.070,0.999,0.886,0.774,0.581,0.475,
qf(183)=0.505,0.629,0.857,0.946,0.976,0.976,1.011,1.021,1.011,
1.040,1.055,1.055,1.040,1.065,1.065,1.040,1.065,1.065,1.045,
1.040,1.050,1.026,0.961,0.892,0.753,0.677,
qf(209)=0.614,0.742,0.976,1.044,1.044,1.015,1.015,0.995,0.966,
0.976,0.976,0.966,0.947,0.966,0.966,0.947,0.976,0.986,0.986,
1.005,1.044,1.064,1.044,1.015,0.927,0.879,
x(1)=0.00,0.09,0.21,0.37,0.52,0.67,0.82,0.98,1.13,1.28,
1.43,1.58,1.74,1.89,2.04,2.19,2.35,2.50,2.65,2.80,2.96,
3.11,3.26,3.41,3.57,3.66,
x(27)=0.00,0.09,0.21,0.37,0.52,0.67,0.82,0.98,1.13,1.28,
1.43,1.58,1.74,1.89,2.04,2.19,2.35,2.50,2.65,2.80,2.96,
3.11,3.26,3.41,3.57,3.66,
x(53)=0.00,0.09,0.21,0.37,0.52,0.67,0.82,0.98,1.13,1.28,
1.43,1.58,1.74,1.89,2.04,2.19,2.35,2.50,2.65,2.80,2.96,
3.11,3.26,3.41,3.57,3.66,
x(79)=0.00,0.09,0.21,0.37,0.52,0.67,0.82,0.98,1.13,1.28,
1.43,1.58,1.74,1.89,2.04,2.19,2.35,2.50,2.65,2.80,2.96,
3.11,3.26,3.41,3.57,3.66,
x(105)=0.00,0.09,0.21,0.37,0.52,0.67,0.82,0.98,1.13,1.28,
1.43,1.58,1.74,1.89,2.04,2.19,2.35,2.50,2.65,2.80,2.96,
3.11,3.26,3.41,3.57,3.66,
x(131)=0.00,0.09,0.21,0.37,0.52,0.67,0.82,0.98,1.13,1.28,
1.43,1.58,1.74,1.89,2.04,2.19,2.35,2.50,2.65,2.80,2.96,
3.11,3.26,3.41,3.57,3.66,
x(157)=0.00,0.09,0.21,0.37,0.52,0.67,0.82,0.98,1.13,1.28,
1.43,1.58,1.74,1.89,2.04,2.19,2.35,2.50,2.65,2.80,2.96,
3.11,3.26,3.41,3.57,3.66,
x(183)=0.00,0.09,0.21,0.37,0.52,0.67,0.82,0.98,1.13,1.28,
1.43,1.58,1.74,1.89,2.04,2.19,2.35,2.50,2.65,2.80,2.96,
3.11,3.26,3.41,3.57,3.66,
x(209)=0.00,0.09,0.21,0.37,0.52,0.67,0.82,0.98,1.13,1.28,
1.43,1.58,1.74,1.89,2.04,2.19,2.35,2.50,2.65,2.80,2.96,
3.11,3.26,3.41,3.57,3.66,
ProblemTime=0.0010,0.1000,0.2000,0.3000,0.4000
0.5000,0.6000,0.7000,0.8000,0.9000
1.0000,1.1000,1.4937,1.8874,2.0000
3.0000,4.0000,5.0000,6.0000,7.0000
8.0000,9.0000,10.0000,11.0000,12.0000
13.0000,14.0000,15.0000,18.0000,21.0000
24.0000,27.0000,30.0000,35.0000,40.0000
45.0000,50.0000,60.0000,70.0000,80.0000
90.0000,100.0000,115.0000,130.0000,145.0000
160.0000,175.0000,190.0000,205.0000,220.0000
235.0000,250.0000,265.0000,280.0000,295.0000
310.0000,325.0000,340.0000,355.0000,370.0000
385.0000,400.0000,415.0000,430.0000,445.0000
460.0000,475.0000,483.3333,483.5833,498.5833
513.5833,528.5833,543.5833,558.5833,573.5833
```

588.5833,603.5833,618.5833,633.5833,648.5833
663.5833,678.5833,693.5833,708.5833,723.5833
738.5833,753.5833,768.5833,783.5833,798.5833
813.5833,828.5833,843.5833,858.5833,873.5833
888.5833,903.5833,918.5833,933.5833,948.5833
963.5833,966.6667,966.9167,981.9167,996.9167
1011.9167,1026.9167,1041.9167,1056.9167,1071.9167
1086.9167,1101.9167,1116.9167,1131.9167,1146.9167
1161.9167,1176.9167,1191.9167,1206.9167,1221.9167
1236.9167,1251.9167,1266.9167,1281.9167,1296.9167
1311.9167,1326.9167,1341.9167,1356.9167,1371.9167
1386.9167,1401.9167,1416.9167,1431.9167,1446.9167
1450.0000
qmpy= 0.00,1.25,2.50,3.75,5.00
6.25,7.50,8.75,10.00,11.25
12.50,13.75,18.67,23.59,25.00
25.00,25.00,25.00,25.00,25.00
25.00,25.00,25.00,25.00,25.00
25.00,25.00,25.00,25.00,25.00
25.00,25.00,25.00,25.00,25.00
25.00,25.00,25.00,25.00,25.00
25.00,25.00,25.00,25.00,25.00
25.00,25.00,25.00,25.00,25.00
25.00,25.00,25.00,25.00,25.00
25.00,25.00,25.00,25.00,25.00
25.00,25.00,25.00,23.50,23.50
23.50,23.50,23.50,23.50,23.50
23.50,23.50,23.50,23.50,23.50
23.50,23.50,23.50,23.50,23.50
23.50,23.50,23.50,23.50,23.50
23.50,23.50,23.50,23.50,23.50
23.50,23.50,23.50,23.50,23.50
23.50,23.50,18.25,18.25,18.25
18.25,18.25,18.25,18.25,18.25
18.25,18.25,18.25,18.25,18.25
18.25,18.25,18.25,18.25,18.25
18.25,18.25,18.25,18.25,18.25
18.25,18.25,18.25,18.25,18.25
18.25,
$end

Seabrook Annular Pellet Case

```
*****************************************************************************
* frapcon3, steady-state fuel rod analysis code, version 3 *
*---------------------------------------------------------------------- *
* *
* CASE DESCRIPTION: Seabrook 6.5mil gap, constant power *
* *
*UNIT FILE DESCRIPTION *
*---- ------------------------------------------- *
* Output : *
* 6 STANDARD PRINTER OUTPUT *
* *
* Scratch: *
* 5 SCRATCH INPUT FILE FROM ECH01 *
* *
* Input: FRAPCON2 INPUT FILE (UNIT 55) *
* *
*****************************************************************************
* GOESINS:
FILE05='nullfile', STATUS='scratch', FORM='FORMATTED',
CARRIAGE CONTROL='LIST'
*
* GOESOUTS:
FILE06='void-EPSiC-FRASP.out', STATUS='UNKNOWN', CARRIAGE CONTROL='LIST'
FILE66='void-plot-EPSiC-FRASP.out', STATUS='UNKNOWN', CARRIAGE CONTROL='LIST'
/*****************************************************************************
43: Seabrook 6.5mil gap, constant power
$frpcn
im=136, na=17, ngasr=30, nr=25,
$end
$frpcon
nunits=0, pitch=1.259e-2, dco=9.5e-3, thkcld=5.71e-4, thkgap=8.25e-5,
hplt=9.83e-3, hdish=2.87e-4, dishsd=4.01e-3, den=95.0, enrch=4.5,
roughc=5.1e-7, roughf=7.6e-7, idxgas=1, fgpav=2.41e6, cpl=0.254,
totl=3.66, rc=1.29e-3, rsntr=97.2, dspg=8.19e-3, dspgw=1.27e-3, vs=28,
icor=0, crdt=0.0, crdtr=0.0, iplant=-2, icm=4, nsp=0,
p2=15.5e6, tw=565.82, go=3336, nplot=1, iq=0, fa=1.0,
jn=9*26, jst=46*1,11*2,11*3,12*4,11*5,11*6,12*7,10*8,12*9, slim=0.05, jdlpr=0,
qf(1)=0.396,0.509,0.716,0.854,0.932,0.966,1.044,1.078,1.078,
1.139,1.173,1.173,1.165,1.199,1.199,1.156,1.182,1.165,1.122,
1.087,1.052,0.975,0.845,0.725,0.552,0.458,
qf(27)=0.477,0.608,0.847,0.959,1.000,0.996,1.037,1.042,1.025,
1.062,1.075,1.066,1.054,1.079,1.079,1.042,1.070,1.066,1.042,
1.037,1.037,1.008,0.930,0.847,0.707,0.630,
qf(53)=0.557,0.706,0.979,1.067,1.075,1.035,1.043,1.019,0.987,
1.003,0.995,0.979,0.963,0.979,0.979,0.947,0.979,0.987,0.979,
1.003,1.035,1.051,1.019,0.971,0.858,0.797,
qf(79)=0.389,0.526,0.776,0.906,0.970,0.994,1.059,1.092,1.083,
1.140,1.164,1.156,1.148,1.172,1.172,1.132,1.156,1.140,1.100,
1.075,1.043,0.978,0.857,0.729,0.534,0.427,
qf(105)=0.498,0.631,0.874,0.972,1.002,0.997,1.031,1.040,1.023,
1.061,1.070,1.057,1.040,1.065,1.065,1.036,1.061,1.057,1.036,
1.031,1.031,1.010,0.938,0.858,0.720,0.645,
```

```
qf(131)=0.629,0.758,0.996,1.060,1.051,1.014,1.014,0.996,0.968,
0.987,0.977,0.959,0.932,0.959,0.959,0.941,0.968,0.977,0.977,
0.996,1.032,1.060,1.041,1.014,0.941,0.901,
qf(157)=0.397,0.520,0.744,0.856,0.917,0.948,1.019,1.060,1.070,
1.121,1.151,1.162,1.151,1.182,1.182,1.151,1.172,1.162,1.121,
1.090,1.070,0.999,0.886,0.774,0.581,0.475,
qf(183)=0.505,0.629,0.857,0.946,0.976,0.976,1.011,1.021,1.011,
1.040,1.055,1.055,1.040,1.065,1.065,1.040,1.065,1.065,1.045,
1.040,1.050,1.026,0.961,0.892,0.753,0.677,
qf(209)=0.614,0.742,0.976,1.044,1.044,1.015,1.015,0.995,0.966,
0.976,0.976,0.966,0.947,0.966,0.966,0.947,0.976,0.986,0.986,
1.005,1.044,1.064,1.044,1.015,0.927,0.879,
x(1)=0.00,0.09,0.21,0.37,0.52,0.67,0.82,0.98,1.13,1.28,
1.43,1.58,1.74,1.89,2.04,2.19,2.35,2.50,2.65,2.80,2.96,
3.11,3.26,3.41,3.57,3.66,
x(27)=0.00,0.09,0.21,0.37,0.52,0.67,0.82,0.98,1.13,1.28,
1.43,1.58,1.74,1.89,2.04,2.19,2.35,2.50,2.65,2.80,2.96,
3.11,3.26,3.41,3.57,3.66,
x(53)=0.00,0.09,0.21,0.37,0.52,0.67,0.82,0.98,1.13,1.28,
1.43,1.58,1.74,1.89,2.04,2.19,2.35,2.50,2.65,2.80,2.96,
3.11,3.26,3.41,3.57,3.66,
x(79)=0.00,0.09,0.21,0.37,0.52,0.67,0.82,0.98,1.13,1.28,
1.43,1.58,1.74,1.89,2.04,2.19,2.35,2.50,2.65,2.80,2.96,
3.11,3.26,3.41,3.57,3.66,
x(105)=0.00,0.09,0.21,0.37,0.52,0.67,0.82,0.98,1.13,1.28,
1.43,1.58,1.74,1.89,2.04,2.19,2.35,2.50,2.65,2.80,2.96,
3.11,3.26,3.41,3.57,3.66,
x(131)=0.00,0.09,0.21,0.37,0.52,0.67,0.82,0.98,1.13,1.28,
1.43,1.58,1.74,1.89,2.04,2.19,2.35,2.50,2.65,2.80,2.96,
3.11,3.26,3.41,3.57,3.66,
x(157)=0.00,0.09,0.21,0.37,0.52,0.67,0.82,0.98,1.13,1.28,
1.43,1.58,1.74,1.89,2.04,2.19,2.35,2.50,2.65,2.80,2.96,
3.11,3.26,3.41,3.57,3.66,
x(183)=0.00,0.09,0.21,0.37,0.52,0.67,0.82,0.98,1.13,1.28,
1.43,1.58,1.74,1.89,2.04,2.19,2.35,2.50,2.65,2.80,2.96,
3.11,3.26,3.41,3.57,3.66,
x(209)=0.00,0.09,0.21,0.37,0.52,0.67,0.82,0.98,1.13,1.28,
1.43,1.58,1.74,1.89,2.04,2.19,2.35,2.50,2.65,2.80,2.96,
3.11,3.26,3.41,3.57,3.66,
ProblemTime=0.0010,0.1000,0.2000,0.3000,0.4000
0.5000,0.6000,0.7000,0.8000,0.9000
1.0000,1.1000,1.4937,1.8874,2.0000
3.0000,4.0000,5.0000,6.0000,7.0000
8.0000,9.0000,10.0000,11.0000,12.0000
13.0000,14.0000,15.0000,18.0000,21.0000
24.0000,27.0000,30.0000,35.0000,40.0000
45.0000,50.0000,60.0000,70.0000,80.0000
90.0000,100.0000,115.0000,130.0000,145.0000
160.0000,175.0000,190.0000,205.0000,220.0000
235.0000,250.0000,265.0000,280.0000,295.0000
310.0000,325.0000,340.0000,355.0000,370.0000
385.0000,400.0000,415.0000,430.0000,445.0000
460.0000,475.0000,483.3333,483.5833,498.5833
513.5833,528.5833,543.5833,558.5833,573.5833
```

```
588.5833,603.5833,618.5833,633.5833,648.5833
663.5833,678.5833,693.5833,708.5833,723.5833
738.5833,753.5833,768.5833,783.5833,798.5833
813.5833,828.5833,843.5833,858.5833,873.5833
888.5833,903.5833,918.5833,933.5833,948.5833
963.5833,966.6667,966.9167,981.9167,996.9167
1011.9167,1026.9167,1041.9167,1056.9167,1071.9167
1086.9167,1101.9167,1116.9167,1131.9167,1146.9167
1161.9167,1176.9167,1191.9167,1206.9167,1221.9167
1236.9167,1251.9167,1266.9167,1281.9167,1296.9167
1311.9167,1326.9167,1341.9167,1356.9167,1371.9167
1386.9167,1401.9167,1416.9167,1431.9167,1446.9167
1450.0000
qmpy= 0.00,1.25,2.50,3.75,5.00
6.25,7.50,8.75,10.00,11.25
12.50,13.75,18.67,23.59,25.00
25.00,25.00,25.00,25.00,25.00
25.00,25.00,25.00,25.00,25.00
25.00,25.00,25.00,25.00,25.00
25.00,25.00,25.00,25.00,25.00
25.00,25.00,25.00,25.00,25.00
25.00,25.00,25.00,25.00,25.00
25.00,25.00,25.00,25.00,25.00
25.00,25.00,25.00,25.00,25.00
25.00,25.00,25.00,25.00,25.00
25.00,25.00,25.00,25.00,25.00
25.00,25.00,25.00,23.50,23.50
23.50,23.50,23.50,23.50,23.50
23.50,23.50,23.50,23.50,23.50
23.50,23.50,23.50,23.50,23.50
23.50,23.50,23.50,23.50,23.50
23.50,23.50,23.50,23.50,23.50
23.50,23.50,23.50,23.50,23.50
23.50,23.50,18.25,18.25,18.25
18.25,18.25,18.25,18.25,18.25
18.25,18.25,18.25,18.25,18.25
18.25,18.25,18.25,18.25,18.25
18.25,18.25,18.25,18.25,18.25
18.25,18.25,18.25,18.25,18.25
18.25,18.25,18.25,18.25,18.25
18.25,
$end
```

Uprated Seabrook Annular Case

```
*******************************************************************************
* frapcon3, steady-state fuel rod analysis code, version 3 *
*------------------------------------------------------------------ *
* *
* CASE DESCRIPTION: Seabrook 6.5mil gap, constant power *
* *
*UNIT FILE DESCRIPTION *
*---- ------------------------------------------- *
* Output :  *
* 6 STANDARD PRINTER OUTPUT *
* *
* Scratch:  *
* 5 SCRATCH INPUT FILE FROM ECH01 *
* *
* Input:  FRAPCON2 INPUT FILE (UNIT 55) *
* *
*******************************************************************************
* GOESINS:
FILE05='nullfile', STATUS='scratch', FORM='FORMATTED',
CARRIAGE CONTROL='LIST'
*
* GOESOUTS:
FILE06='uprate-EPSiC-FRASP.out', STATUS='UNKNOWN', CARRIAGE CONTROL='LIST'
FILE66='uprate-plot-EPSiC-FRASP.out', STATUS='UNKNOWN', CARRIAGE CONTROL='LIST'
/*****************************************************************************
43:  Seabrook 6.5mil gap, constant power
$frpcn
im=136, na=17, ngasr=30, nr=25,
$end
$frpcon
nunits=0, pitch=1.259e-2, dco=9.5e-3, thkcld=5.71e-4, thkgap=8.25e-5,
hplt=9.83e-3, hdish=2.87e-4, dishsd=4.01e-3, den=95.0, enrch=4.5,
roughc=5.1e-7, roughf=7.6e-7, idxgas=1, fgpav=2.41e6, cpl=0.254,
totl=3.66, rc=1.29e-3, rsntr=97.2, dspg=8.19e-3, dspgw=1.27e-3, vs=28,
icor=0, crdt=0.0, crdtr=0.0, iplant=-2, icm=4, nsp=0,
p2=15.5e6, tw=565.82, go=3670, nplot=1, iq=0, fa=1.0,
jn=9*26, jst=46*1,11*2,11*3,12*4,11*5,11*6,12*7,10*8,12*9, slim=0.05, jdlpr=0,
qf(1)=0.396,0.509,0.716,0.854,0.932,0.966,1.044,1.078,1.078,
1.139,1.173,1.173,1.165,1.199,1.199,1.156,1.182,1.165,1.122,
1.087,1.052,0.975,0.845,0.725,0.552,0.458,
qf(27)=0.477,0.608,0.847,0.959,1.000,0.996,1.037,1.042,1.025,
1.062,1.075,1.066,1.054,1.079,1.079,1.042,1.070,1.066,1.042,
1.037,1.037,1.008,0.930,0.847,0.707,0.630,
qf(53)=0.557,0.706,0.979,1.067,1.075,1.035,1.043,1.019,0.987,
1.003,0.995,0.979,0.963,0.979,0.979,0.947,0.979,0.987,0.979,
1.003,1.035,1.051,1.019,0.971,0.858,0.797,
qf(79)=0.389,0.526,0.776,0.906,0.970,0.994,1.059,1.092,1.083,
1.140,1.164,1.156,1.148,1.172,1.172,1.132,1.156,1.140,1.100,
1.075,1.043,0.978,0.857,0.729,0.534,0.427,
qf(105)=0.498,0.631,0.874,0.972,1.002,0.997,1.031,1.040,1.023,
1.061,1.070,1.057,1.040,1.065,1.065,1.036,1.061,1.057,1.036,
1.031,1.031,1.010,0.938,0.858,0.720,0.645,
```

```
qf(131)=0.629,0.758,0.996,1.060,1.051,1.014,1.014,0.996,0.968,
0.987,0.977,0.959,0.932,0.959,0.959,0.941,0.968,0.977,0.977,
0.996,1.032,1.060,1.041,1.014,0.941,0.901,
qf(157)=0.397,0.520,0.744,0.856,0.917,0.948,1.019,1.060,1.070,
1.121,1.151,1.162,1.151,1.182,1.182,1.151,1.172,1.162,1.121,
1.090,1.070,0.999,0.886,0.774,0.581,0.475,
qf(183)=0.505,0.629,0.857,0.946,0.976,0.976,1.011,1.021,1.011,
1.040,1.055,1.055,1.040,1.065,1.065,1.040,1.065,1.065,1.045,
1.040,1.050,1.026,0.961,0.892,0.753,0.677,
qf(209)=0.614,0.742,0.976,1.044,1.044,1.015,1.015,0.995,0.966,
0.976,0.976,0.966,0.947,0.966,0.966,0.947,0.976,0.986,0.986,
1.005,1.044,1.064,1.044,1.015,0.927,0.879,
x(1)=0.00,0.09,0.21,0.37,0.52,0.67,0.82,0.98,1.13,1.28,
1.43,1.58,1.74,1.89,2.04,2.19,2.35,2.50,2.65,2.80,2.96,
3.11,3.26,3.41,3.57,3.66,
x(27)=0.00,0.09,0.21,0.37,0.52,0.67,0.82,0.98,1.13,1.28,
1.43,1.58,1.74,1.89,2.04,2.19,2.35,2.50,2.65,2.80,2.96,
3.11,3.26,3.41,3.57,3.66,
x(53)=0.00,0.09,0.21,0.37,0.52,0.67,0.82,0.98,1.13,1.28,
1.43,1.58,1.74,1.89,2.04,2.19,2.35,2.50,2.65,2.80,2.96,
3.11,3.26,3.41,3.57,3.66,
x(79)=0.00,0.09,0.21,0.37,0.52,0.67,0.82,0.98,1.13,1.28,
1.43,1.58,1.74,1.89,2.04,2.19,2.35,2.50,2.65,2.80,2.96,
3.11,3.26,3.41,3.57,3.66,
x(105)=0.00,0.09,0.21,0.37,0.52,0.67,0.82,0.98,1.13,1.28,
1.43,1.58,1.74,1.89,2.04,2.19,2.35,2.50,2.65,2.80,2.96,
3.11,3.26,3.41,3.57,3.66,
x(131)=0.00,0.09,0.21,0.37,0.52,0.67,0.82,0.98,1.13,1.28,
1.43,1.58,1.74,1.89,2.04,2.19,2.35,2.50,2.65,2.80,2.96,
3.11,3.26,3.41,3.57,3.66,
x(157)=0.00,0.09,0.21,0.37,0.52,0.67,0.82,0.98,1.13,1.28,
1.43,1.58,1.74,1.89,2.04,2.19,2.35,2.50,2.65,2.80,2.96,
3.11,3.26,3.41,3.57,3.66,
x(183)=0.00,0.09,0.21,0.37,0.52,0.67,0.82,0.98,1.13,1.28,
1.43,1.58,1.74,1.89,2.04,2.19,2.35,2.50,2.65,2.80,2.96,
3.11,3.26,3.41,3.57,3.66,
x(209)=0.00,0.09,0.21,0.37,0.52,0.67,0.82,0.98,1.13,1.28,
1.43,1.58,1.74,1.89,2.04,2.19,2.35,2.50,2.65,2.80,2.96,
3.11,3.26,3.41,3.57,3.66,
ProblemTime= 0.0010,0.1000,0.2000,0.3000,0.4000
0.5000,0.6000,0.7000,0.8000,0.9000
1.0000,1.1000,1.4579,1.8158,2.0000
3.0000,4.0000,5.0000,6.0000,7.0000
8.0000,9.0000,10.0000,11.0000,12.0000
13.0000,14.0000,15.0000,18.0000,21.0000
24.0000,27.0000,30.0000,35.0000,40.0000
45.0000,50.0000,60.0000,70.0000,80.0000
90.0000,100.0000,115.0000,130.0000,145.0000
160.0000,175.0000,190.0000,205.0000,220.0000
235.0000,250.0000,265.0000,280.0000,295.0000
310.0000,325.0000,340.0000,355.0000,370.0000
385.0000,400.0000,415.0000,430.0000,445.0000
460.0000,475.0000,483.3333,483.5833,498.5833
513.5833,528.5833,543.5833,558.5833,573.5833
```

```
588.5833,603.5833,618.5833,633.5833,648.5833
663.5833,678.5833,693.5833,708.5833,723.5833
738.5833,753.5833,768.5833,783.5833,798.5833
813.5833,828.5833,843.5833,858.5833,873.5833
888.5833,903.5833,918.5833,933.5833,948.5833
963.5833,966.6667,966.9167,981.9167,996.9167
1011.9167,1026.9167,1041.9167,1056.9167,1071.9167
1086.9167,1101.9167,1116.9167,1131.9167,1146.9167
1161.9167,1176.9167,1191.9167,1206.9167,1221.9167
1236.9167,1251.9167,1266.9167,1281.9167,1296.9167
1311.9167,1326.9167,1341.9167,1356.9167,1371.9167
1386.9167,1401.9167,1416.9167,1431.9167,1446.9167
1450.0000,
qmpy= 0.00,1.38,2.75,4.13,5.50
6.88,8.25,9.63,11.00,12.38
13.75,15.13,20.05,24.97,27.50
27.50,27.50,27.50,27.50,27.50
27.50,27.50,27.50,27.50,27.50
27.50,27.50,27.50,27.50,27.50
27.50,27.50,27.50,27.50,27.50
27.50,27.50,27.50,27.50,27.50
27.50,27.50,27.50,27.50,27.50
27.50,27.50,27.50,27.50,27.50
27.50,27.50,27.50,27.50,27.50
27.50,27.50,27.50,27.50,27.50
27.50,27.50,27.50,25.85,25.85
25.85,25.85,25.85,25.85,25.85
25.85,25.85,25.85,25.85,25.85
25.85,25.85,25.85,25.85,25.85
25.85,25.85,25.85,25.85,25.85
25.85,25.85,25.85,25.85,25.85
25.85,25.85,20.08,20.08,20.08
20.08,20.08,20.08,20.08,20.08
20.08,20.08,20.08,20.08,20.08
20.08,20.08,20.08,20.08,20.08
20.08,20.08,20.08,20.08,20.08
20.08,20.08,20.08,20.08,20.08
20.08,
$end
```